The present thesis was submitted to
the Department of Concrete and Masonry Structures (CTU Prague)
and the Institute of Building Materials Research (RWTH Aachen)

Master's Thesis

Experimental investigation of the folding behaviour of extruded cement-bound concretes

Submitted by:
Ludwig Josef Werum
Matriculation Number (RWTH Aachen):
349725
Personal ID number (CTU Prague):
490435

Submission date:
8th of June 2021

Supervisors:	M. Sc. Matthias Kalthoff (RWTH Aachen)
	Prof. Ing. Petr Štemberk, Ph.D., D.Eng. (CTU Prague)
1st Examiner:	Univ.-Prof. Dr.-Ing. Thomas Matschei (RWTH Aachen)
2nd Examiner:	Univ.-Prof. Dr.-Ing. Michael Raupach (RWTH Aachen)

Abstract

The innovative and high-performance building material textile reinforced concrete (TRC) has the potential to significantly reduce the enormous resource consumption and CO_2 emissions of the construction industry. To exploit the full potential of this revolutionary building material, however, innovative construction principles are required. Based on the form-follows-force principle, new ideas for structural component geometries can be found in nature, mathematics, and mechanics. In order to produce the found shapes, adequate manufacturing methods are required. Generative manufacturing by means of extrusion is an efficient method to produce filigree TRC components. Within the scope of this master's thesis the subsequent forming or folding behavior of extruded fiber reinforced concrete (FRC) and TRC has been investigated. Furthermore, the influence of different fiber types and contents was analyzed. For this purpose, new folding tools were developed first, which allowed the production of specimens with varying bending radii in transverse and longitudinal direction. Thus, strongly curved specimens were produced using the fold-in-fresh principle. TRC specimens exhibited lower flexibility, which resulted in defects at significantly larger bending radii. Moreover, double-curved specimens were produced and tested in three-point bending tests for their flexural strength. The TRC specimens showed no significant resistance after the critical crack, which led to brittle failure in the FRC specimens. This behavior can be traced back to the test setup, which allowed large horizontal deformations. A possible future use of these double-curved elements is a structural system for ceilings.

Kurzfassung

Der innovative und hochleistungsfähige Baustoff Textilbeton (TRC) besitzt das Potential, den enormen Ressourcenverbrauch und CO_2-Ausstoß des Bauwesens signifikant zu reduzieren. Um das volle Potential dieses revolutionären Baustoffs ausnutzen zu können, bedarf es jedoch innovativer Konstruktionsprinzipien. Basierend auf dem form-follows-force Prinzip können neue Ideen für Bauteilgeometrien aus der Natur, Mathematik und Mechanik gewonnen werden. Um die gefundenen Formen herstellen zu können, bedarf es adäquater Fertigungsmethoden. Die generative Fertigung mittels Extrusion stellt dabei ein effizientes Verfahren zur Herstellung filigraner Textilbeton-bauteile dar. Im Rahmen dieser Masterarbeit wurde das anschließende Umform- bzw. Faltverhalten von extrudiertem Faserbeton (FRC) und TRC untersucht. Weiterhin wurde der Einfluss unterschiedlicher Fasertypen und -gehälter analysiert. Dafür wurden zunächst neue Faltwerkzeuge entwickelt, welche das Herstellen von Probekörpern mit unterschiedlichen Biegeradien in transversaler sowie longitudinaler Richtung ermöglichten. So konnten im fold-in-fresh Verfahren stark gekrümmte Probekörper hergestellt werden. TRC Probekörper zeigten geringere Flexibilität, welche bei deutlich größeren Biegeradien zu Fehlstellen führte. Weiterhin wurden doppelt gekrümmte Probekörper hergestellt und in Dreipunktbiege-versuchen auf ihre Biegezugfestigkeit geprüft. Die TRC Probekörper zeigten dabei keinen signifikanten Widerstand nach dem kritischen Riss, welcher in den FRC Probekörpern zum spröden Versagen führte. Dieses Verhalten kann auf den Versuchsaufbau zurückgeführt werden, welcher große horizontale Verformungen zuließ. Eine mögliche zukünftige Verwendung dieser doppelt gekrümmten Bauteile ist eine Deckenkonstruktion.

Table of Contents

List of Abbreviations

AM	Additive manufacturing
ar-glass	Alkali-resistant glass
CNC	Computerized Numerical Control
CRC	Collaborative Research Center
EAM	Extrusion-based additive manufacturing
ECC	Engineered Cementitious Composite
FRC	(Short) fiber reinforced concrete
MC	Methyl cellulose
PCE	Polycarboxylate ether
PU-foam	Polyurethane foam
PVA	Polyvinyl alcohol
rpm	Revolutions per minute
RWTH	RWTH Aachen University
RC	(Steel) reinforced concrete
TRC	Textile reinforced concrete
TUD	Technische Universität Dresden
UDL	Uniformly distributed load

List of Figures

List of Tables

1 Introduction

1.1 Definition of the problem

The population on earth has grown rapidly in recent years. By 2050 it is estimated that 9.7 billion people will live on earth [Sta19] of which approximately 70 % (6.7 billion) will live in urban areas [Sta18]. Consequently, the demand for construction materials will increase. Currently, most structures are made from cement-bound materials such as reinforced concrete. However, the cement industry is one of the major contributors for greenhouse gas emissions, producing 5 % of global CO_2 emissions [Ber07]. In addition, the resources on earth are limited. Sand and gravel are the second most used natural resources after water [Uni19] and are main components of concrete. Therefore, the goal must be to create building components with minimized weight, optimized load-bearing behavior, and high durability.

Since reinforced concrete structures are prone to corrosion, they have a concrete cover layer to protect the steel reinforcement. From 1999 to 2011, research was conducted at two Collaborative Research Centers (CRCs), RWTH Aachen University (RWTH) and Technische Universität Dresden (TUD) [Cur11b, Cur12], to find a way of replacing the steel reinforcement with non-corrosive, high-performance textiles. The use of carbon textiles offers great potential in this context which is why it has been and will be subject of further research [Cur19, Gär19].

An efficient way of producing filigree concrete structures is generative manufacturing in terms of extrusion [Ald98, Sha01]. Extrusion is a widely used industrial process e. g. to produce bricks or aluminum profiles. Materials ranging from solid to viscous consistency are pressed through a mouthpiece under high pressure and, if necessary, temperature. Compared to common manufacturing procedures, resulting components have a denser structure and can have complex cross-sections, leading to improved mechanical properties [Lan92, Per18]. In order to extrude fine-grained concrete, the rheology of the material makes challenging demands: it must be soft enough to be processable by the extruder while also having sufficient green strength to maintain its shape after extrusion.

The current use of textile reinforced concrete (TRC) is based on traditional construction principles adapted from reinforced concrete (RC). However, to use the full potential of TRC, new design and construction principles must be developed. Through multidisciplinary research and consultation, specifically botany, mathematics, and biology, the goal is to develop structural shapes whose load transfer behaviors perform well under normal stresses. [Cur19]

In general, form-finding is a process of shaping a structure according to the forces acting on it. It can be observed in the formation of natural objects such as trees, shells, or bones and is based on the form-follows-force principle [Lew16b]. To produce efficient structural TRC components in aforementioned shapes, they need to be formed or folded, respectively. Currently, two principles are followed for shaping TRC: the fold-and-grout principle where the concrete is folded after curing along folding edges, and the fold-in-fresh principle where the concrete is folded in its fresh state [Woe17, Woe13].

1.2 Aim of this master's thesis

The extrusion of TRC is a promising method to produce slender, high-performance building components. However, currently no suitable methods for the efficient forming of extruded FRC or TRC are available. Thus, within this master's thesis, efficient folding or forming methods for extruded concrete will be developed and tested. Furthermore, the influence of different types and amounts of microfibers is investigated. Minimal possible bending radii will be determined and ultimately the limits of the folding or forming procedure shall be shown.

2 State of the Art

Within this chapter the state of the art on TRC will be presented from the basics to current practice. Furthermore, the industrial manufacturing process of extrusion of materials such as clay, plastics, aluminum, and others will be explained; and finally, its importance and application for cement-bound materials will be presented. Moreover, folding and forming methods for cementitious materials based on the two principles fold-in-fresh and fold-and-grout will be presented. The connection of these three topics (TRC, extrusion, and folding) resulted in the research done within this thesis: the experimental investigation of the folding behavior of extruded TRC.

2.1 Textile reinforced concrete

Steel reinforced concrete has many technical and economic advantages such as being ubiquitous, universally applicable, and comparatively cheap. Nevertheless, during the sixties and seventies the disadvantages of RC brought its use in construction into disrepute. Disadvantages include corrosion problems of the reinforcement and concrete spalling. [Wei09] Since these circumstances are unsatisfying, the search for an alternative reinforcing material began. As early as the mid-1990s, researchers in Aachen and Dresden developed the idea of using textile fabrics made from corrosion resistant endless fibers with high tensile strength as a reinforcement in concrete. [Sch15]

Since 1999 the two CRCs SFB 532 and SFB 528 at RWTH and TUD have been conducting basic research in the field of TRC. After 12 years of funding, in 2012 the SFB 528 presented their final report on textile reinforced concrete for structural reinforcement and repair, see [Cur12]. SFB 532 conducted its research on the development of a new technology and the use of textile reinforced concrete for thin-walled and highly resilient components [Cur11b].

Subsequently, in 2014 the TUD initiated the project “C³ - Carbon Concrete Composite”. The project is being carried out by a consortium of over 140 interdisciplinary partners and aims to establish carbon concrete as construction method, which is a corrosion-resistant and resource-efficient alternative to common reinforced concrete construction. The vision is to replace reinforcing steel with carbon in the long term. The change of material can reduce the energy consumption and carbon dioxide emissions by almost 50 %. By 2021 the prerequisites for introducing carbon concrete to the market shall be created and by 2025 the construction method shall be established. [Car21a, Gär19, Reu15]

This master’s thesis is part of research currently being carried out at another CRC of RWTH and TUD called SFB TRR 280. The research carried out within the CRC is based on previously collected information from the fundamental research carried out by SFB 528 and SFB 532 as well as the application-oriented consortium C³ (Figure 2-1). However, in the C³ project familiar construction principles are used. In order to develop the full potential of carbon concrete, SFB TRR 280 aims to develop new design and construction strategies for innovative and sustainable structures. New concrete structures, inspired by interdisciplinary fields such as biology (especially botany), mathematics, mechanics, and art are being researched. [Cur19]

The core goals are [Cur19]:

- Reduction of Resource Consumption
- Reduction of Environmental Impact
- Increased Life-Span through Increased Durability
- Aesthetic Design Language

Within the intended 12 years of funding, the design, construction, testing, and production of structures shall be rethought based on new construction principles that go far beyond two-dimensional or slightly curved components. Building upon the form-follows-force principle (chapter 3.1), new methods in the designing and dimensioning of structures including the development of material and process technology, shall be developed. Carbon concrete is an example of a construction material that meets the requirements of being corrosion-resistant, having high load-bearing capacities, and allowing filigree structures with planar or curved topology. Therefore, new production methods specifically generative manufacturing or extrusion will be investigated. [Cur19]

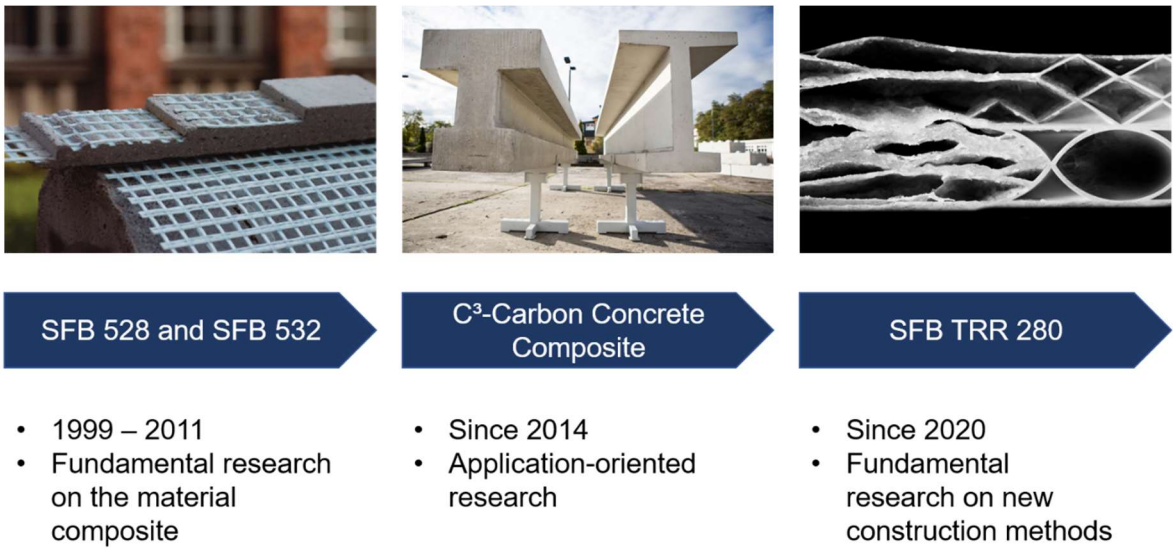

Figure 2-1: Research subject of SFB/TRR 280 based on previous research on textile reinforced concrete cf. [Cur19] – Sources of the figures left to right: [Cur11a] [Car16] [Son20]

RWTH and TUD now play a leading role in the field of carbon concrete due to their long-term collaboration. However, in the last 20 years, TRC research has gained momentum worldwide, especially regarding carbon concrete. This trend is supported by an increase in publications globally, as shown in Figure 2-2, promoting the expansion of current and future research. The numbers are based on search results found in the two citation libraries “Scopus” and “Web of Science” connected to carbon concrete. Especially European countries, South-East-Central Asia, and North America have made major scientific contributions. [Car21b] Exact values can be found in Appendix A.1.

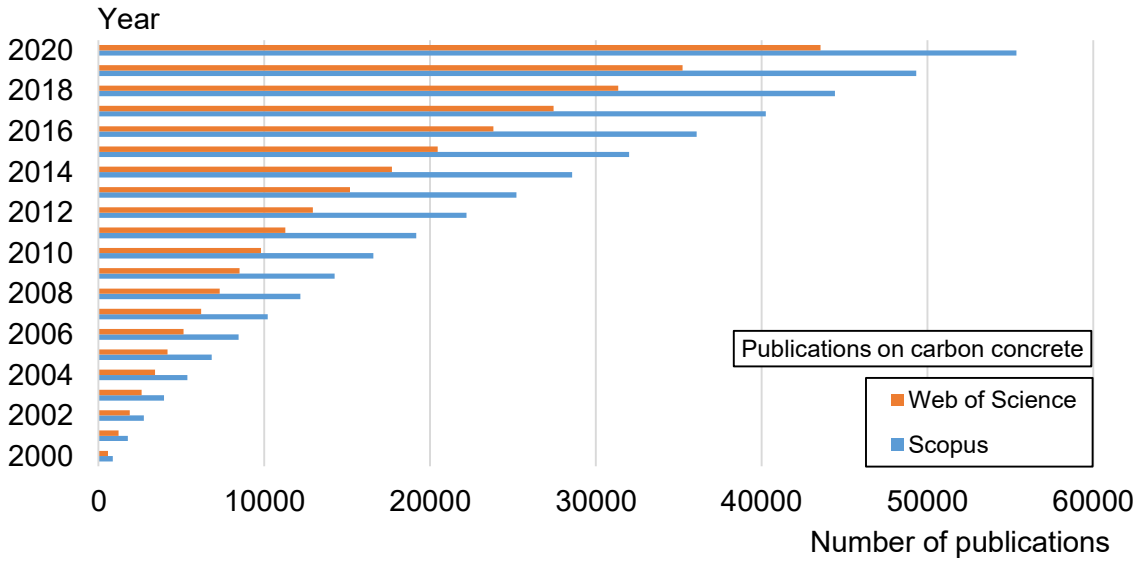

Figure 2-2: Development of publications on carbon concrete from 2000 to 2020 [Car21b]

In the following chapters a summary of research results on TRC will be given from fundamental research to current practice.

2.1.1 Textile reinforcements: short fibers and fabrics

The role of reinforcement in structural concrete is mainly to carry tensile stresses. The nearly perfect combination of steel and concrete made RC to be the most used and most successful building material of the past century. In general, concrete carries the compressive stresses, and the reinforcement steel carries tensile stresses. When the concrete tensile strength is reached and cracks occur, the reinforcement must be able to absorb the released concrete tensile stresses as well. Besides carrying the compressive stresses, another effect of the concrete as a matrix material is, that it has a high pH-value and thus is strongly alkaline, which protects the reinforcement steel from corrosion. [Cur09] To guarantee this, a minimal concrete cover of 10 to 65 mm is necessary [DIN11]. This induces minimal dimensions for components made from RC of approximately 50 to 100 mm. Therefore, when less concrete is needed for carrying the compressive stresses, and it is mainly used to protect the reinforcement from corrosion, the structure is inefficient in terms of its load-bearing capacity. Textile reinforcements made from high-performance fibers provide a more efficient solution for these structures, since their tensile strength is significantly higher than that of construction steel (Table 2-1, page 7). Furthermore, they do not need to be protected from corrosion making a minimal concrete cover obsolete. This makes it possible to reach overall better performance and thinner component dimensions. To describe the new composite material, a distinction must be made between FRC and TRC. FRC contains short fibers randomly distributed in the concrete mixture, whereas in TRC fibers are connected into so-called rovings and arranged in the form of fabrics, see figure below. [Cur09]

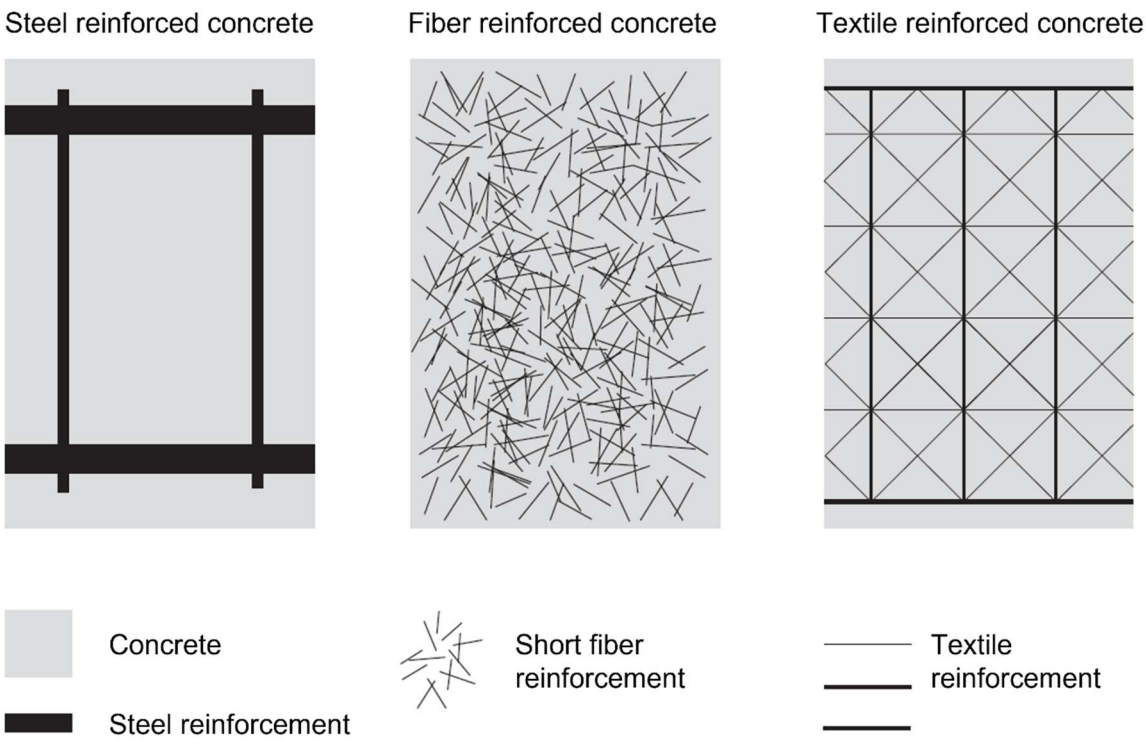

Figure 2-3: Comparison of different reinforcement types cf. [Jes10]

2.1.2 Fiber material and its production

The characteristics of textile reinforcement are greatly impacted by the properties, the amounts, and the arrangements of the fiber materials used. This places various demands on the fiber material and its make-up. In principle, all fibers with high tensile strength, good bonding properties, high modulus of elasticity, and high elongation at break are suitable as reinforcement materials for the use in concrete. Having a high Young's Modulus compared to concrete is especially important, otherwise crack formation would drastically reduce the composites stiffness. Furthermore, the fibers need to be chemically and physically compatible with the alkaline matrix material, so that they do not lose their properties over time and assure a long-term reinforcing effect (more in chapter 2.1.6). Alkali-resistant glass (ar-glass), carbon, and aramid are potential substitutes for the steel reinforcement as they meet aforementioned requirements. Other fiber materials such as steel, various plastic fibers (e.g. polypropylene, polyethylene, polyvinyl alcohol), and basalt fibers have proven to be suitable as short fiber reinforcements. [Gri06, Wei09]

To produce textile reinforcements, single fibers (so-called filaments) are connected to multi-filament yarns (rovings). One roving consists of 800 up to 2000 filaments for ar-glass and carbon fibers have even more (Table 2-1, page 7). Thus, the stress-strain behavior of a filament yarn is influenced by the position of the single filament in the yarn. Ideally, they should all be parallel and straight, but deviations may occur during manufacturing. Furthermore, a coating or size is applied on the filaments during manufacturing which is crucial for further processing. The sizing influences the properties of a yarn significantly and enhances the adhesion between filament and matrix material, which impacts the load-bearing behavior of the composite. Additionally, the sizing can improve the alkali-resistance e. g. of ar-glass and basalt. [Gri06, Off04]

Table 2-1: Properties of different fiber materials for textile reinforced concrete in comparison to reinforcing steel [Cur09]

Property	Unit	Construction Steel BSt 500	Alkali-resistant glass	Carbon
Strength	MPa	500	2500	4200
Youngs Modulus	GPa	200	74 … 80	240
Elongation at break	‰	50	35	18
Density at 20 °C	g/cm³	7.85	2.74 … 2.80	1.78
Diameter of reinforcement	mm	6 … 28	~1 … 2	~1 … 2.5
Area of reinforcement per rod	mm²	28 … 615	0.23 … 0.88	0.44 … 1.9
Cost	€/kg	~1 … 1.5	~4 … 5	~20 … 30
Load-bearing capacity in kN per € and m	kN/(€∗m)	42 … 64	36 … 46	37 … 56
Fineness	tex	–	640 … 2400	800 … 3500
Filaments per Roving	pieces	–	800 … 2000	12000 … 50000

When textiles are used as reinforcement, civil engineers are confronted with terminology from textile technology. For example, in steel reinforcement, the diameter of the rebars and the cross-sectional area are used as measurement. However, for textiles, the fiber weight in grams per 1000 m is used instead of the cross-section area. This resulting unit of measurement is called tex. Dividing it by the density ρ of the material gives the cross-sectional area A. [Cur09] A calculation example of an 800 tex carbon fiber is given in the following equation.

$$800\ tex = 800\ {}^{g}/_{1000\ m} = 800\ {}^{g}/_{10^5\ cm} \tag{2-1}$$

$$A = \frac{tex}{\rho} \tag{2-2}$$

$$\Rightarrow A = \left(800\ {}^{g}/_{10^5\ cm} : 1.80\ {}^{g}/_{cm^3}\right) * \left(10^2\ {}^{mm^2}/_{cm^2}\right) \approx 0.44\ mm^2 \tag{2-3}$$

With: A Cross-section area
tex Unit for the fiber weight in grams per 1000 meter
ρ Density in g/cm^3

Ar-glass

The basic materials used to produce ar-glass are silica sand, clay, and limestone. To provide alkali resistance, ar-glass contains at least 16 % of zirconia. The mixture is molten at temperatures of up to 1350 °C and is then pulled from a spinning nozzle with a velocity of up to 150 m/s. The diameter of the resulting single fibers ranges from 9 to 27 µm.

Afterwards, the sizing is applied to the filaments before they get connected to multi-filament yarns. Ar-glass shows strong adhesion with the concrete matrix and has low cost compared to carbon. [Off04, Pur06]

Carbon

Carbon is a synthetic polymer used in aviation, automobiles, and sporting goods. It is made from polyacrylonitrile, which is spun into anisotropic fibers after pretreatment. Afterwards, during carbonization, the properties of the fibers are defined. Depending on the desired fiber characteristics they are treated at temperatures between 1500 °C and 3000 °C. Advantages of carbon fibers are high tensile strength, low heat elongation, little creep tendency, and high resistance against acids and alkalis. However, the adhesion properties are inferior to ar-glass. Thus, special sizes have to be implemented to improve filament properties and achieve better reinforcement action in the building component. [Gri06, Off04]

As Table 2-1 shows, in comparison to ar-glass, carbon fibers are approximately 4 to 6 times more expensive. However, the difference in density reduces the price per kg. Also, the strength of carbon fibers is nearly twice as high as ar-glass, and ar-glass loses strength in some concrete mixtures, so that over a lifetime of 50 to 80 years a loss of approximately 50 % must be considered. Finally, looking at the load-bearing capacity in kN per € and m, carbon fibers seem to be the more economical alternative (Table 2-1, page 7). [Cur09]

Aramid

Aramid is a synthetic fiber made from aromatic polyamides. Due to its high tensile strength and modulus of elasticity, aramid fibers belong to the high-performance fibers. Compared to carbon or ar-glass fibers, aramid has a lower density and lower brittleness. However, it has a negative thermal extension. If thermal extension of reinforcement and concrete differ, tension arises in the adhesion zone. Another disadvantage of aramid fibers is its general lack of alkali-resistance. [Gri06]

Basalt

Basalt fibers can be used as short fiber reinforcement in FRC. They are made through a melting process from the natural resource of basalt rock which is available in abundance in places like Russia. One advantage of using basalt fibers are the cost savings, as it contains no additives. However, when compared to carbon fiber, basalt fiber has worse resistance against alkalinity, which is prevalent in concrete. In [Sim05] the alkali-resistance of basalt, carbon, and glass fibers was investigated by immersing the fibers in a 1 M NaOH solution. The basalt and glass fibers showed a significant volume loss and thus a loss of strength under caustic conditions. This was caused by the reaction between SiO_2 and the alkali solution, resulting in a strength loss of more than 80 % after 28 days of immersion. For carbon fibers immersed in the same solution, only a 13 % loss was observed after 28 days. However, under thermal conditions basalt fibers showed significantly better behavior than glass and carbon fibers. [Sim05]

Polyvinyl alcohol

Besides basalt, fibers made from polyvinyl alcohol (PVA) can be used as short fiber reinforcement. The fibers are widely used in industrial, agricultural, and fishing applications. Furthermore, they feature suitable characteristics as a reinforcement for cementitious materials such as high tensile strength, good bonding with the concrete matrix, and high

modulus of elasticity while being a reasonable cost alternative. Compared to ar-glass, PVA fibers have a better strength to weight ratio and will not degrade in highly alkali cement. [Hor06]

2.1.3 Textile fabrics

In order to use textiles as a two-dimensional concrete reinforcement, multifilament rovings (Figure 2-4) are connected to open-meshed fabrics (Figure 2-5). These fabrics must have a sufficient openness and resistance against displacement. The openness is necessary so that the fibers get fully covered in concrete and to avoid the formation of a separation gap [Vos08]. Therefore, minimal distances within the meshes must be considered. In previous applications, girder structures with openings of approximately 3 times the maximum grain diameter have proven their suitability [Cur09] (more in chapter 2.1.6). The figures below show a carbon fabric and the roving it was made of. The textile reinforcement was used for the production of a TRC footbridge in Albstadt, Germany [Rem18].

Figure 2-4: Multifilament roving made from carbon fibers [Rem18]

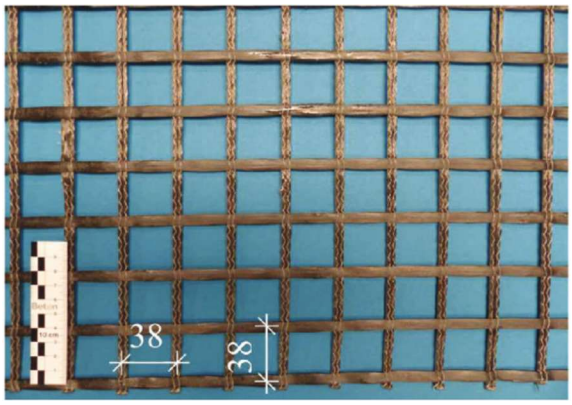

Figure 2-5: Laid carbon scrim with 38 mm spacing [Rem18]

The resistance against displacement is necessary for an adequate handling and can be achieved by a variety of textile fabrication processes. However, only a few can be used for concrete reinforcement. Three common types of fabrics are: laid scrims, woven fabrics, and knit fabrics. Knit fabrics are produced from only one thread and are known from domestic use. However, those structures are only conditionally suitable for the use as concrete reinforcement. Laid scrims consist of at least two systems of superposing thread scrims which are connected by a knitting thread (Figure 2-6). If two thread systems are used bi-axial scrims are produced, while three or more systems form multiaxial scrims. Thereby, the orientation of the rovings can be adapted according to the intended purpose of the fabric. For the highest tensile load-bearing capacity, yarns should be orientated in load direction. Fibers in 0° direction are called warp and the fibers in transverse direction are called weft. The advantage of laid scrims is that all yarns are straight and thus achieve high stiffness and strength. Woven fabrics are produced by shedding two rectangular thread systems (Figure 2-6). The disadvantage of those structures is the alternating position of warp and weft causing deviation forces which can lead to damage on the yarns. Thus, common woven fabrics are unsuitable as textile reinforcement. [Gri06, Jes10, Mol05, Off04]

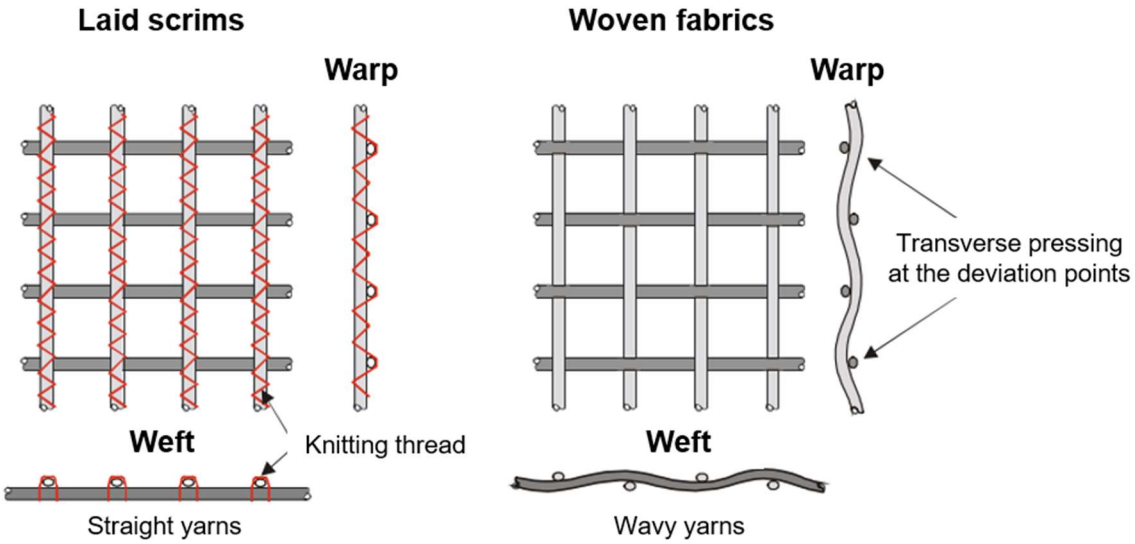

Figure 2-6: Schematic illustration of laid scrims and woven fabrics cf. [Mol05]

After connecting the rovings, in most cases, the fabric will be covered in a special coating based on a polymer suspension. The coating influences the connection between the individual filaments and between concrete and filaments, which further directly influences the load-bearing capacity of the whole fabric. Furthermore, it increases the resistance against displacement and the bending stiffness. For good handling, more stiff textiles are used in planar components than in three-dimensional geometries or profiled cross-sections. [Cur09]

2.1.4 Load-bearing behavior of textile reinforced concrete

The mechanical properties of TRC and RC are similar due to equal load-bearing and failure mechanisms. The behavior of TRC under load can be described by separating it in different stages (Figure 2-7) [Cur09]:

- Stage I: The concrete is uncracked and the composite material behaves according to the stiffness of the concrete.
- Stage IIa: The concrete tensile strength is exceeded and the concrete cracks.
- Stage IIb: No further cracks can be developed. Further loading only leads to elongation of the reinforcement.

RC shows a third stage which is characterized by the plastic work capacity of the steel reinforcement. However, neither ar-glass nor carbon exhibit such a work capacity and thus TRC fails in a brittle manner. Nevertheless, TRC has advantageous properties compared to RC such as the significantly higher tensile strength, corrosion resistance, and fine crack pattern. [Cur09]

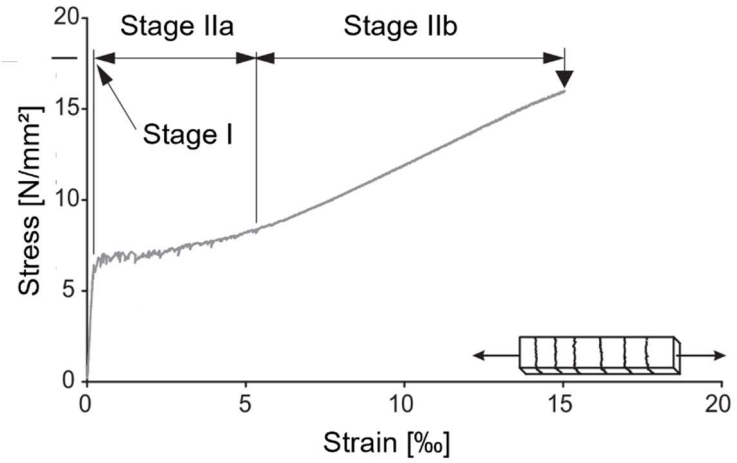

Figure 2-7: Stress-strain diagram of a TRC specimen subjected to centric tension cf. [Jes10]

For an analysis of the load-bearing behavior of the textile itself, there needs to be a distinction between the strength of a filament and a roving. Testing a roving on its tensile load-bearing capacity, the weakest fibers fail first. Consequently, the tensile stress is transferred to the remaining fibers which are then subjected to higher stress and thus, more fibers fail. Since the load at failure is projected on the cross-sectional area, the load-bearing capacity of a roving will always be smaller than the average strength of a filament. [Wei09]

In the further process of creating a fabric from the roving, more strength-reducing influences such as abrasion or transverse pressing of a filament can occur. Furthermore, the stiffness of the fabric changes through a slight waviness and not ideally parallel or stretched filaments and rovings – the stress-strain curve is flatter and can partially be non-linear. [Wei09] The following figure shows an example of the different stress-strain curves of a filament, a roving, and a fabric made of ar-glass under similar testing conditions. The utilization coefficient between filament and roving is approximately 60 to 70 % and between roving and fabric it is approximately 90 %. [SFB01]

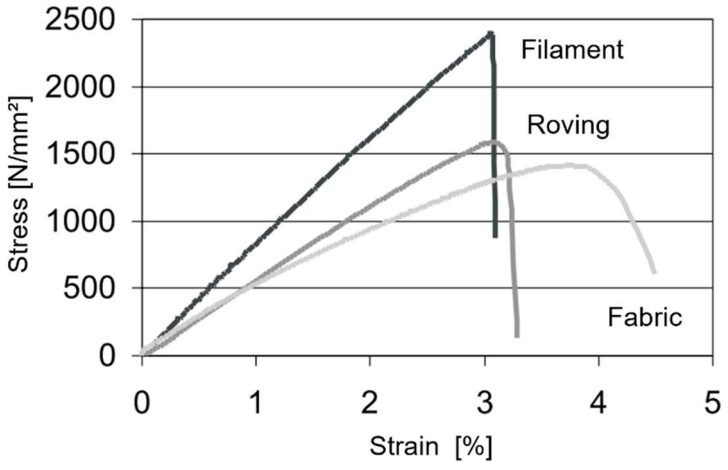

Figure 2-8: Exemplary stress-strain diagram of filament, roving, and fabric made from ar-glass cf. [SFB01]

FRC shows a different failure mode, in comparison to steel or TRC. In FRC the fibers will be pulled out in the state of break. The work done in this process gives the FRC high ductility. Yet, it must be considered that the load should not exceed the tensile strength of

the fibers or brittle failure might occur. Thus, a full utilization of the fiber strength is not possible. On the other hand, RC and TRC fail when reaching the material strength of the reinforcement. The ductility thereby comes exclusively from the plastic deformation of the reinforcement. [Cur09]

2.1.5 Short fiber reinforced concrete

As mentioned above, the failure mode of concrete is a multi-stage process. Pre-existing cracks in the order of micrometers grow under an applied load and eventually join to form macrocracks. The macrocracks then propagate at a stable level until conditions of unstable propagation are fulfilled and a rapid fracture occurs. [Ban05] To increase stresses at which first cracks occur, enhance ductility, and optimize the crack development of concrete mixes, short fibers can be added [Hin09]. The short discontinuous fibers are mixed with the concrete and thus, they are randomly distributed in the matrix material. The fibers reach every part of the element, which is optimal for structures influenced by an undirected force. For structures under a directed force, the random distribution of the reinforcement is inefficient, but due to the simple manufacturing process it is economical for some load-bearing structures. [Cur09] Even so, a given fiber can only provide reinforcement within a limited range of strains. For an optimal response, different types of fibers can be combined. [Ban05] In [Hin09] different types and combinations of fibers (hybrid fiber mixes) were investigated to achieve the best mechanical properties. The stress-strain behavior of conventional TRC without short fibers and TRC with different types and combinations of fibers can be seen in the figure below.

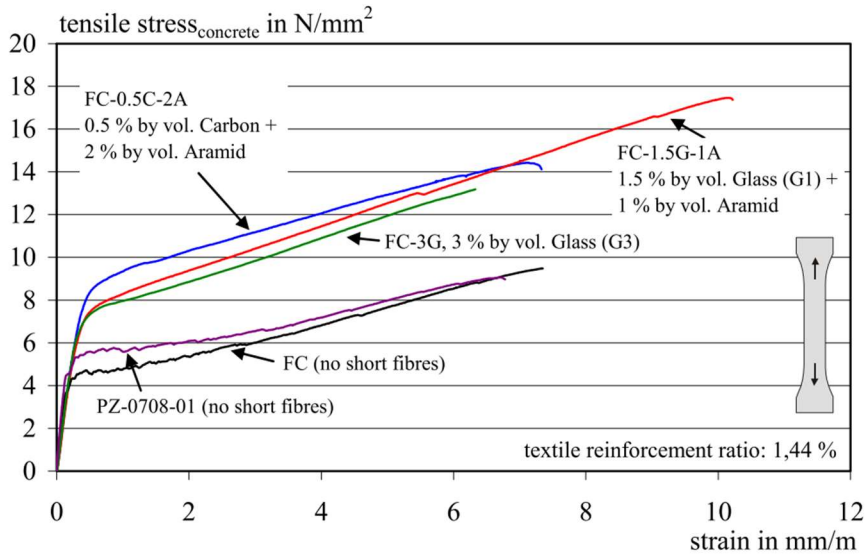

Figure 2-9: Stress-strain behavior of TRC with and without short fibers [Hin09]

As shown in the figure above, using short fibers improves the stress-strain behavior of the TRC. The short fibers 1) contribute to higher first crack stresses of the concrete and 2) show a strain hardening behavior after the initial crack formation, where the short fibers help to bridge the cracks and improve the crack pattern. Both contributions place different demands on the short fibers and thus, a combination of fibers of different materials, sizes, and shapes seems advantageous. Microfibers can increase the first crack stress of the concrete by reducing the micro-crack formation. After a first macro-crack is formed, the macrofibers further increase the load bridging of the cracks [Ban05]. Consequently, both fiber types

provide reinforcement on different fracture levels, meaning that their combination and synergy provide improved stress-strain behavior. In [Hin09] carbon fibers of 3 mm length and glass fibers of 6 mm length were used for increasing the first crack stress and aramid fibers of 20 mm length were used for bridging the macro-cracks. The results showed an increase of the first crack-stress by approximately 40 % and a more ductile load-transfer from concrete to textile. [Hin09]

2.1.6 Fine-grained concrete

The concrete used as a matrix for textile reinforcement needs to fulfill several requirements that are different to the ones used in RC. It must ensure a force-fit and durable embedding of the textile reinforcement. Therefore, a major requirement is the maximum grain diameter which generally should be adapted to the distance between the reinforcement bars. Usually, the smallest dimension of a component should be at least 3 times the size of the maximum grain diameter. For components in the scale of several millimeters to centimeters, as they are common for TRC, the maximum grain diameter results in approximately 1 to 4 mm. Due to this fine structure, the matrix material could be classified as a mortar according to DIN EN 206 [DIN17], but this would not satisfy the potential of the material. The composition of the material is rather similar to a high-performance concrete; therefore, it is called fine-grained concrete. The two CRCs in Aachen and Dresden developed several basic mixtures in accordance with the reinforcement structure and manufacturing requirements (Table 2-2). The fibers used were mainly made from ar-glass and carbon. [Cur09, Lie15]

Table 2-2: Exemplary sprayable fine-grained concrete mixtures developed in SFB 528 [Jes10]

Component	Unit	Mixture 1	Mixture 2	Mixture 2
CEM I 32.5	kg/m³	-	564.8	-
CEM III/B 32.5		628.0	-	468.4
Sand 0 … 1 mm		942.0	1122.4	1122.4
Silica fume		100.5	56.6	56.6
Fly ash		265.6	253.1	253.1
Water	l/m³	214.6	221.5	221.5
Superplasticizer		10.5	12.0	3.8
Water to binder ratio	-	0.33	0.36	0.42

Generally, the fine-grained concrete needs to be chemically compatible with the fiber material, its rheological properties, and the curing behavior needs to suit the manufacturing process. While a high pH-value of the concrete matrix is desired for steel reinforcement, the durability of textile fibers in a strong alkaline environment is limited. High silica fume or fly ash contents result in a drop of pH-value in the pore solution, which increases the risk of depassivation of the steel reinforcement [Wie95]. However, the lower alkalinity might be beneficial for the textile reinforcements. In terms of processability, depending on its

application, the consistency of the concrete needs to be soft to flowable to ensure good embedment of the textile reinforcement. Furthermore, if the concrete is used as a reinforcement for existing concrete structures, it needs to have good bonding properties with the substrate. [Lie15]

A main difference between fine-grained concrete and conventional concrete mixtures is the high binder and fine grain aggregate content. This is necessary to achieve an all-round coating of the multifilament yarns to ensure the bond between the fine-grained concrete matrix and the textile reinforcement. Due to the compact packing of the multifilament yarns usually only a partial penetration in dependence of the diameter of the filaments can be achieved. The outer filaments are encapsulated by hydration products ensuring that the bond between reinforcement and matrix material is achieved. The activation of the inner filaments comes through the friction within the yarn. If an impregnation is applied during the manufacturing process of the rovings, the transmitted forces between matrix and reinforcement and between the individual filaments of a yarn, are increased. This influences the crack formation as well as the stress-strain diagram of TRC. [Lie15]

To achieve high strength of the composite material, the properties of the concrete need to be adjusted specifically. Concrete mixtures with fly ash and microsilica have proven themselves to be suitable since their combination will create delicate calcium silicate hydrate phases that have particularly well bonding properties with the filigree reinforcement and create a homogeneous fresh concrete with a low segregation tendency. The exact composition of the binders, the moisture and temperature conditions, and the surface properties of the filaments determine the morphology of the resulting hydration products and thus the performance of the bond between the filaments and the fine-grained concrete matrix. Through the small grain size of the microsilica and fly ash (approximately 1/10 of the cement) a filling effect is achieved within the microstructure of the concrete. Furthermore, they positively influence the processability of the concrete. The fine-grained concrete has a high density and in combination with the usual fine crack pattern due to the textile reinforcement, the durability is positively influenced. Usually, the amount of water added to the mixture is limited by the amount necessary for hydration to achieve high-performance concrete properties. Thus, the water to binder ratio is commonly between 0.3 and 0.4. To still achieve processable fresh concrete properties, super plasticizers on the basis of polycarboxylate ether (PCE) are generally used. [Cur09, Lie15]

2.1.7 Production methods of TRC elements

New building materials need to prove their suitability for practical use. However, the manufacturing methods must meet the practical requirements. For the application of TRC, casting, laminating, spraying, and spinning have already been successfully utilized. In the casting technique the textile reinforcement is placed in a formwork and afterwards the concrete is cast. Therefore, the fine-grained concrete mixture must be of a very flowable consistency. However, this method reaches its limit when the textile fabric is too close-meshed and can no longer be penetrated by the fine-grained concrete, or when the textile reinforcement is not stiff enough and thus a stable position in the concrete can no longer be guaranteed. The area of use of this method is therefore limited to two-dimensional slabs and simple three-dimensional elements. [Bra16] The cast method was used already in 2005 to produce elements for a diamond-shaped lattice arch made of TRC [Heg08]. At

first, the inner formwork was placed, and the fabrics were clamped around it. Then spacers were placed between the individual fabric layers and the formwork was completed. The fine-grained concrete was then cast into the mold (Figure 2-10). After curing it was demolded resulting in the finished diamond-shaped TRC element (Figure 2-11). [Bra16]

Figure 2-10: Casting a diamond shaped TRC element [Bra16]

Figure 2-11: Finished cast TRC element for a lattice arch [Bra16]

During the laminating process of TRC elements, the fine-grained concrete and the fabric are alternately placed in the formwork layer upon layer until the desired number of layers and thickness are reached. Uncoated two-dimensional fabrics with a flat structure should be used so that they can be placed smoothly in the concrete. The fabrics are then pushed into the fine-grained concrete with a roller to improve the penetration and thus the bond. The fine-grained concrete can have differing viscosities, where a high flowability allows for more penetration of the yarns by the concrete. However, it turned out that the waviness of the fabric is increased compared to cast elements and thus the maximum load-bearing capacity of laminated elements is lower. The lamination method is suitable for two-dimensional and simple three-dimensional slabs as well as for simple shell structures. [Bra16]

Spraying or shotcreting is based on a low-pressure system with up to 8 bar. It is very similar to the laminating method since the fine-grained concrete and the fabric are applied alternatingly in layers. Hence, the requirements for the fabric are the same for both methods. However, textiles coated with soft polymeric materials can be used to increase the load-bearing capacity. Another parallel between both methods is that the fabrics should be rolled into the fine-grained concrete in order to ensure a good penetration and bonding. An advantage of this method is that vertical surfaces can also be sprayed. Thus, this method is suitable for manufacturing multiple curved shells. Yet, the fine-grained concrete mixture must fulfill different requirements in contrast to the laminating method. It must be pumpable and sprayable and thus it must have a higher viscosity and adhesion. With this technique, furthermore, larger surfaces of arbitrary geometry can be cast quickly. [Bra16] A practical example for the use of this method can be found in [Sch09]. There it is described how a 100 years old RC roof structure which is under historic preservation was reinforced with sprayed TRC in Zwickau, Germany (Figure 2-12).

Figure 2-12: Application of TRC reinforcing layer on a historic roof structure in Zwickau, Germany [Sch09]

In order to produce poles, tubes, or columns, the spinning method is a possible alternative manufacturing procedure. In this method, the concrete is compacted by fast rotation around the axis of the formwork. In an early test, a turning lathe was used for spinning, where the tubes were axially clamped and spun evenly (Figure 2-13). Suitable concrete mixtures should feature a flowable consistency and can be used with or without short fibers. Uncoated and coated two-dimensional fabrics can be used. However, uncoated fabrics cannot keep their position during production in one work step and thus, to insert the fabrics, the spinning process must be interrupted. This process is very time consuming. Coated fabrics are stiffer and by using spacer they allow for the production with the spinning method in one work step. Accordingly, circular TRC profiles with a defined position of textile reinforcement can be produced (Figure 2-14), which can considerably reduce the self-weight of poles or tubes made from steel reinforced concrete. [Bra16]

Figure 2-13: Clamped tube during spinning process [Bra16]

Figure 2-14: Spun tube with four layers of textile reinforcement [Bra16]

A continuous manufacturing process of building components has the advantage of low manufacturing costs due to an automated production. The process of extrusion describes a continuous process where viscous materials are pressed under high pressure (and if needed temperature) through a mouthpiece. The material is compacted by a screw or ram and the required cross-section is determined by the shape of the mouthpiece through which the material is pressed. Cross-sections that can be extruded are for example I-profiles, channel sections, or honeycomb slabs. However, a concrete mixture, suitable for extrusion must fulfill several requirements regarding its rheology. [Bra16] Yet, after overcoming this challenge and implementing the textile in the manufacturing process, it is possible to extrude TRC. The manufacturing process of extrusion with a special focus on the extrusion of TRC will be described in more detail later in chapter 2.3.6.

The manufacturing methods and practical examples presented above show the impressive versatility of TRC as a building material. It can be used for load-bearing structures, as a reinforcement for existing structures, and for various light-weight slender components with high requirements on corrosion resistance and appearance. A selection of more practical examples for the application of TRC can be found in [Ehl12, Heg06] and [Heg08].

2.2 Folded plate structures and folding methods

TRC with fabrics made from ar-glass or carbon has the property of being flexible and consequently pliable. This flexibility makes it possible to create thin folded plate structures by using folding methods. In this master's thesis two general folding principals are presented.

Within the first folding principle the concrete is formed while it is fresh; ergo soft enough to be formed – the so-called: fold-in-fresh principle. The concrete is placed into a formwork, and when sufficiently cured, the formwork is removed, and the concrete retains its shape (chapter 2.2.1). The second possibility is to produce concrete in straight elements with folding joints. The joints are created by recess elements which are put into the concrete while its fresh. When cured the element gets folded along its joint. Afterwards the joint is filled with some kind of mortar or grout – this method is called: fold-and-grout principle (chapter 2.2.3). [Woe18b] Later in this thesis, specific folding procedures for extruded cement-bound concrete will be developed and tested. This chapter summarizes the existing folding methods for TRC.

2.2.1 Fold-in-fresh

Within the fold-in-fresh principle the concrete gets folded while still soft enough to be put in shape. An exemplary way to use this principle for folding textile reinforced structures can be found in [Woe17]. There, a joint was placed in the formwork so that the folding mechanism was not in the concrete but in the formwork. By folding the formwork, the flat plate is put from the plane into the desired shape (Figure 2-15 and Figure 2-16). The textile reinforcement keeps the concrete in place and prevents it from flowing out of shape. After curing, the formwork is removed and the folded plate structure is finished. [Woe18b] However, the size of the folded plate is limited so that for building larger elements methods for joining are essential. Nevertheless, the elements can be transformed into a spatial structure while no laborious formwork is needed. [Woe17]

Figure 2-15: Components of a foldable formwork [Woe17]

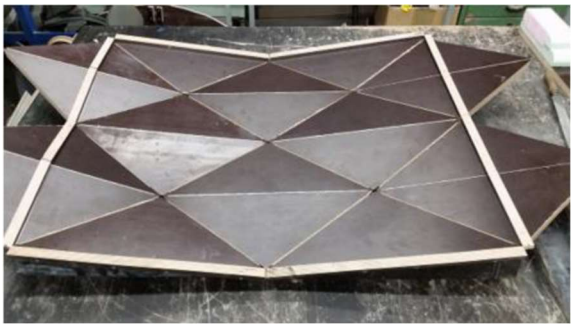

Figure 2-16: Foldable formwork in folded state [Woe17]

In [Woe17] the authors constructed a vault using folded segments of TRC made by the above mentioned principle. The authors intended to apply this approach and create folding

elements with a so-called YOSHIMURA[1] crease pattern. Therefore, the formwork was built out of hinges and facets. As first step the concrete of the lower half was poured into the formwork, followed by the installation of the textile reinforcement. Then the second layer of concrete was poured for the upper half. After smoothening the surface, the folding process began. Therefore, wedges were placed below the formwork (Figure 2-15) and thus, the concrete was formed in its fresh state. After the concrete cured the wedges were removed and the desired YOSHIMURA crease pattern was achieved (Figure 2-17). The prototype elements had a thickness of 2 cm and two layers of fabric. [Woe17]

Since the size of the elements is limited, a way of connecting them had to be found as well. Several ways of connecting the elements were discussed and for the prototype purpose a screw connection was chosen. Therefore, eight holes were drilled into each element. Two elements were then connected with four screws. Since the elements were overlapping and imperfections occurred, rubber disks were placed to the screws for compensation. The final vault element spanned approximately 2.75 m with a height of 1.25 m (Figure 2-18). [Woe17]

Figure 2-17: Folded segments produced by fold-in-fresh method [Woe17]

Figure 2-18: Final vault element made from connected segments [Woe17]

Later, the authors discussed the use of screws. During the connection of the elements a gap between the elements of the outside layer occurred with an increasing offset if elements are placed radial to the outside. However, if grout was used for connecting the elements instead of screws, the issue is not critical since the offset gets filled. Furthermore, drilling holes into the concrete had a high danger of breaking and the screwed connection itself led to a very concentrated force introduction which forms a weak point. A full-surface bonding with mortar could increase the load-bearing capacity. This could be achieved by connecting the elements with screws in the production phase, leaving sufficient space for introducing the mortar subsequently. [Woe17]

In [Pid16] another way of folding TRC elements in their fresh state is presented. The goal of the authors was to produce façade elements with complex geometries in a more efficient way than the conventional manufacturing process with individual formworks. To evaluate different concrete mixtures and their folding behavior preliminary tests with a folding tool were carried out (Figure 2-19). The fresh concrete was produced in a formwork with the

[1] The Yoshimura crease pattern was developed from the buckling behavior of a circular cylindrical shell under axial compression [Yos55]. It can be seen in the formwork in Figure 2-16 and in the final TRC product in Figure 2-17.

laminating method and after reaching sufficient green strength[1], it was carried to the folding tool with the help of a plastic foil.

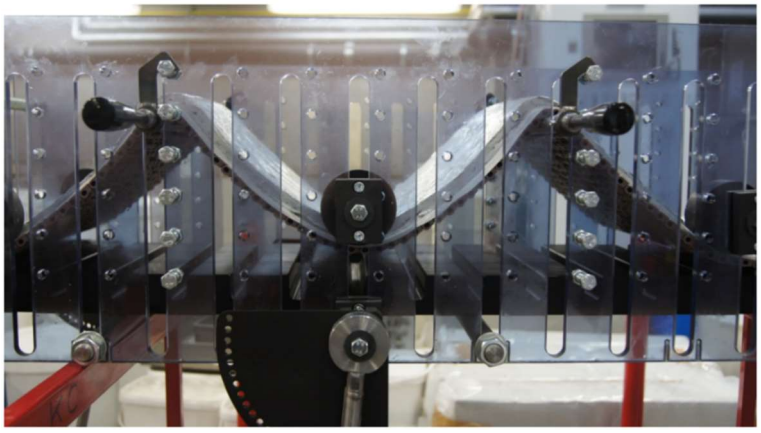

Figure 2-19: Folding tool with fresh concrete and two high points [Pid16]

Within the framework of this project the Institute of Textile Technology of the RWTH developed a biaxial textile mesh with locally adjusted bending stiffness (Figure 2-20). Two stiffer textile meshes were connected with a more flexible mesh to receive some kind of textile joint which allowed better formability. [Pid16]

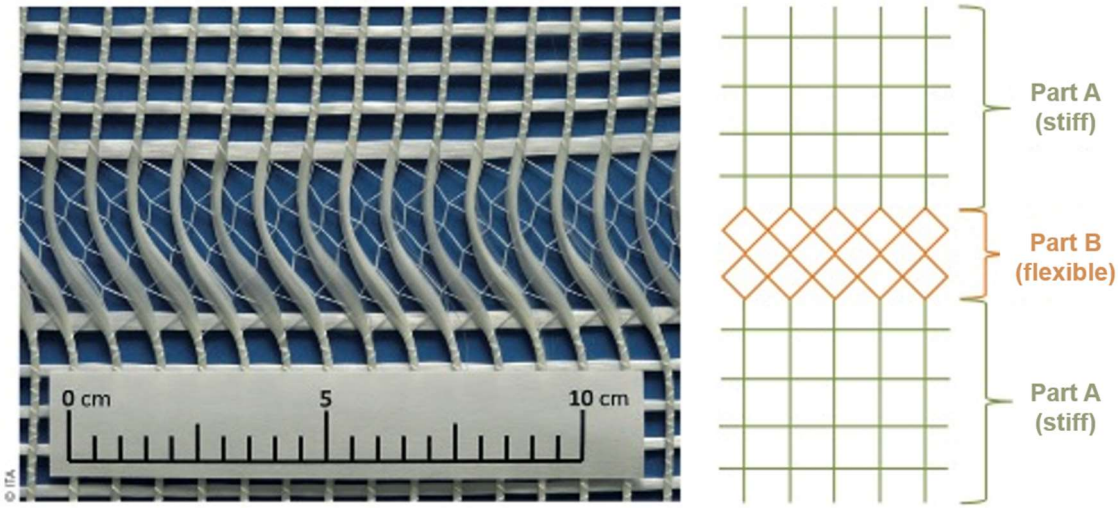

Figure 2-20: Textile reinforcement mesh with locally adjusted stiffness cf. [Pid16]

Later in the project, a new folding tool was developed that was adapted to the application case of façade elements. 25 TRC elements were produced with varying geometries for a prototype wall (Figure 2-21). [Pid16]

[1] Green strength is the property of fresh concrete to be sufficiently stable that it does not change its geometric shape without formwork.

Figure 2-21: Prototype wall made from 25 folded TRC elements [Pid16]

2.2.2 Testing of folded structures

Besides the three-dimensionally shaped prototypes, small scale experiments were conducted in [Woe17] to assess the load-bearing capacity. In this study a foldable formwork defined by a central mountain fold was created (Figure 2-22). Both ends of the formwork were furthermore folded up for a better anchorage of the textile reinforcement. For the specimens two different types of textile reinforcement were used – ar-glass and carbon. [Woe17]

The bending test performed on the specimens was similar to a four-point bending test. The set-up can be seen in Figure 2-23. The valley folds were placed on a horizontally displaceable bearing. Furthermore, elastomer strips were placed between the bearing and the specimen to compensate for imperfections. The load was then introduced in two points with a twistable traverse to avoid stress concentrations. Thus, the mountain fold was only exposed to bending moments. Since the cross-section was very thin, the moment of first cracking was defined as failure of the specimens. [Woe17]

Figure 2-22: Formwork of specimen in folded configuration [Woe17]

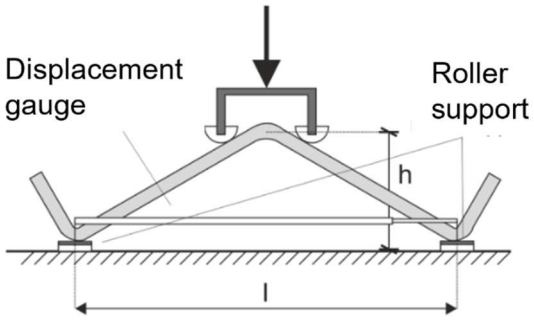

Figure 2-23: Experimental set-up for determining bending resistance cf. [Woe17]

2.2.3 Fold-and-grout

The second approach for creating thin-walled folded plate structures is the fold-and-grout principle. With the development of TRC, the folding of concrete structures was made possible in the first place. Since the textiles used in TRC are very flexible, they can be folded

easily and thus, they can be used as line joints between stiff concrete plates (Figure 2-24). Therefore, recess elements that follow the desired crease pattern are placed in the formwork below and above the textile reinforcement, before pouring the concrete. After the concrete has cured the recess elements are removed (Figure 2-25) and the plate can be folded along the edge creating a line joint. After bringing the panel into the desired shape, the edge is grouted with mortar, which fixes the folding plate in place. [Woe14, Woe13]

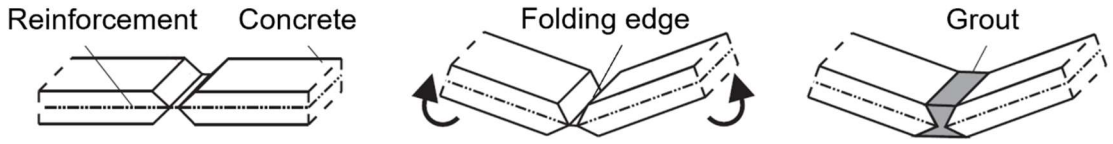

Figure 2-24: Basic fold-and-grout principle for thin concrete plates cf. [Woe13]

WOERD ET AL. proved the functionality of the fold-and-grout method by building several shell structures e. g. [Woe14, Woe13]. In [Woe14] they described an example of the use of their so-called Oricrete, which is a combination of the Japanese word “Origrami”[1] and the word “concrete”, and describes filigree folded concrete structures (Figure 2-26). In combination with high-performance concrete Oricrete provides an approach to realize lightweight structural elements according to the form-follows-force principle (chapter 3.1). By parameterization and modularization, the folded elements could be produced economically and with high variability. Before building those structures, a specific form finding analysis had to be carried out, since only for very simple cases the shape is obvious. Furthermore, a lifting and folding machine had to be developed. For these reasons, WOERD ET AL. developed a simulation platform which helped finding a suitable shape, modeled the manufacturing process, and simulated the load-bearing behavior. [Woe14]

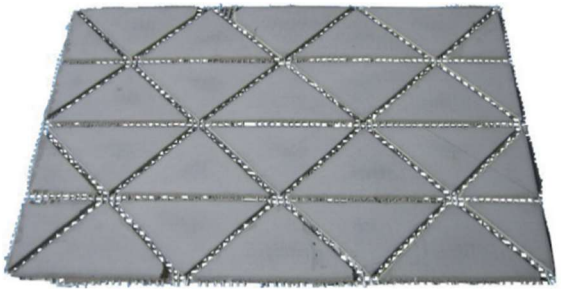

Figure 2-25: Oricrete-plate with Yoshimura crease pattern [Woe13]

Figure 2-26: Finished folded structure of a single curved shell segment [Woe13]

To showcase a lightweight and filigree folding structure, WOERD ET AL. realized a folded dome in small scale. The so-called Oridome is a versatile usable folded structure. Since the folding refers not only to the final shape of the structure but also to the manufacturing process, it is truly a folding structure made from TRC. The structure of the Oridome serves as a building envelope and load-bearing structure simultaneously. Due to its shape a very favorable load transfer can be achieved mainly by means of membrane forces. The dome was made from 20 similar Segments (rectangular YOSHIMURA crease pattern) casted in a reusable formwork. Thanks to the folding concept the free-formed, three-dimensional folding structure could be manufactured economically, although the geometry was relatively

[1] Generally, Origami designates the art of folding paper (from Japanese: “ori” – folding; “gami” – paper). It is a collective term for various types of folding. [Woe14, Woe18b.]

complex. The final structure had a diameter of 120 cm and a height of 40 cm (Figure 2-27). [Woe14]

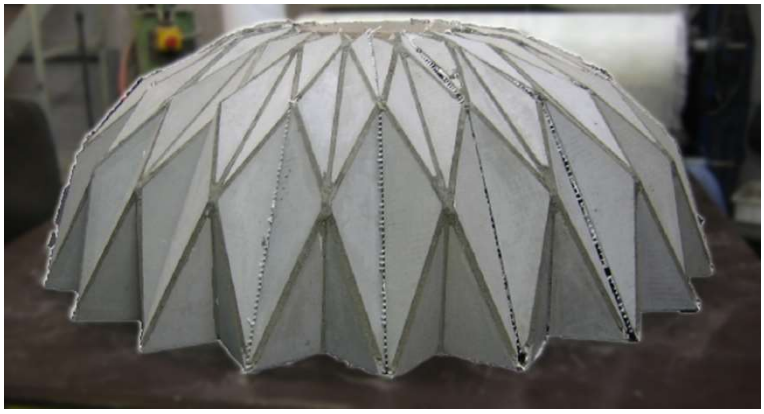

Figure 2-27: Oridome made from 20 segments in model scale [Woe18a]

2.2.4 Comparison of fold-in-fresh and fold-and-grout

In [Woe17] the authors state, that no method is clearly superior to the other. Either method has specific qualities and thus its own application purposes. Small and detailed patterns could be realized by the fold-in-fresh method. The folding of the formwork has a high precision and furthermore, since the elements have no grouted folding edges, they have very high-quality surfaces. On the other hand, the crease patterns created with the fold-and-grout method will not provide perfect hinge lines. However, this method allows very steep inclination angles of 90° and lower, while this angle is limited in the fold-in-fresh method due to slipping of the concrete. [Woe18b, Woe17]

Another aspect is the production time. While new crease patterns made with the fold-and-grout method can be created very fast, producing identical segments is very time consuming, since the production steps must be redone. Fold-in-fresh provides less flexibility, since the production of the formwork requires much more effort but once the formwork is built, identical segments can be cast very fast. These identical elements could be made in precast plants and then be stacked and transported. Yet, unfolded elements might have an advantage in storage and transportation. A combination of the fold-and-grout and fold-in-fresh method promises further expansion of the design and manufacturing of folded elements. [Woe17]

WOERD outlines a concept where both approaches could be combined and thus a very steeply sloped element with a fine surface could be produced. Therefore, the crease pattern must be divided in folding edges that are folded in the fresh state and folding edges that are fold-and-grouted after curing. Thus, some parts of the element are produced in fold-in-fresh method and some parts in fold-and-grout method using the advantages of both principles. [Woe18b]

2.3 Extrusion

Extrusion is a process in which solid to viscous materials are continuously pressed through a mouthpiece under high pressure and if necessary, temperature. It is a widely used industrial process e. g. in clay, food, plastic, or aluminum industry (chapter 2.3.1). However, extrusion is often referred to by the term “additive manufacturing” (AM), which in a non-technical context is often used as a synonym for 3D printing. Certainly, additive

manufacturing is a collective term for many manufacturing processes in which three-dimensional objects are produced by applying material layer by layer. Yet, it can be based on extrusion – so-called material extrusion and is defined in ISO / ASTM 52900 [ISO15]. In the construction industry extrusion based additive manufacturing is used to produce objects like in-situ walls for buildings by the computer-controlled placement of extruded cement-based mortar, which is pumped through a nozzle often mounted to a robotic arm [Bus18]. The figure below shows an example of this process. An overview of current progress on this field can be found in e. g. [Bus18, Moh21, Nem17, Val19].

Figure 2-28: 3D-printed in-situ concrete wall by Apis Cor [Api19]

However, this master's thesis does not investigate the computer-controlled production of 3D objects, but the linear and continuous production of TRC using a stationary extruder. Here two general methods can be distinguished: the ram extrusion and the auger or screw extrusion. Ram extrusion is not a common way to process materials on an industrial scale since it is not a continuous process. However, it can be used on a laboratory scale to examine the extrusion flow or rheological behavior of various materials [Zho05]. Auger extrusion on the other hand, is a common extrusion technique. The material is continuously fed into a feeding vessel and an auger is then used to convey the material towards the mouthpiece (Figure 2-29). With an appropriate feeding system, it becomes a highly productive manufacturing method on an industrial scale which can still be used on laboratory scale for mixture optimization and testing material on its extrudability. [Per18]

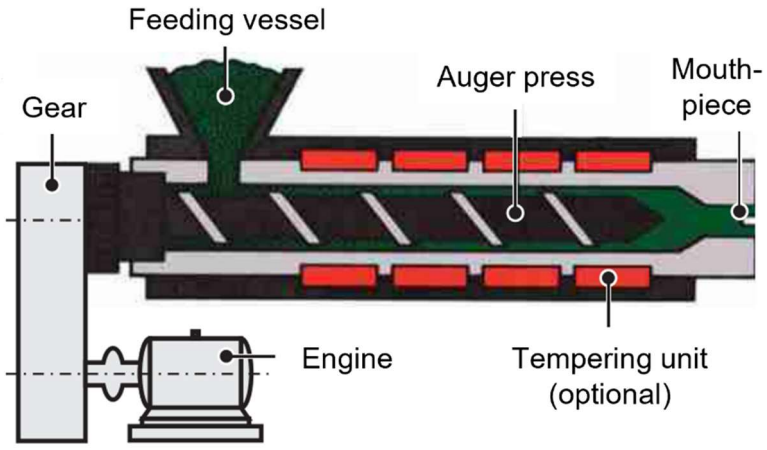

Figure 2-29: Structure of an anger extruder cf. [Rau19]

The inner surface of an auger extruder is designed with longitudinal grooves to direct the flow of the material along the auger and towards the mouthpiece. Furthermore, a vacuum de-airing system is often added to reduce air entrapped within the mixture and thus, increase density and durability of the extrudate. [Per18]

Within this master's thesis the extrusion of textile reinforced cement-bound concrete will be explained and discussed. A general overview of extrusion as an industrial process and its development will be given in the following chapter.

2.3.1 Extrusion – an overview

The continuous manufacturing process of extrusion is not a new process and has been used for metal products since the end of the 18th century. Early state extrusion started with liquid lead which can be formed at 80°C with relatively low force. This explains why it was the only important material used for extrusion until the end of the 19th century. Lead pipes for water supply could be produced from solid billets through a multipart bridge die. Furthermore, with the electrification a new market for lead evolved as a cable sheathing material. A process where the lead could be extruded directly onto the cable core, was built by BORRELL 1879 and improved by WERNER VON SIEMENS. [Bau06]

Later on, ALEXANDER DICK the so-called "father of extrusion" succeeded in developing the extrusion of metals with higher melting points than lead, e. g. 1894 he developed a brass extrusion press. With the start of the 20th century extrusion completely replaced previous standard processes for the production of bars, sections, and wires in copper alloys and 1914 even steel sections could be extruded. With the introduction of electric heating, instead of the previously used coal or gas heating, aluminum could be processed. Breakthrough in its extrusion came with the construction of airships and aircrafts. [Bau06] A timeline of the development of extrudable materials can be seen in the figure below.

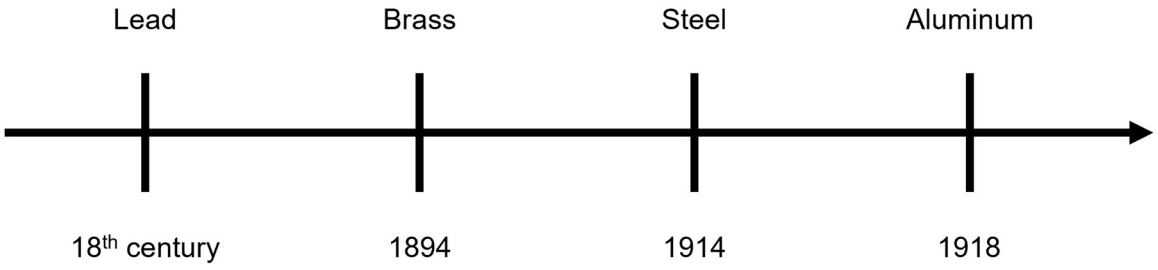

Figure 2-30: Development of extrudable materials over time

Nowadays generative manufacturing by extrusion is a well-established industrial process which is widely used in different fields e. g. plastic, metal, and clay industries (Figure 2-31 and Figure 2-32). Since the process of manufacturing is continuous, high production rates for different types of cross-sections and materials can be achieved. [Alf05]

Figure 2-31: Brick production from endless extruded string [Zie21]

Figure 2-32: Strut profile made from extruded Aluminum [Bos16]

2.3.2 Extrusion of cement-based materials

In the past extrusion was used to produce asbestos-cement products such as pipes and sheets but mostly it was used for wall panels with simple cross-sections. However, since the potential of extrusion technology is very high (continuous and thus very effective process that fulfills the new market needs, such as sustainability, low environmental impact, recyclability, and low cost) new applications have been developed. Non-traditional concrete markets, where the cement-based materials are used as a substitute to plastics and metals, can be conquered. [Alf05]

Already in 1998 a group of researchers from Northwestern University in Illinois published a paper in which they describe how they tested different mixtures for the production of extruded fiber reinforced pipes (Figure 2-33) [Ald98]. Further tests with similar aims were made e.g. [Sta99], where a material developed by the University of Michigan so-called Engineered Cementitious Composite (ECC) was used and slightly modified to extrude pipes.

Figure 2-33: Extrusion of FRC pipes onto Teflon tubes [Ald98]

The conventional use of extrusion of cement-bound materials might be considered as a marginal market since it is used for specific applications in the precast industry [Per18]. However, pipes made from ECC [Ald98, Sta99], plates and wall panels from cement-bound materials [Hän19, Zho15], and fiberboards [Sha01] are just some examples that prove what can be made by extrusion of cement-bound concretes. Furthermore, the company Händle

for example uses the extrusion technology to produce fiber reinforced cement-bound concrete components such as panels, plates, claddings, and formwork elements (Figure 2-34 and Figure 2-35). Advantages are the economic production technology which allows the manufacturing of various products, and ecological aspects since waste material can be used. [Hän19]

Figure 2-34: Industrial-scale extruder for fiber reinforced cement-bound material by Händle GmbH [Hän19]

Figure 2-35: Extruded fiber reinforced cement-bound element [Hän19]

2.3.3 Rheology of cement-based materials used for extrusion

Due to its quite infrequent use the process of extruding cement-bound materials has not been studied intensively. The theoretical knowledge is therefore based on the extrusion of ceramics [Ben93]. Both materials behave in a visco-plastic[1] manner and show non-Newtonian[2] behavior in respect to yield-stress. But besides these similarities both have critical differences mainly caused by the size and shape of their particles. Cement-based materials tend to be more sensitive to water drainage unlike the platelet-shaped clay particles. [Per18] Thus, special attention must be paid to the flow characteristics and rheological properties of the concrete mixture.

Short fiber reinforced concrete mixtures suitable for extrusion are different from usual cement pastes, mortars, and suspensions which have a greater water-cement ratio and better fluidity. Compared to them, extrudable mixtures are viscous pastes with almost no fluidity and high cohesion. [Zho05] The material should be soft enough to flow through the mouthpiece of the extruder, whilst simultaneously being stiff enough to maintain its shape (so-called green strength). [Alf05]

[1] Visco-plastic materials show non-reversible as well as rate-dependent behavior [Ste21].
[2] Non-Newtonian fluids do not follow Newton's law of viscosity i. e. they do exhibit constant viscosity independent of stress.

Generally, the extrudability of a cement-bound concrete is given if three conditions are fulfilled [Per18]:

- The load capacity of the extruder is sufficient.
- The material remains homogeneous during extrusion.
- The extrudate maintains its shape under the load of gravity.

The basic properties which need to be achieved with the mix design are [Alf05]:

- dispersion of the components
- plasticity, cohesion, and particle lubrication
- suitable strength of extruded products
- easy manipulation of extruded products (cutting, curing)

A lack of plasticity, cohesion, or particle lubrication can lead to defects in the extruded products. To avoid these defects, some reference compositions must be determined at a laboratory level before it is possible to scale up the process on an industrial level and optimization of the technology can be achieved. Furthermore, correlations between the rheological behavior of the mixtures and the structural stability of the extruded product can be derived. [Alf05]

2.3.4 Extrusion of fiber reinforced concrete

In [Bra15] initial experiences with the production of FRC and TRC via extrusion are shown. A special equipped laboratory extruder for optimizing mixture designs and mixing processes was used (Figure 2-36). It consists of a pre-worm gear and a main worm gear which transport the concrete to the nozzle. During extrusion various parameters can be measured such as velocity of extrusion, air temperature, vacuum if applied, press power, motor current, and revolution speed of the main worm gear and pre-worm gear. [Bra15]

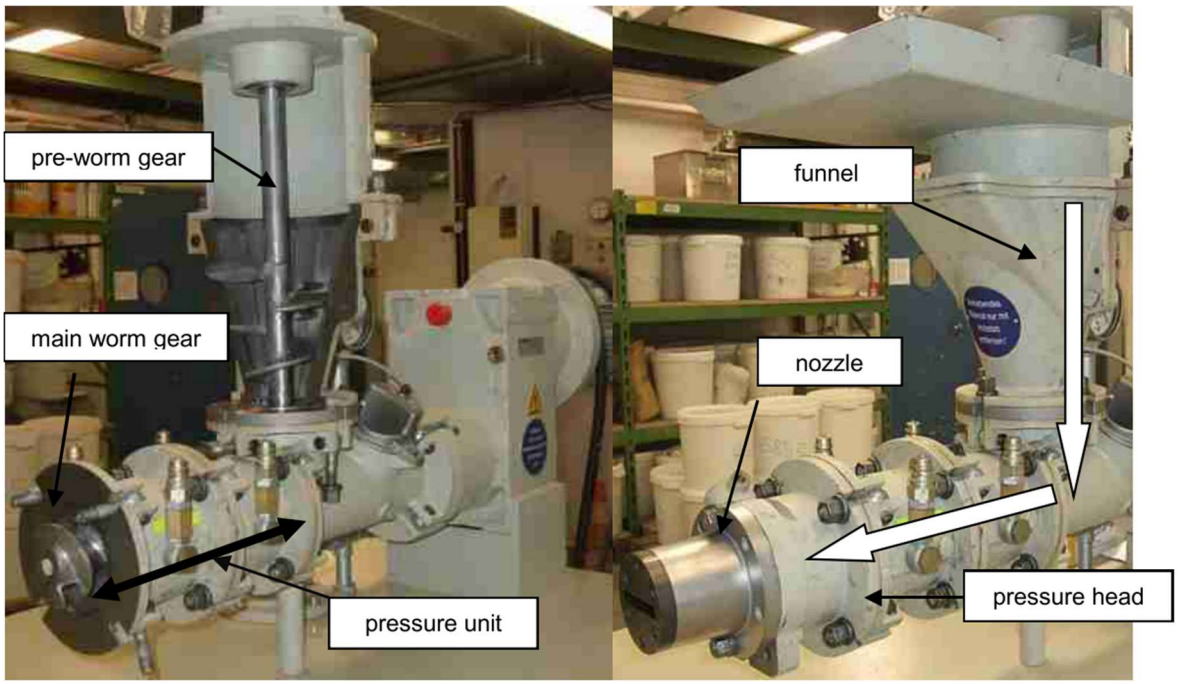

Figure 2-36: Laboratory extruder used in [Bra15]

In order to produce extruded FRC or TRC elements, a suitable concrete mixture and a mixing process had to be found first. Two basic mixtures have been designed and were used in the first steps in [Bra15]. However, they did not lead to suitable mixtures for extrusion (Figure 2-37).

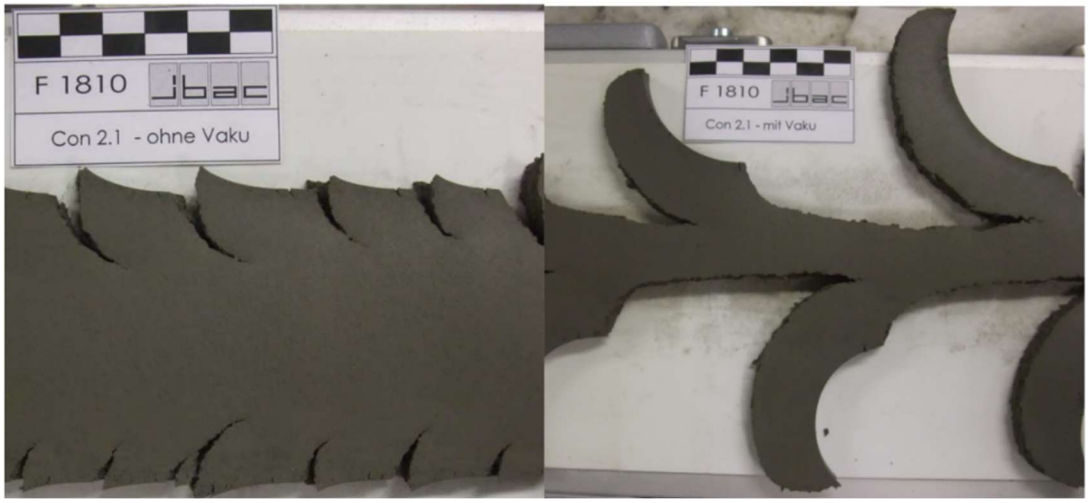

Figure 2-37: Results of extrusion with unsuitable concrete mixtures – Left: no vacuum applied Right: vacuum applied [Bra15]

In [Kra15] a suitable concrete mixture was found (Table 2-3). The mixture developed was similar to the one in [Bra15] but since the extrudability is very sensitive to minor changes it led to a extrudable concrete mixture.

Table 2-3: Extrudable concrete mixture used in [Kra15]

Component	Unit	Amount
Cement	kg/m³	700
Quarzitic aggregate 0 … 0.6 mm		987
Fly ash		210
Silica fume		70
Water		256
Methyl cellulose		7
PVA fibers (6 mm)		5

As indicated in the table, the mixture has a high binder content and consequently a small amount of water. Mixtures like these can be difficult, or sometimes impossible to process, and thus additives such as superplasticizers are required for processing. Superplasticizers may facilitate the extrusion process, but the extruded concrete loses its green strength. Thus, the mixture contains the extrusion aid methyl cellulose (MC). In placed in contact with water, MC forms a gel-like substance which surrounds the solid particles and embeds dispersed air. The embedded air improves the processability due to its lower resistance to deformation, while the gel ensures that the extrudate remains its shape. However, to fully

develop the effect of the MC a high mixing intensity is required, which would result in very long mixing times using conventional mixing techniques. Therefore, instead of mixing and dispersing, a high-speed intensive mixer was chosen to prepare the concrete mix. The intensive mixer by the company Gustav Eirich has variable revolution speed and the possibility of measuring various parameters of the mixing process (revolution speed, torque, and current uptake). The automated control system of the intensive mixer allows the mixing vessel and the mixing tool to be controlled separately, enabling optimum homogenization of the mixture in a short mixing time [Rau19]. For the mixing procedure two different regimes have been tested: with a constant revolution speed of 500 revolutions per minute (rpm) and with a revolution speed of 500 rpm for the first 90 seconds (dry mixing) followed by 800 rpm mixing after a short interruption for adding water. The measured revolution speed, torque, and current uptake can indirectly be used as a flow indicator of the concrete. Due to the high viscosity of the concretes used for extrusion no direct methods for measuring the consistency and flow limits exist. An increase in torque is accompanied by a decrease in viscosity of the concrete and a constant revolution means that the dispersion is finished. [Bra15]

The mouthpieces

The central element of the extrusion process is the mouthpiece. The extruder mass is pressed through it into the desired shape by an all-round rejuvenation of the cross-section under nearly constant volume flow. Simple cross-sections, were used for the development and characterization of the fine-grained concrete (Figure 2-38). Here, the square cross-section allows the production of test specimens according to DIN EN 196-1 [DIN16] (Prisms of 40 mm x 40 mm) on which compressive and flexural strength as well as shrinkage can be measured. Furthermore, the quality of the extrudates in terms of sharpness could be analyzed and the additive dosing could take place. [Kra15]

Figure 2-38: Mouthpieces for circular and square cross-sections [Kra15]

Initially, elements with two-dimensional shapes should be extruded. Therefore, two mouthpieces of 60 mm x 10 mm and 60 mm x 6 mm were produced. The lower the ratio of the cross-section height to width, the more attention had to be given to the transportation of the extrudate after leaving the mouthpiece. Therefore, a conveyor belt was used which was driven by the exit velocity of the extrudate. However, the friction between extruded element and conveyor belt created a velocity gradient within the extrudate, slowing down the lower

part of it while transporting the upper part at a nearly constant rate. This problem could be controlled by transporting the material on the conveyor belt with as little friction as possible, which in the present article was achieved by using a thin foil between conveyor belt and extrudate. [Kra15]

If all problems mentioned above are mastered, elements of arbitrary length with high compressive strength (more than 70 N/mm² after 28-days) could be produced. Furthermore, those elements featured high load-bearing reserves in terms of tensile and flexural strength through the combination of short fibers and textile reinforcement. [Kra15]

Different types and amounts of microfibers

The extrudability of the above mentioned concrete mixture when adding different types and amounts of microfibers was investigated in [Jan19]. JANISSEN ET AL. used three different mouthpieces resulting in extruded concrete with cross-sections of dimensions 40 mm x 40 mm, 60 mm x 10 mm, and 60 mm x 6 mm. Since there was no standardized test procedure for assessing the extrudability, a concrete mixture was classified as extrudable if a 60 mm x 10 mm test specimen could be extruded without visible surface damage i. e. cracks or strand widening. Adversely, when surface damage occurred, the extruder clogged, the maximum possible press pressure was reached, or no vacuum could be applied the mixtures were classified as non-extrudable. PVA fibers of 6 mm and 8 mm length as well as aramid fibers of 6 mm length were used. Preliminary tests showed that fibers made from carbon did not withstand the intensive mixing process and therefore were not suitable for extrusion. Microscopic investigations with 40 times magnification showed that only fragments of the fibers were left. Furthermore, 6 mm long aramid fibers did not lead to an extrudable mixture and only PVA fibers were used for further investigations. [Jan19]

As preliminary tests showed the extrudability can greatly be improved by adding the extrusion aid MC. For the investigations of the extrudability of the concrete mixtures, the amount of cement, fly ash, silica fume, and water was kept constant while the amount of MC, fibers, and aggregate was adapted. In the first step, MC with an amount of 1.5 mass-% (percent of mass) of the cement and 2.0 vol.-% (percent of volume) of PVA fibers of 8 mm length were added. However, the produced extrudate had an inconsistent surface topology and it was not possible to apply a vacuum. A reduction of the MC content while keeping the amount of fibers constant led to a smoother surface, however, strand widening occurred and the mixture became as non-extrudable. Even the step-wise reduction of the amount of fibers to 0.5 vol.-% and an increase of the binder content by 5 % and 10 %, respectively, did not produce extrudable mixtures. These factors lead to the conclusion that the PVA fibers of 8 mm length were not suitable for extrusion. [Jan19]

In the next step, PVA fibers of 6 mm length were used. First, the fiber content was set to 0.5 vol.-% and the MC content was set to 1.0 m.-%. Furthermore, 0.2 mass-% of the cement of a superplasticizer based on PCE were added in order to compensate for the increased water demand caused by the fibers. The resulting mixture was extrudable without any defects for the 60 mm x 10 mm and the 40 mm x 40 mm cross-section (Figure 2-39), and an equal distribution of the fibers within the matrix and fiber alignment along the extrusion axis was observed. [Jan19]

Investigations on aramid fibers of 6 mm length did not lead to extrudable concrete mixtures. The fiber content was set to 0.5 vol.-% and the MC content was set to 1.0 m.-%. Since the aramid fibers significantly increased the water demand according to manufacturer specifications (approx. 7 mass-%), the water content was increased by 5 mass-%. However, the mixture could not be extruded under maximum press pressure since it was already stiffened. Based on the findings mentioned above solely PVA fibers of 6 mm length were considered for further investigations. [Jan19]

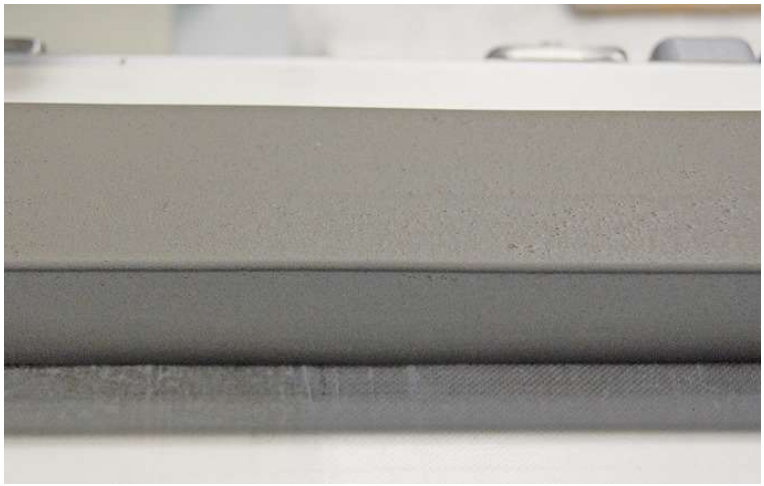

Figure 2-39: Flawless extruded specimen 0.5 vol-% of 6 mm PVA fibers and 1.0 mass-% of MC [Jan19]

Vacuum pump

Furthermore, the investigations carried out in [Jan19] showed that the bulk density of extruded prisms under vacuum could significantly be increased (Figure 2-40). Due to the resulting lower porosity of the concrete, the compressive strength could be significantly increased – in numbers: an increase of 25 – 45 % in compressive strength could be achieved. However, the flexural strength did not increase. This was probably based on imperfections within the microstructure, which could not be reduced even by the improved deaeration.

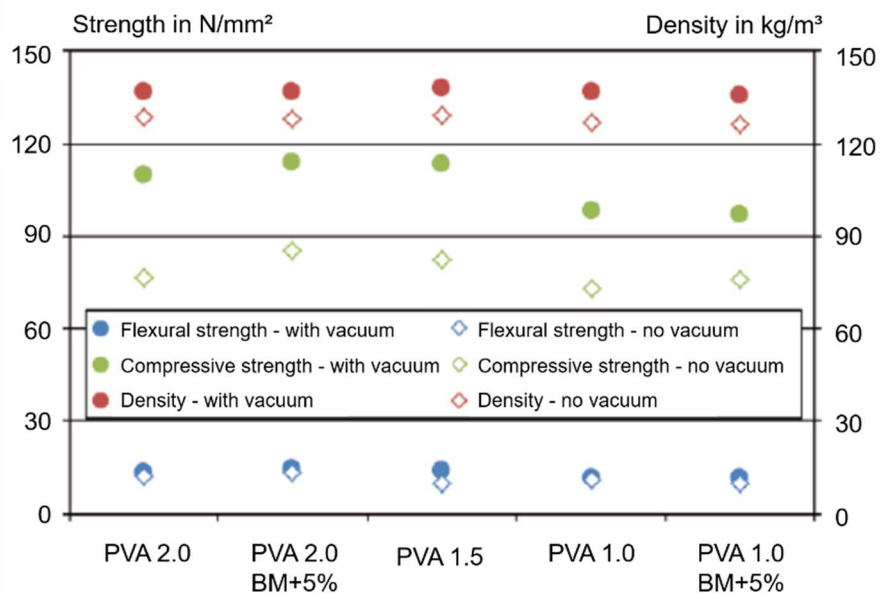

Figure 2-40: Bulk density and strength of extruded prisms with PVA fibers of 8 mm length cf. [Jan19]

2.3.5 Fiber alignment during extrusion

For FRCs a beneficial effect occurs during extrusion: a large portion of the fibers get aligned along the direction of extrusion. Research carried out in [Lan92] approved this hypothesis for extruded short fiber reinforced glass. Their investigations at the Technical University of Kaiserslautern showed that in the transformation zone of the extruder, the desired orientation of the short fibers parallel to the extrusion direction took place. In this way, unidirectionally reinforced glass composites with fiber volumes of up to 30 % could be produced. Theoretical and experimental tests on the alignment of the short fibers were carried out. First, with the help of simple model assumptions, it was calculated that decent alignment of the short fibers parallel to the extrusion direction could be achieved. Since these model assumptions were based on many simplifications a supplementary Finite Element Analysis of the fiber movement was subsequently carried out. This analysis allowed much more detailed investigations and confirmed that a parallel orientation of a portion of the short fibers into the matrix material could be achieved with the help of the extrusion process. At last, experimental investigations were carried out where extruded products were cut, and fiber surfaces were examined with the aid of an image analysis system. The analysis showed that the fibers were mostly oriented along the direction of extrusion (Figure 2-41). The distribution of angular deviations from a fiber running exactly 0° parallel to the direction of extrusion resembled a steep bell curve. It was found that at least 71 % of the fibers were within a range of $\pm 10°$. Thus, extrusion proved to be a suitable manufacturing process for the production of nearly unidirectional short-fiber reinforced composites. [Lan92]

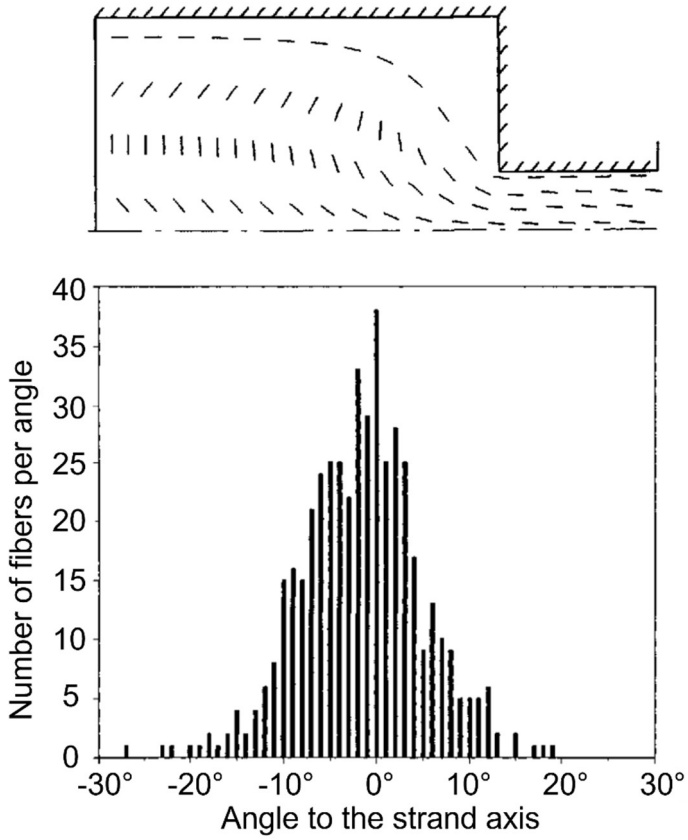

Figure 2-41: Analysis of fiber movement during extrusion – top: computationally simulated movement bottom: measured distribution of fiber angles ref. [Lan92]

The combination of short fibers and textile reinforcement seems useful for various applications. The orientation of fibers in the direction of extrusion often impairs the embedding of the textile in the concrete matrix, especially when the length of the short fibers is greater or equal to the mesh widths of the textile reinforcement. [Kra15]

2.3.6 Extrusion of textile reinforced concrete

TRC can be produced using different methods such as casting, spinning, spraying, and laminating (chapter 2.1.7). As these methods are designed for the production of prototypes instead of production at scale e. g. [Cur07, Heg08], the labor intensive processes drive up the cost of producing this material [Bra15]. However, thin TRC elements might be produced more economically in a continuous process such as extrusion (Figure 2-42). The potential load-bearing capacity of TRC can be utilized especially in three-dimensional cross-sections similar to steel sections. The production of three-dimensional members, however, is relatively complex. Extrusion seems highly suitable for this since the extruded concrete products exhibit high quality in terms of sharpness and accuracy [Mot12]. Furthermore, continuous production has the advantage over single piece production in that the formwork effort is not connected to the number of pieces produced. However, for the extrusion of TRC two main issues occur that require attention: First, the fresh concrete properties must meet the requirements of the extrusion process. Second, a system needs to be developed that guides the textile into the concrete without disturbing the inner structure of the concrete or the structure of the textile. [Bra15, Mot12]

Figure 2-42: Extrusion with feeding device for fabrics [Bra15]

The textile feeding system

The same extruder as mentioned in chapter 2.3.4 has been modified so that textile reinforcement could be guided from outside into the flow of the concrete matrix. Since the textile reinforcement should be in a statically optimized position, an extension was made to the pressure head with a textile guiding channel (Figure 2-42) fully covering the textile reinforcement in fine-grained concrete. The narrowing cross-section at the end of the mouthpiece pressed the concrete into the meshes of the textile, which was then pushed through the mouthpiece by friction between it and the concrete. The guiding channel, however, interrupted the homogeneous matrix flow so that a cavity was formed behind it. As a result, the laminar flow was interrupted and the velocity distribution in the mouthpiece

became uneven. Consequently, the concrete flow through the meshes of the textile was too slow and generated unsuitable results (Figure 2-43). [Bra15, Kra15]

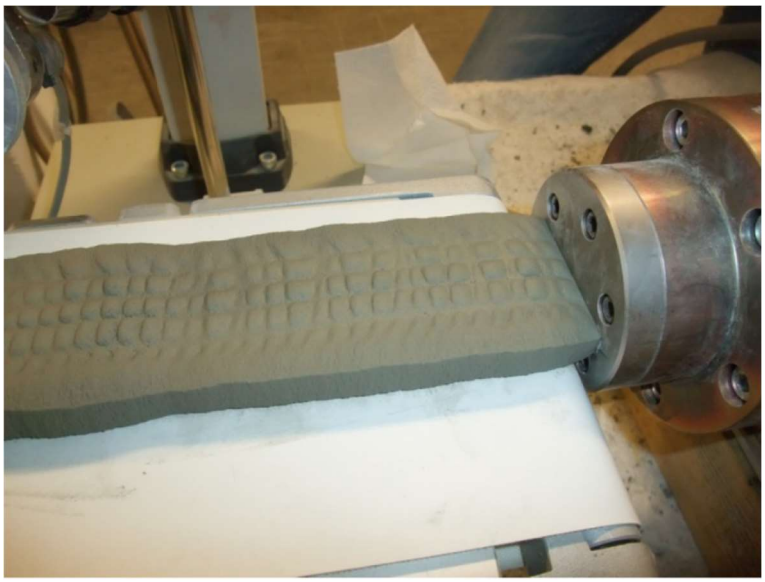

Figure 2-43: Unadjusted concrete flow leading to unsuitable extrusion results [Bra15]

To achieve good bonding properties, the matrix must be pressed against the textile from all sides at the same speed. In order to regulate the matrix velocity, narrowing elements in form of screw bolts with adjustable penetration depth were attached to the mouthpiece (Figure 2-44). Thus, an equally large flow cross-section above and below the textile could be achieved. [Jan19]

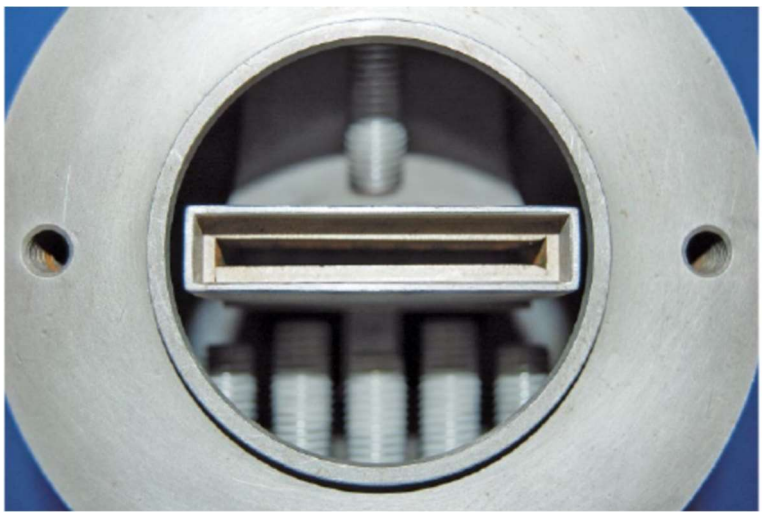

Figure 2-44: Adjustable screw bolts to regulate the concrete flow [Jan19]

However, even after this change to the mouthpiece an uneven surface was observed on the extruded products and furthermore, the textile reinforcement was visible. The reason for the unequal velocity below and above the textile were identified as the friction between the extruded concrete and the conveyor belt, which was solely driven by the velocity of the extruded concrete. To reduce this effect, a plastic foil was placed between concrete and conveyor belt. However, a slight waviness remained. [Jan19]

Textile reinforcements

Besides the feeding system, another issue which had to be addressed was the choice of suitable textiles. In tests carried out in [Jan19] two different types of textiles were used as a reinforcement for the extruded concrete: one made from uncoated ar-glass (Figure 2-45) and the other one made from coated carbon (Figure 2-46). Due to their pliability, both were generally suitable for being fed into the concrete during extrusion which happened under an angle of approximately 75-90°. After extrusion tensile tests were carried out on 60 mm x 6 mm specimens at 2 days of age. [Jan19]

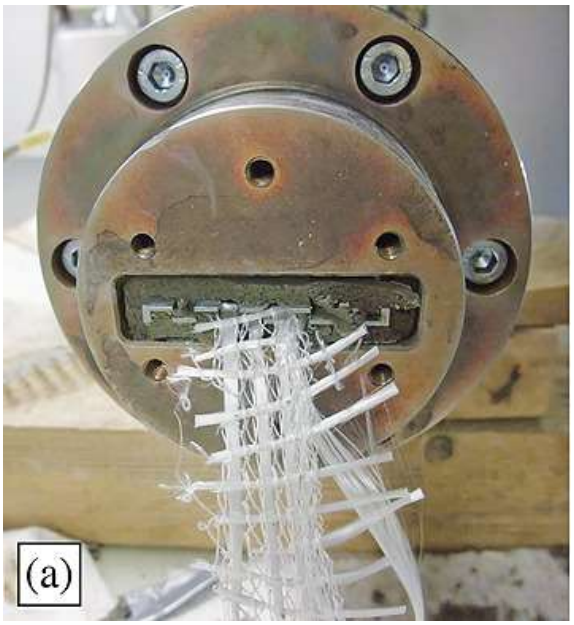

Figure 2-45: Uncoated alkali-resistant glass fabric at the beginning of extrusion [Jan19]

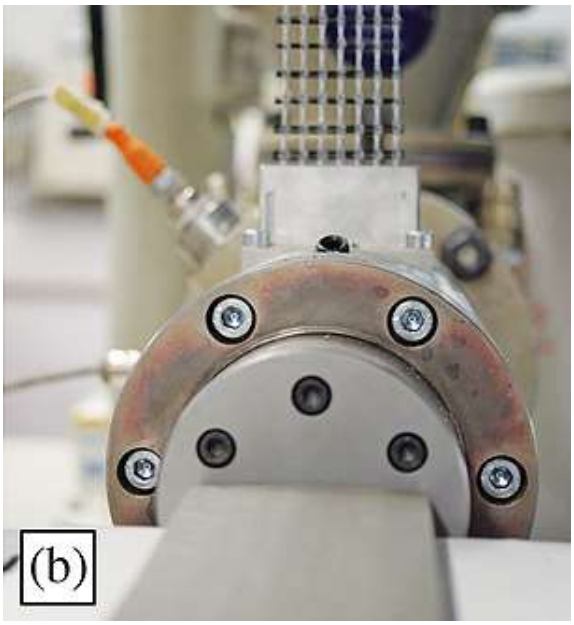

Figure 2-46: Coated carbon fabric during extrusion [Jan19]

However, the flexibility of the textiles used caused similar issues as already mentioned in [Kra15]. During the feeding process the textile was compressed and after leaving the mouthpiece the textile elongated again, leading to corrugated surfaces. In order to address this problem, the mouthpiece was extended so that the resulting compression already reduced within the area of the mouthpiece. However, the ar-glass textile did still not lead to extrudable results. [Jan19]

Tensile tests

After curing, the extruded products from [Bra15] were tested on their tensile strength to evaluate if the extrusion process had an influence on the tensile behavior of the composite. The rapid strength development of the mixture allowed tensile tests to be carried out already 48 hours after production. Extruded concrete specimens with coated carbon textiles and a cross-section of 60 mm x 6 mm were tested and compared to specimens made by lamination. The textiles used were the same in both manufacturing processes but due to the viscosity of the concrete the MC had to be substituted by a superplasticizer in the concrete used for the laminating method. Even though this made a direct comparison difficult since the rheological properties changed, there was no other way to compare the specimens. [Bra15, Jan19]

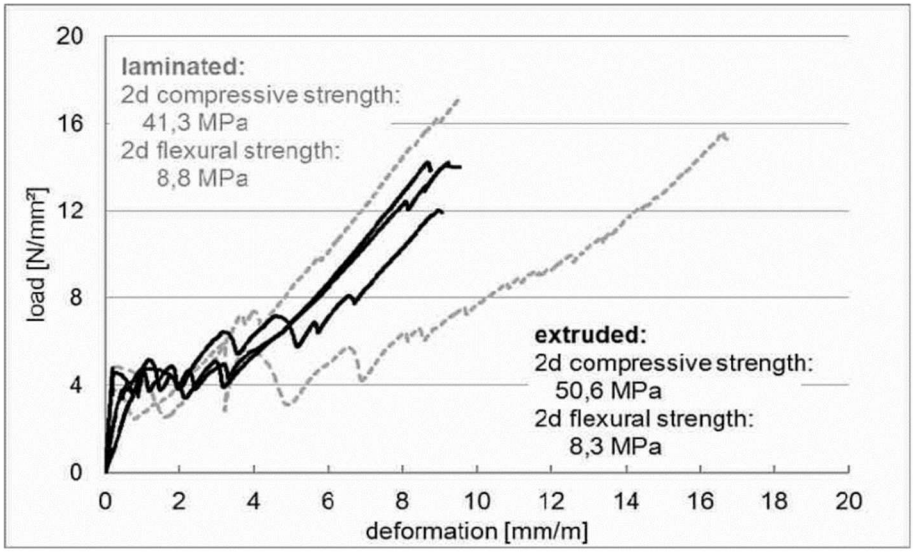

Figure 2-47: Comparison of tensile tests with laminated and extruded TRC [Bra15]

The results show that the load-bearing behavior was comparable between laminated and extruded concrete (Figure 2-47). However, the extruded concrete showed higher strength, but the results tended to scatter further. This was caused by the geometric deviations of the extruded products which are of high importance especially when determining the tensile strength. The higher strength proved the position accuracy of the textile reinforcement in the concrete achieved by the extrusion process. Furthermore, the microfibers aligned along the extrusion axis and thus strengthened the compound zone. [Jan19]

At last, JANISSEN ET AL. recommend further investigations optimizing the geometry of the mouthpiece and thus the composite of textile reinforcement and concrete. Furthermore, the textile feeding system could be tested for more filigree and complex geometries. A mouthpiece in the shape of an H-profile was already produced where the textile could be fed into both flanges.

3 Mathematical and Physical Background

In order to exploit the full potential of the innovative construction material TRC, intelligent design principles for efficient and thus sustainable structures must be found. Therefore, traditional construction principles must be questioned. New idea providers for the lightweight construction with TRC can be found in biology (especially in botany), mathematics, mechanics, and art. The goal of SFB TRR 280 is to find structural shaped in which forces are to be predominantly transferred by normal stresses. [Cur19]

The process of shaping structures according to the forces acting on them undergoes the form-follows-force principle which is originated in nature. In the following chapter this principle will be explained from its origin and early use to the importance for this master's thesis. Special attention will be paid to the shape a free hanging rope or chain solely affected by gravity adopts – the so-called catenary, which is a mathematical function based on the hyperbolic cosine. Derived from this principle, ideal arches and vaults which are aimed to be moment-less are presented in the following chapter.

3.1 Form-follows-force principle

In general, form-finding is a process of shaping structures according to the forces acting on them. In the formation of natural objects such as trees, shells, bones, or soap-films this process can be observed and follows the so-called form-follows-force principle. Structures which are created by form-finding (Figure 3-1 and Figure 3-2) show evidence to be efficient in terms of load transfer, have high durability, and the material used is minimal. The process of form-finding can be carried out by physical and computational modelling. [Lew16b]

Thereby, three basic form-finding techniques can be distinguished, depending on the structure being modelled [Lew16b]:

- Soap-film analogy
- Inflated membrane models
- Inverted hanging models

Soap-films are examples of ideal lightweight tension membranes. They feature a constant surface stress and a minimum surface area. Furthermore, their configuration achieves a minimal potential energy and thus they are stable. In a physical model, loose threads are attached to several posts before being dipped into a soapy solution for form-finding. In a computational model, an initial surface is guessed and iteratively adjusted until constant tension and an equilibrium are achieved. The principle of minimizing the surface area and achieving constant stress is also observed in other natural processes such as in the growth and healing of trees. Nevertheless, using this approach in engineering has been criticized since architectural fabrics are anisotropic, unlike soap-films. However, the principle behind the formation of soap-films in the conceptual design of fabric structures can improve their properties. [Lew16b, Lew17a]

Figure 3-1: Prophet's Mosque in Madinah, Saudi Arabia: convertible umbrellas [Lew17c]

Figure 3-2: Prophet's Mosque in Madinah, Saudi Arabia: Soap-film model [Lew17c]

The swiss engineer HEINZ ISLER (1926-2009) developed numerous shell structures. For finding ideal shapes, he used various methods including inflated latex rubber membranes. The membranes were fixed over a plan resulting in a surface subjected to pure tension. Consequently, when a structure with the same shape is subjected to the opposite loading, resulting stresses are purely compression. ISLER used shapes like this for industrial shells. [Chi10] However, this method is similar to hanging models but with loads acting upwards and normal to the surface. In the following the use of inverted hanging models will be explained in more detail.

3.1.1 Inverted hanging models

The mechanic of a rope already served as a basis for the classic mechanics and the infinitesimal calculus. The physicist ROBERT HOOKE (1635-1702) rediscovered the catenary as statically ideal shape for an arch in the 17th century and encrypted his findings on the relationship between hanging chain and the statics of an arch in a Latin anagram, which translates to "As hangs the flexible line, so but inverted will stand the rigid arch." [Hey98]. Based on this finding the Italian physicist GIOVANNI POLENI (1683-1761) analyzed the structural stability of the Saint Peter's Basilica in Rome, Italy. Therefore, he used a hanging model which considered the variable distribution of the dome mass in form of spheres with different sizes and weights (Figure 3-3). [Tra01]

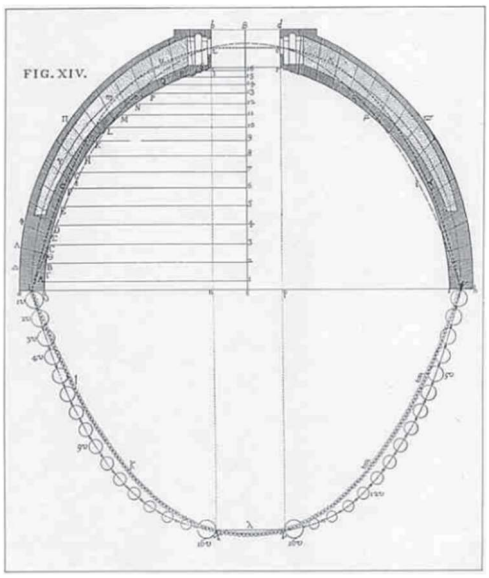

Figure 3-3: Poleni's hanging model with weights attached to check the stability of St. Peter's Basilica [Pol47]

The modified catenary of the composite model was at all points within the dome cross-section, proving that the cupola was stable despite its cracks [Tra01]. Later, the English mathematician DAVID GREGORY (1659-1708) added to HOOKE's statement that the true form of a vault is solely the catenary, yet a vault not having the shape of a catenary can be stable if and only if it includes the catenary within its cross section. [Kur16]

Inverted hanging models were also used for finding ideal vault shapes by ANTONI GAUDÍ (1852-1926) for designing the arches of the Sagrada Família in Barcelona, Spain. At first, he hung a simple cable and calculated the loads that would act on an arch of similar shape by measuring vertical distances (self-weight of the walls above). Then he added the corresponding load of the floor in form of weights which changed the shape of the cable. Afterwards the self-weight needed to be recalculated and the added weights had to be changed accordingly. After this iterative process was done, the cable adopted a shape that was very close to the exact mathematical shape that supports the load. However, the calculation of arches is a two-dimensional problem, whereas a vault is a three-dimensional problem. To master this, vaults were analyzed by slicing them into simple arches and supporting those on cross arches – the so-called cross vault. To show the volume of the model, he then took a photograph of it and drew on it (Figure 3-5) or he placed cloth or paper over the model (Figure 3-4). By using this technique, GAUDÍ integrated the structural design in the process of architectural design and as far as we know, it was the first time that this approach was exploited in its full capacity. [Hue06]

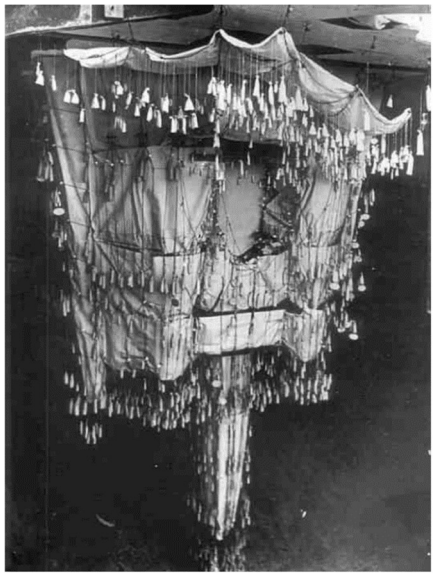

Figure 3-4: Gaudí's hanging model [Mah03]

Figure 3-5: Inverted photograph used for rendering the form by Gaudí [Mah03]

A more recent example of the use of the catenary for an arch is the Gateway Arch in St. Louis, USA (Figure 3-6). The designer EERO SAARINEN (1910-1961) might have been influenced by HOOKE'S statement that the hanging flexible line is the ideal shape for arches. However, the catenary was viewed as the optimal shape for arches of constant cross-section, unlike the Gateway arch which has a varying cross-section. In a later design stage, SAARINEN changed the original catenary shape by eye and came up with a flattened catenary which is described in [Oss10] by OSSERMAN. [Lew17b]

Figure 3-6:The Gateway Arch in St. Louis, USA [Bup07]

A significant difference between the flattened catenary shape of the Gateway Arch and a constant-stress shape (shape of a hanging cable of varied cross section under its self-weight) is that the latter is a moment-less arch and the flattened catenary is not. [Lew17b] BRUCE DETMERS, who worked with SAARINEN on the arch, said that SAARINEN'S choice on the shape of the arch was purely esthetic. Furthermore, many more factors besides the self-weight needed to be considered such as wind, earthquakes, and thermal expansion and contraction. Yet, by choosing the shape of a flattened catenary the designer satisfied the structural needs of greater strength to the bottom and more slenderness near the top. [Oss10]

In general, the form-finding process has great potential to generate efficient structures. However, the main challenge is to answer the question of which acting forces should be considered on the model, since it is not possible to optimize a structure for every load case imaginable. While living structures such as trees can compensate a change in the load conditions by adapting its growth, engineering structures are not capable of doing that. Consequently, the most critical load case combinations needs to be found and considered for form-finding. [Lew16b, Lew17a]

3.2 Mathematics of the catenary

If two ropes are considered of different weight – e. g. one is lightweight made from wool and the other one is heavy weight made from steel – they will hang in exactly the same shape as long as their hanging points are equally distanced, and the ropes have the same length. By changing the distance between the hanging points different shapes of the rope can be observed. Each of these shapes can be described by a mathematical equation which is called catenary. The figure below shows three different catenaries. They all have the same rope length (100 cm) but differently spaced fixing points.

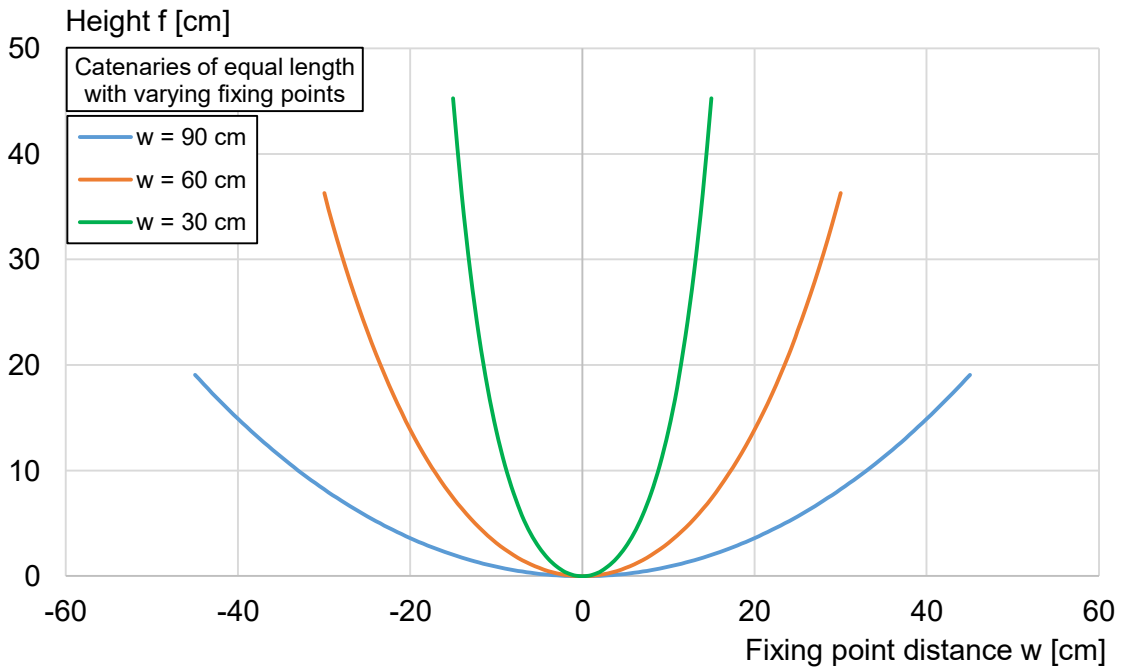

Figure 3-7: Catenaries of equal length with varying fixing points

The catenaries look very similar to parabolas which might explain why GALILEO GALILEI (1564-1642) stated that the catenary corresponds in shape and content to the throwing parabola. Shortly after 1600 he described the flight path of a projectile as a parabola by the superposition of a freefall motion and a straightforward motion, neglecting the air drag. His explanation why the catenary corresponds to the throwing parabola is based on the forces acting on both objects: a projectile is propelled by two forces – a propelling, horizontal force, and a downward force of the weight; a hanging rope or chain is also deformed by two forces – a horizontal, tensile force, and a vertical force due to its weight. Both mechanisms are very similar. [Kur16] Today the mathematical description of the catenary is known. GOTTFRIED WILHELM LEIBNIZ (1646-1716) derived the exact formula of it in 1690 [Haj16]. The equation that describes the curve is based on the hyperbolic cosine and can be written as cf. [Haj16]:

$$f(x) = a * \cosh\left(\frac{x - x_0}{a}\right) + y_0 \tag{3-1}$$

With: a Bending radius at the vertex
x_0 Displacement in x-direction
y_0 Displacement in y-direction

The formula can be derived from the equilibrium of forces acting on the hanging chain or from the potential energy of the system. In the following, the derivation from the equilibrium of forces is shown. The following forces are acting on the system (Figure 3-8): the vertical force $F_V(x)$, the horizontal force $F_H(x)$, and the tensile force $T(x)$ which is the resulting force of $F_V(x)$ and $F_H(x)$. Here the horizontal force of the chain must be constant in every point to achieve equilibrium. If it was not constant, the chain would still move to balance the forces $\Rightarrow F_H(x) = H$. The force $F_V(x)$ results from the product of the length of the chain $s(x)$, the mass per meter μ, and the acceleration due to gravity g. [Haj16] Thus, it follows:

$$F_V(x) = \mu * g * s(x) = \mu * g * \int_0^x \sqrt{1 + y'^2}\, dx \tag{3-2}$$

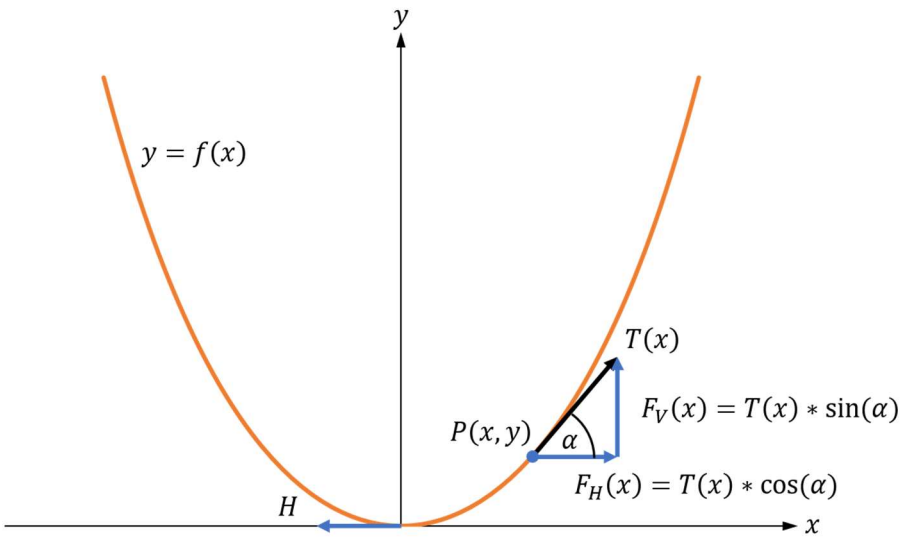

Figure 3-8: Forces acting on a hanging chain

However, the forces can also be written in the following way [Haj16]:

$$F_V(x) = T(x) * \sin(\alpha) \tag{3-3}$$

$$F_H(x) = T(x) * cos(\alpha) \tag{3-4}$$

$$\Rightarrow y' = \tan(\alpha) = \frac{F_V(x)}{F_H(x)} = \frac{\mu * g}{H} * s(x) \tag{3-5}$$

$$\Rightarrow y'' = k * \sqrt{1 + y'^2}, k := \frac{\mu * g}{H} \tag{3-6}$$

Here, (3-6) is the differential equation of the catenary. The solution can be found by substitution and integration [Haj16]:

$$y = \frac{1}{k} * \cosh(kx + C_1) - C_2 + C_3 \tag{3-7}$$

Where C_1, C_2, and C_3 are integration constants. It seems useful to put equation (3-7) in a handier form as it is in equation (3-1).

The result shows that the catenary in fact is not a parabola as assumed by GALILEI. However, a parabola and a catenary can look very similar (Figure 3-11, page 45). Furthermore, under certain circumstances, a hanging chain will rather hang in a parabola-like shape: in case of a big uniformly distributed load q along the span of the chain (e. g. a suspension bridge), the self-weight of the chain is neglectable. Thus, the vertical load on the chain changes and the resulting equation (3-10) gives a parabola [Haj16]:

$$F_V(x) = q * g * x \tag{3-8}$$

$$\Rightarrow y' = \frac{q * g}{H} * x \tag{3-9}$$

$$\Rightarrow y = \frac{q * g}{H} * x^2 + c, c \in \mathbb{R} \tag{3-10}$$

As equation (3-1) shows, the shape of the catenary is solely driven by the parameter a. If the shape of a specific hanging chain shall be determined, only the length of the rope l and the distance between the fixing points w is needed. Knowing those two parameters, the shape of the hanging chain is physically defined, and a can be calculated to define the hanging chain mathematically. However, the calculation of a from given parameters w and l is not very pleasant. The equation to look for needs to satisfy the following condition:

$$l = 2 * s\left(\frac{w}{2}\right) = 2 * \int_0^{w/2} \sqrt{1 + y'^2}\, dx \tag{3-11}$$

$$\text{Using: } y = a * \cosh\left(\frac{w/2}{a}\right)$$

$$\Rightarrow y' = \sinh\left(\frac{w/2}{a}\right)$$

$$\Rightarrow l = 2 * \int_0^{w/2} \sqrt{1 + sinh^2\left(\frac{w/2}{a}\right)}\, dx$$

$$\Leftrightarrow l = 2 * \int_0^{w/2} \sqrt{cosh^2\left(\frac{w/2}{a}\right)}\, dx$$

$$\Leftrightarrow l = 2 * \int_0^{w/2} cosh\left(\frac{w/2}{a}\right) dx$$

$$\Leftrightarrow l = 2 * a * sinh\left(\frac{w/2}{a}\right) \tag{3-12}$$

One can imagine that the mathematical solution of this equation to a is very unpleasant. It is much more convenient to use a solving algorithm which has (3-12) as a boundary condition to find the (nearly) correct value for a. Furthermore, negative values are neglected to receive a unique solution. The software Microsoft Excel allows the usage of an evolutionary algorithm finding the parameter a. The boundary conditions are here satisfied with a precision of 0.000001 (one millionth), which is by far enough for the calculations done within this master's thesis. Thus, the mathematical equation defining the shape is received. The calculated parameter a then gives the radius of the curvature at the vertex (Figure 3-9, right), besides the displacement in y-direction (Figure 3-9, left).

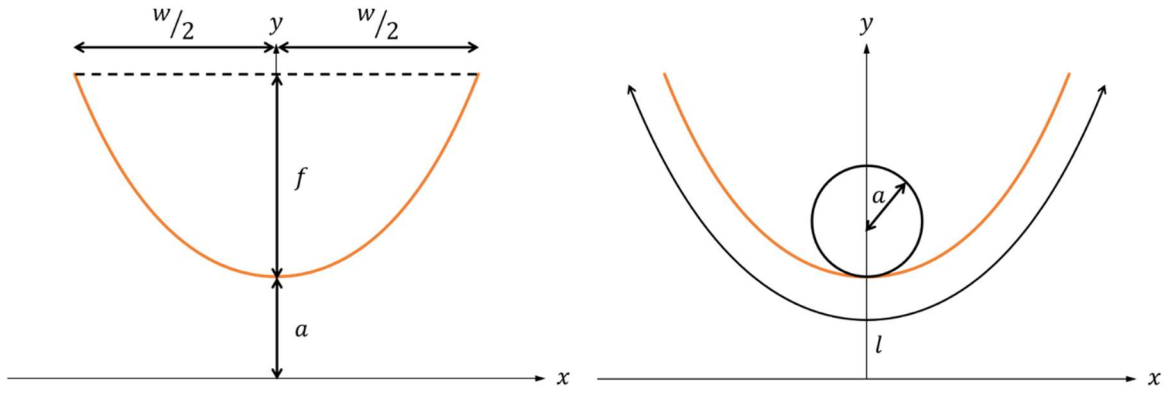

Figure 3-9: Parameters of a catenary

3.3 Ideal vaults and moment-less arches

In general, the structural shape is viewed as an architectural matter, usually resulting in one of three idealized shapes: circular, parabolic, or catenary arches. Under certain load conditions these shapes become moment-less which can be reproduced by a physical experiment. A chain under its self-weight hangs in a catenary shape; a weightless chain under a uniformly distributed load (UDL) along its span forms a parabola, and a weightless chain under a UDL applied perpendicular along its length produces a circular shape. Inverting those shapes will lead to moment-less arches under the given loads. This technique for finding optimal arches was used in the past for the construction of various arches (chapter 3.1.1). For building materials that are weak in tension, such as masonry or concrete, having zero bending moment in the arch is desirable. [Lew16a]

The form-finding process can be used to optimize many types of structures. The following chapter deals with the optimization of arches. In [Lew16a] a mathematical model of a moment-less arch is presented. The model predicts the geometrical shape of rigid, two-pin, moment-less arches of constant cross section made of a material that is weak in tension. It includes the self-weight of the arch as well as a uniformly distributed load per unit span. Two classical moment-less arch shapes, namely the parabola and the catenary, are derived with the model and compared with the calculated geometries. Therefore, a necessary and sufficient condition for pure axial force in the arch is derived. [Lew16a]

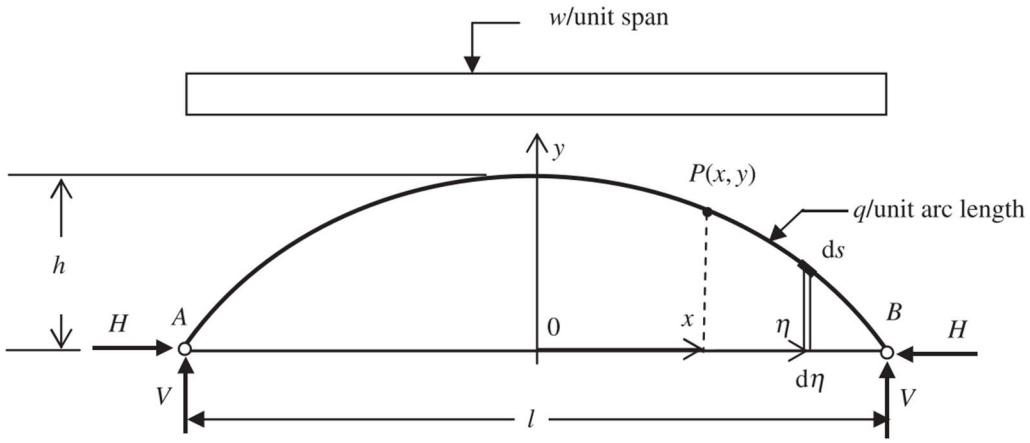

Figure 3-10: Parameters and forces acting on a two-pin arch [Lew16a]

The figure above shows the arch structure considered by LEWIS for the calculation of the mathematical model. The forces to be considered are an external UDL per unit span w and the self-weight of the structure q, taken as a uniformly distributed density per unit arch length. Internal forces to be considered are the axial force T, shear force S, and bending moment M. The reactions at the pin support are the horizontal force H and the vertical force V and the variables h and l represent the height and span of the arch. [Lew16a]

Considering there is only compression in the arch, the shear force needs to be zero at any point of the arch. This leads to a constant moment within the cross section and consequently with zero bending moment in the pins the moment is zero everywhere. Thus, the necessary and sufficient condition for a two-pin arch to be solely under axial force is that the shear force is zero everywhere. Using this condition, LEWIS derived the two known forms of moment-less arches, which are 1) the parabola – where arch self-weight is neglected and 2) the catenary – where the UDL on the deck is neglected. Since in both cases assumptions are made, LEWIS derived the general case of a moment-less arch including self-weight and a UDL. The result is a parametric solution for the x and y coordinate separately. Furthermore, three different cases for the ratio of external UDL to self-weight ($r = w/q$) occur of which only the case $w > q$ i. e. the deck load is bigger than the self-weight is considered to be of structural importance. [Lew16a]

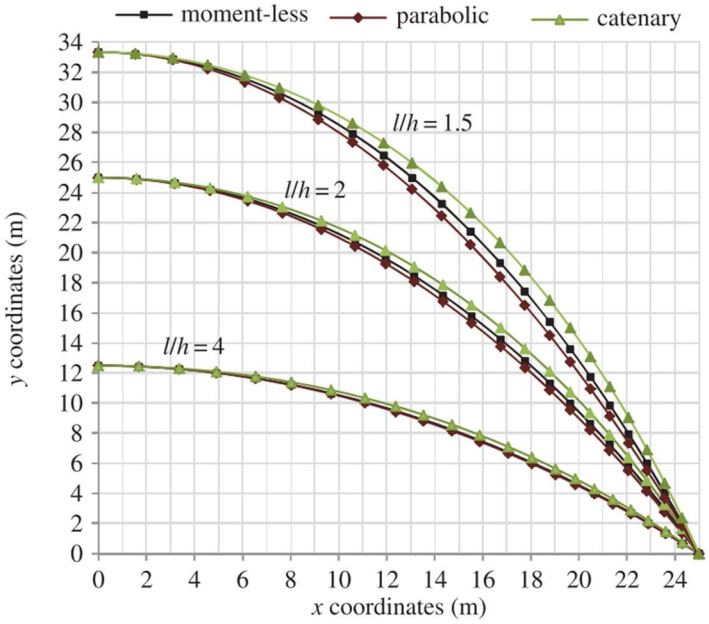

Figure 3-11: Shapes of a moment-less, parabolic, and catenary arch for $r = 2$ (ratio between UDL and self-weight) and varied l/h ratios [Lew16a]

The figure above shows the shapes of the mathematically moment-less, parabolic, and catenary arch with a span of 50 m and varying l/h ratios. The cross-section of the arch is 0.68 m $*$ 1.47 m (depth times width) giving an area of 1 m². The moment-less arch seems to be correct since it lies between the two limits: the catenary (UDL neglected) and the parabola (self-weight neglected). Comparing the parabola to the moment-less arch, especially in the case of medium rise arches ($l/h = 4$) the differences in the geometries are, in practical terms, insignificant (maximum difference of 0.075 m). For further stress analysis, only the parabola was chosen since it would be the usual case for $r > 1$. The

analysis showed that even though the geometrical differences are very small, there are significant differences in the stresses of the arches. The resulting stresses in the parabolic arch vary from tension to compression across the cross-section which is in sharp contrast to the moment-less arch which is solely under compression. Furthermore, significant bending moments develop in the parabolic arch (resulting stresses and bending moment can be found in Appendix A.3). Thus, it is found that relatively small differences in the geometry of the arches can result in large differences in stresses. The moment-less arch furthermore, does not follow a mathematical simple equation and thus the question arises: how much accuracy can be achieved in construction? However, the current equipment allows the production of large objects in a scale of mm rather than cm and thus, a precise production should be possible. [Lew16a]

4 Testing Program and Execution of Tests

The scope of this master's thesis is to develop a suitable process for the efficient folding or forming of extruded (textile reinforced) concrete structures. Furthermore, the influence of different types and amounts of microfibers on the forming process has been investigated. For the analysis microfibers made from PVA and basalt were used. At first, minimum bending radii were determined. The final aim was to demonstrate technical limits of the folding process. Therefore, various tests have been carried out at the Institute of Building Materials Research of the RWTH. Besides the feasibility of different bending radii for varying fiber contents, the load-bearing capacity of resulting components was investigated.

4.1 Testing program

The testing program carried out within this master's thesis consisted of two different types of tests: 1) the extrusion of (textile reinforced) concrete with subsequent forming and 2) three-point bending tests of double curved extruded elements. In total 8 extrusion test series were carried out with varying types and amounts of fibers. During each test series longitudinally and transversally formed concrete specimens were produced. After the first half of test series, it was concluded to produce double curved specimens in order to evaluate the flexural load-bearing capacity of curved concrete elements. The formwork for these double curved elements was produced just before the 5th test series and thus, it was used from that test series on (series 5 to series 8). The following table summarizes the testing program. Properties of the different fiber types can be found in Table 4-3, page 49.

Table 4-1: Summary of the testing program

Test series no.	Type of fibers	Amount [vol.-% of mixture]	Textile reinforcement	3-point bending test
1	PVA "hard"	0.5	-	-
2	PVA "soft"	0.5	-	-
3	Basalt	0.5	-	-
4	-	-	-	-
5	PVA "soft"	0.25	-	Yes
6	Basalt	0.25	-	Yes
7	PVA "soft"	0.5	Ar-glass	Yes
8	PVA "soft"	0.5	Carbon	Yes

The bending radii were chosen differently for forming in the longitudinal and transverse direction. In transverse direction, the specimens were formed using pipes with four different bending radii. A list of all specimens and associated bending radii can be found in Appendix A.11. For longitudinal forming, the bending radii were chosen in an iterative process. Initially, rather conservative assumptions were made to finally demonstrate the limits of the concrete and the folding tool. A complete listing of all intended and achieved longitudinal bending radii can be found in Appendix A.10.

4.2 Test set-up

The basic set-up for the extrusion and forming carried out within this master's thesis consists of three main parts: an intensive mixer, a laboratory extruder, and the forming tools. The laboratory extruder and the intensive mixer are part of the laboratory of the Institute of Building Materials Research of the RWTH and could be used straightforward. However, some modifications were made to the extruder such as a new mouthpiece and conveyor belt (chapter 4.2.2). The basic concrete mixture was adopted from previous investigations [Kra15]. However, it was slightly modified.

The folding tools first needed to be developed since there was no suitable process for the efficient folding of extruded concrete structures. Different ways of forming the extrudate in longitudinal and transverse direction were evaluated. The process of the development can be found in chapter 4.3.

4.2.1 Concrete mixtures and the mixing process

The concrete mixtures used within this master's thesis are based on previous investigations [Kra15]. The development of this mixture was intensively explained in chapter 2.3.4. Due to the MC which is contained in it, an intensive mixing process is required, which would take a lot of time with conventional mixing methods. Thus, an intensive mixer was chosen as mixing equipment. The following table gives the 3 basic concrete mixtures used within this master's thesis.

Table 4-2: Mix designs used within this master's thesis

Component	Unit	No fibers	0.25 vol.-% fibers	0.5 vol.-% fibers
Cement	kg/m³	700	700	700
Quarzitic aggregate 0.1 … 0.5 mm		678	676	671
Millisil W3 0 … 0.25 mm		283	279	277
Fly ash		210	210	210
Silica fume		70	70	70
Water		278	278	278
Methyl cellulose		7	7	7
Microfibers (PVA or basalt)	vol.-% of mixture	-	0.25	0.5

As the table above shows, the content of cement, fly ash, silica fume, MC, and water was kept constant over all tests. Only the content and types of fibers were changed and accordingly, the amount of quarzitic aggregate was changed to achieve equal volume ratios. The concrete mixtures used in the respective test series can be found in Appendix A.7.

Microfibers

The microfibers used were two different types of PVA fibers and basalt fibers. Properties of those fibers can be found in Table 4-3. However, the PVA fibers of type “hard” were neglected after the first test series since new PVA fibers of type “soft” with improved mechanical properties for extrusion were ordered (more in chapter 5.4).

Table 4-3: Properties of fibers used within this master’s thesis

Property	Unit	PVA fibers “soft”	PVA fibers “hard”	Basalt fibers
Tensile strength	MPa	1600	1000	860
Youngs Modulus	GPa	39	27	68
Elongation at break	‰	60	90	15.5
Density	g/cm³	1.3	1.3	2.65
Diameter	µm	26	200	13 … 16
Length	mm	6	6	6.4

Textile fabrics

Besides short fiber reinforcement, it was possible to add a textile reinforcement fabric through a special mouthpiece (Figure 4-9, page 55). Two different textiles were used within this master’s thesis. Since the specimens should be formed after extrusion the main selection criterion was the flexibility and pliability of the fabrics. Furthermore, one textile made from ar-glass and one textile made from carbon should be tested. The used textile fabrics can be seen in the figures below.

Figure 4-1: Textile reinforcement fabric used within this master’s thesis made from carbon

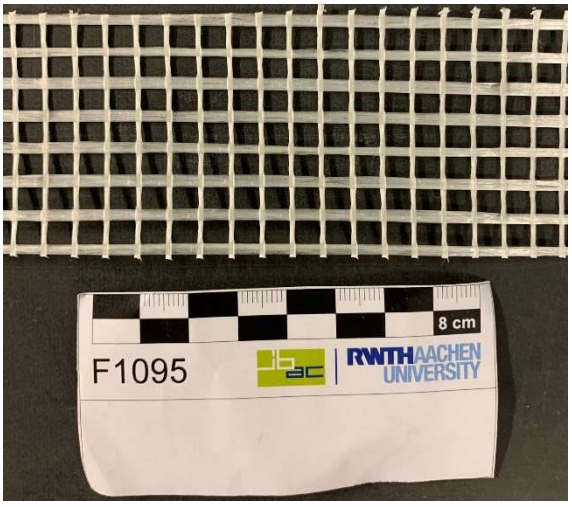

Figure 4-2: Textile reinforcement fabric used within this master’s thesis made from ar-glass

The following table summarizes relevant properties of the two used textiles.

Table 4-4: Properties of the textile fabrics used within this master's thesis

Name	Base material	Grid opening[1] [mm x mm]	Impregnation	Tensile strength approx. [MPa]
SITgrid044 VL	Carbon	11 x 10	Polystyrene	2200
AR - 240	Ar-glass	5 x 5	Styrene-Butadiene	600

Mixing procedure

The intensive mixer used within this master's thesis is made by the company Gustav Eirich and is part of the laboratory of the Institute of Building Materials Research. It mainly consists of a mixing vessel for the concrete mixture, a swirler, and a scraper (Figure 4-3). The mixing vessel holds up to 40 liters. However, for the investigations carried out within this master's thesis not that much concrete was needed so that approx. 18 liters of fine-grained concrete were produced per test series. During the mixing procedure revolution speed, torque, current uptake, and temperature in dependence of time are monitored. As mentioned above, the intensive mixing is necessary to fully develop the effect of the MC.

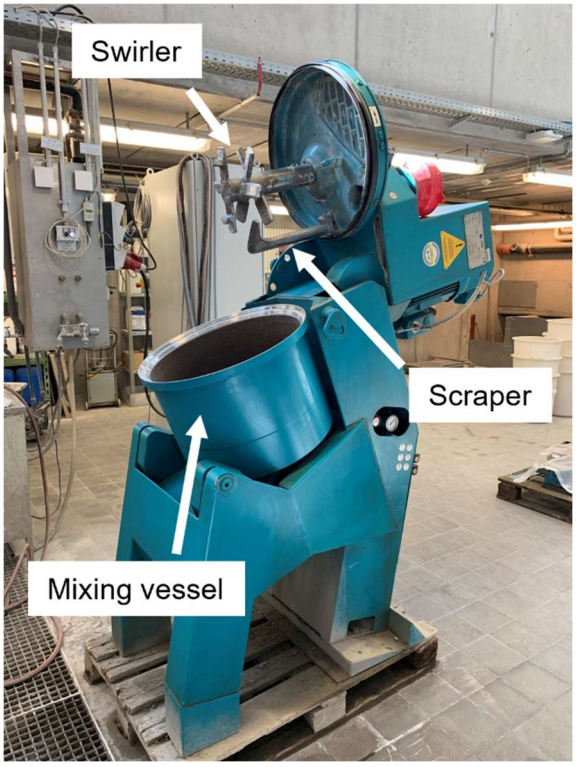

Figure 4-3: Eirich intensive mixer

The mixing procedure was adopted from previous investigations [Kra15]. Here, the necessary mixing time was approximately 4 minutes (Figure 4-4). First, a revolution speed of 500 rpm was used for 90 seconds and only the dry components were mixed (dry mixing). After that time, a 25 second time window opened, in which the machine slowed down to

[1] Clear distance between the rovings according to the producers. Warp x Weft.

66 rpm. During this time, the water was added. Afterwards the intensive mixer speeded up to 800 rpm for 130 seconds (wet mixing) until the mixture was ready for extrusion.

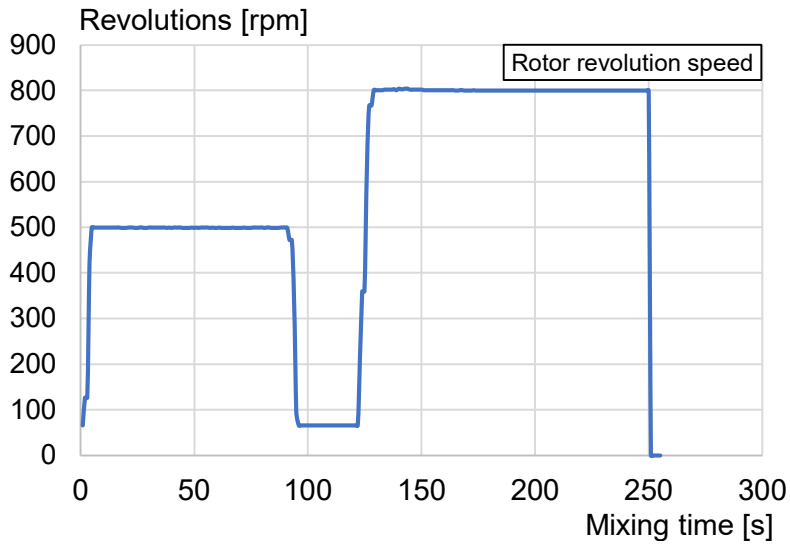

Figure 4-4: Revolution speed of the rotor of the intensive mixer [rpm] during the mixing procedure (mixture PA2 with 0.5 vol.-% of "soft" PVA fibers)

4.2.2 The laboratory extruder

After the fine-grained concrete was mixed, it was put into the laboratory extruder which is made by the company Händle. However, it was important to shorten the time between intensive mixing and starting the extrusion as much as possible since the concrete mixture which included rapid type cement tended to harden fast. Yet, the concrete mixture had to be soft enough to be processable by the extruder. The fine-grained concrete was then compacted by a pre-press and an auger conveyor which pushed the mixture to the pressure head. There, two different mouthpieces for shaping the extrudates were placed: one with textile feeding channel (Figure 4-9, page 55) and one without (Figure 4-7, page 54). Both had a cross section in form of a flat plate with dimensions of 60 mm x 10 mm.

A temperature and pressure sensor near the mouthpiece of the extruder measured the concrete temperature and the pressing pressure continuously. Moreover, the absolute value of the vacuum, the motor current, and the revolution speed of the prepress and the auger press were measured.

After leaving the mouthpiece, the concrete was extruded onto a conveyor belt on which a thin plastic foil was placed. The plastic foil decreased the friction between conveyor belt and extrudate and furthermore was necessary for the transportation of the specimen to the folding tools. After the desired length of the extrudate was reached, it was cut off with a spatula and transported from the conveyor belt to the folding tool. The figure below shows the structure of the laboratory extruder.

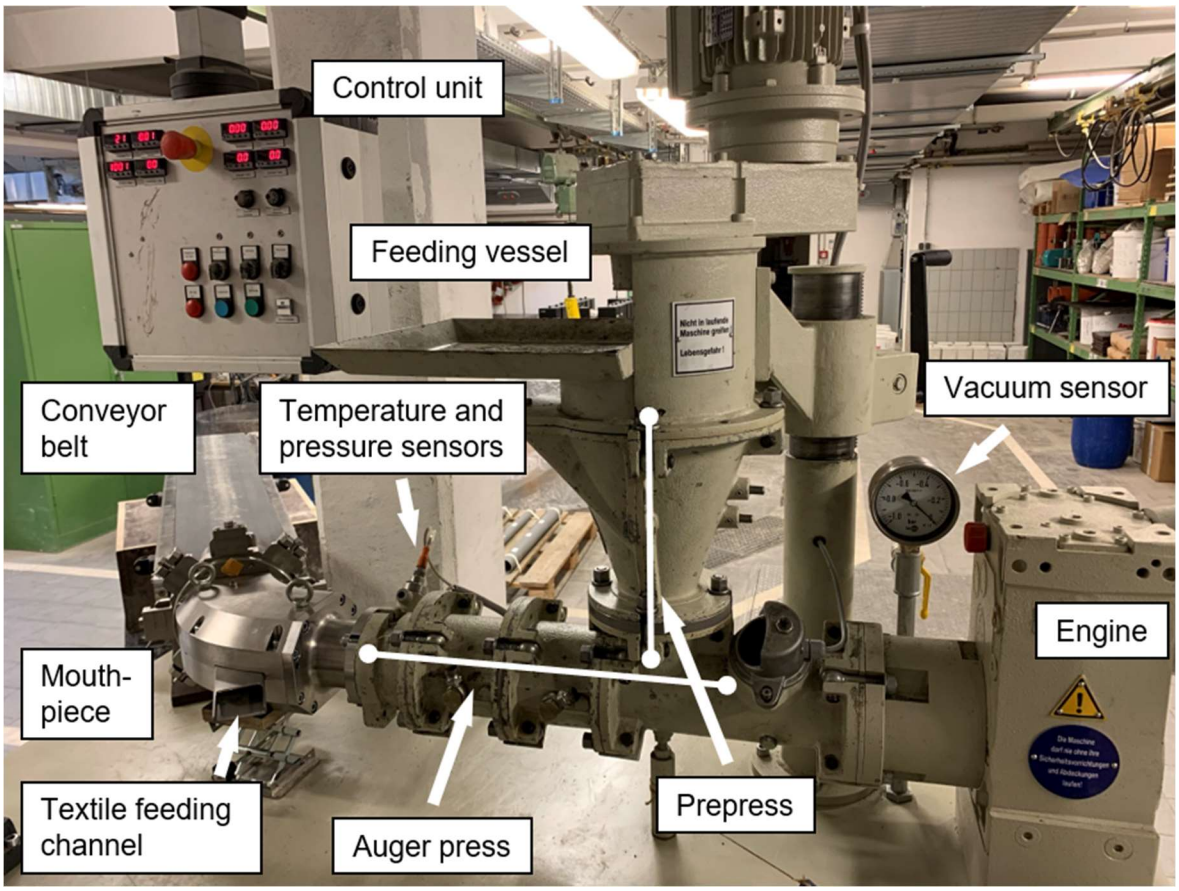

Figure 4-5: Laboratory extruder

Vacuum pump

A vacuum pump could be switched on at the extruder, which removed the air from the fine-grained concrete making it more compact and stiffer. Thus, a vacuum was applied whenever possible to improve extrusion results. However, as explained in chapter 2.3.4 the flexural strength of the specimens would not increase due to deaeration and thus, it was not of great importance to apply vacuum for the flexural tests carried out. Nevertheless, during the extrusion of FRC, it was mostly possible to apply a vacuum. However, when TRC was extruded which included a change of the mouthpiece, a vacuum could not be applied successfully. This might be caused due to the length of the new mouthpiece which is significantly longer than the mouthpiece used for FRC extrusion. Furthermore, the new mouthpiece has a curved shape (Figure 4-8, page 55) so that the extruder press had to push the concrete mixture around a curve in addition to the added distance. This increase in workload, combined with a denser concrete structure due to the applied vacuum, brought the extruder machine to its limit, so that the concrete could no longer be extruded. Thus, no vacuum was applied for TRC specimens.

The table below summarizes the maximum pressing pressure and the average absolute vacuum that was applied on the specimens for all test series. Since the pressing pressure strongly correlates with the velocities of the presses, they are also given. The “old” mouthpiece was used in previous investigations for TRC extrusion (Figure 2-42, page 33), however, for the first two test series of this master’s thesis it was used for FRC extrusion. In test series 1 no proper vacuum could be applied which however could be done in test series 2. Yet, the change of velocity does not allow a direct comparison. From test series 3

on the “new” mouthpiece for TRC extrusion was available. Thus, it was used for the first time in series 3 and later for TRC extrusion in test series 7 and 8. In test series 4 to 6 a “short” mouthpiece was used which was much more convenient for FRC extrusion. It can be seen from the table that the pressing pressure decreased significantly compared to the old mouthpiece with similar velocities in test series 2. Furthermore, the table shows that for the TRC test series (series 7 and series 8) even without vacuum the pressing pressure was significantly higher than for FRC extrusion with approx. equal pressing velocities and the short mouthpiece (series 4 to series 6).

Table 4-5: Vacuum and maximum pressing pressure per test series

Test series	1	2	3	4	5	6	7	8
Textile reinforcement	-	-	-	-	-	-	Yes	Yes
Mouthpiece	Old[1]	Old	New[2]	Short[3]	Short	Short	New	New
Absolute vacuum approx. [mbar]	-300	-1000	-	-1000	-1000	-1000	-	-
Max. pressing pressure [Bar]	2.4	7.7	8.4	3.3	3.6	3.1	10.9	11.0
Prepress velocity [rpm]	2.8	5.8	7.0	5.0	5.7	5.1	5.1	5.1
Auger press velocity [rpm]	2.6	6.2	7.5	6.0	6.6	5.9	5.9	6.0

The mouthpieces

As mentioned above, the mouthpiece used in the first 2 test series was the one used in previous investigations to extrude TRC. However, for the extrusion of fine-grained concrete without textile reinforcement a much simpler mouthpiece could be used (Figure 4-6). Since no textile feeding channel was needed, a cross-section rejuvenation in the form of 60 mm x 10 mm was just necessary to extrude FRC (Figure 4-7).

[1] The “old” mouthpiece can be seen in Figure 2-42, page 33;
[2] The “new” mouthpiece can be seen in Figure 4-9, page 55;
[3] The “short” mouthpiece can be seen in Figure 4-6.

Figure 4-6: Mouthpiece for flat rectangular cross-sections of 60 mm x 10 mm

When the extrudate reached the desired length, the extruder was stopped, and the piece was cut off with a spatula. Afterwards, the extruded concrete strip was measured and trimmed to the desired length. Then a flat metal plate was placed underneath the plastic foil the concrete lied on, to transport the specimens to the folding tool without damaging them.

Figure 4-7: Extruded fine-grained concrete without textile reinforcement

For the extrusion of TRC, the mouthpiece needed to have a textile feeding channel which guided the textile reinforcement into the concrete flow. As presented in Figure 2-42, page 33 and Figure 2-46, page 35 the state of the art from previous tests was a mouthpiece where the textile reinforcement fabric was guided into the concrete flow from above under an angle of 75-90°. However, not all textiles are flexible enough to perform such bending. Thus, a new mouthpiece was developed which can be seen in detail in Figure 4-8.

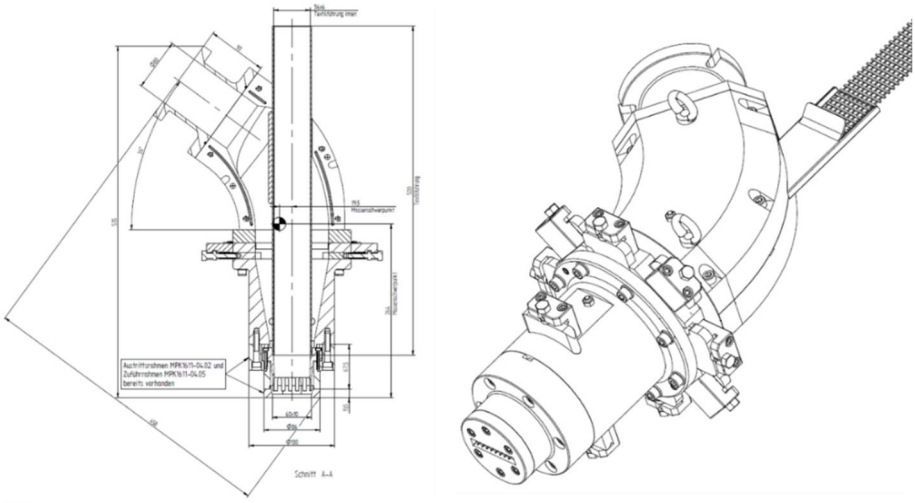

Figure 4-8: New mouthpiece for feeding textile reinforcements parallel to the concrete flow – sketch by ZMB Braun

The aim for the development of this component was to achieve a 0° angle between textile reinforcement and concrete flow during the extrusion process. This allowed less flexible textiles to be guided into the concrete flow without damage. Consequently, the mouthpiece could not be parallel to the extrusion axis anymore resulting in a curved shape. The textile reinforcement was fed into the mouthpiece via a guiding channel similar to the mouthpiece used before, however, it was now under 0° angle to the concrete flow.

To be able to feed the textile reinforcement fabrics into the guiding channel they needed to be cut in shape. For the new mouthpiece this meant that the textile had to be of 56 mm width or less. In the tests carried out within this master's thesis, textile reinforced concrete stripes of approximately 1.10 m length were needed. The figures below show how the textile was fed into the mouthpiece and the resulting extruded TRC specimen.

Figure 4-9: Textile being fed into new mouthpiece

Figure 4-10: TRC specimen extruded with new mouthpiece

Conveyor belt

The existing set-up previous to the investigations carried out within this master's thesis included a conveyor belt which was solely driven by the extruded concrete. Thus, the velocity of extrusion could be measured through the velocity of the conveyor since they would be equal. For the investigations carried out within this master's thesis, further improvements on the test set-up were performed. A new conveyor belt was used which had an electric engine and thus, was self-sufficient and not driven by the extruded concrete. However, it turned out that it was hardly possible to synchronize the velocity of the conveyor belt exactly to the velocity of the concrete flow. Thus, to reduce friction and for transportation reasons a thin plastic foil was used between extruded concrete and conveyor belt.

Furthermore, this allowed the conveyor belt to be driven slightly faster than the concrete flow. If the conveyor belt was put on a velocity lower than the velocity of the extruded concrete, the friction increased, and the concrete started to undulate. Furthermore, the slightly higher velocity of the conveyor belt, constantly pulled on the plastic foil and thus on the extruded FRC with just a good amount of force, so that the extrudate would come out smooth. Another positive side-effect of the slightly higher velocity of the conveyor belt was that even though the conveyor belt tended to get slower when a certain amount of concrete lied on top of, it was still fast enough to prevent undulations. Presumably, this happened because when setting the velocity of the conveyor belt, it was in fact not the velocity that was set, but the motor current of the electric engine, which was not high enough to drive the belt at the same velocity with the increased load from the concrete. However, the velocity of the conveyor belt and extruded FRC were now unequal which made the measurement pointless. Thus, the velocity of extrusion was not measured during this master's thesis.

Figure 4-11: Pulling on the textile fabric – Concrete piling up on transverse rovings

Figure 4-12: Pulling on the textile fabric – Extruded specimen without visible defects

For the extrusion of TRC, by slightly pulling on the textile reinforcement, the concrete could be guided to obtain straighter elements (Figure 4-12). Without pulling, especially for longer elements, the concrete would not necessarily follow an exactly straight line since the concrete matrix tends to sway slightly to the right and left. Furthermore, for the textile reinforcements which were guided into the concrete flow via the feeding channel, the concrete tended to get a wavy surface without pulling. This was caused by concrete piling up on the transverse rovings. By pulling on the textile reinforcement mesh, this effect could be significantly reduced. Thus, the concrete did not need to push the textile reinforcement through the guiding channel by frictional force (or at least with less force) and it did not pile up along the transverse rovings. However, the necessary amount of force had to be applied by hand and with sensitivity because it is different for every specimen. As to be seen in Figure 4-11, a short moment of not pulling on the textile reinforcement would lead to undulations.

4.3 Folding procedure

The goal of this master's thesis is to find minimal bending radii for extruded concrete. Therefore, the extruded concrete was folded separately in longitudinal and transverse direction to analyze the differences in bending behavior between the two directions. Since no suitable folding tool was available at the laboratory, at first, a new folding procedure needed to be developed.

Within this master's thesis the fold-in-fresh method was used as folding principle (chapter 2.2.1). The high green strength of the extruded concrete made it possible to dispense with the formwork and thus, allowed for flexible manageability. As mentioned earlier, the concrete was extruded onto a thin plastic foil and was carried on this foil to the folding tool. At the same time the foil was used to keep the concrete in position during the folding process.

4.3.1 Folding in transverse direction

For the evaluation of the minimal bending radii in transverse direction, pipes of different diameters were used (Figure 4-13). The advantage of using pipes is that their bending radius is defined and that they have a smooth surface. Thus, the extruded concrete could be placed parallel to the axis of the pipe either on top of it or into it. Here the before mentioned plastic foil has another advantage: it prevents the concrete from sticking to the pipes. The fresh concrete should then be formed according to the bending radius of the pipe solely by gravity. Pipes of the following diameter were used: DN[1] 160, DN 110, DN 75, and DN 50.

[1] DN is the nominal outer diameter of a pipe. The pipes used have diameters according to DIN EN 1451-1 [DIN18].

Figure 4-13: Pipes used for transverse folding of extruded concrete

The FRC was extruded in 1 m long stripes as explained above and cut off with a spatula in pieces of approximately 50 cm. To produce TRC, the textile fabrics were cut in pieces of approximately 60 cm length, and accordingly stripes of that length were produced. The stripes were then carried from the conveyor belt to the pipes on a steel plate with the plastic foil in between. Pieces of double-sided adhesive tape were put on top of the smaller grey pipes (DN 75 and DN 50) so that plastic foil and thus the concrete would not slip off. The concrete was aligned by eye to be as straight as possible on top of the pipes. This way transversally formed FRC specimens were produced (Figure 4-14).

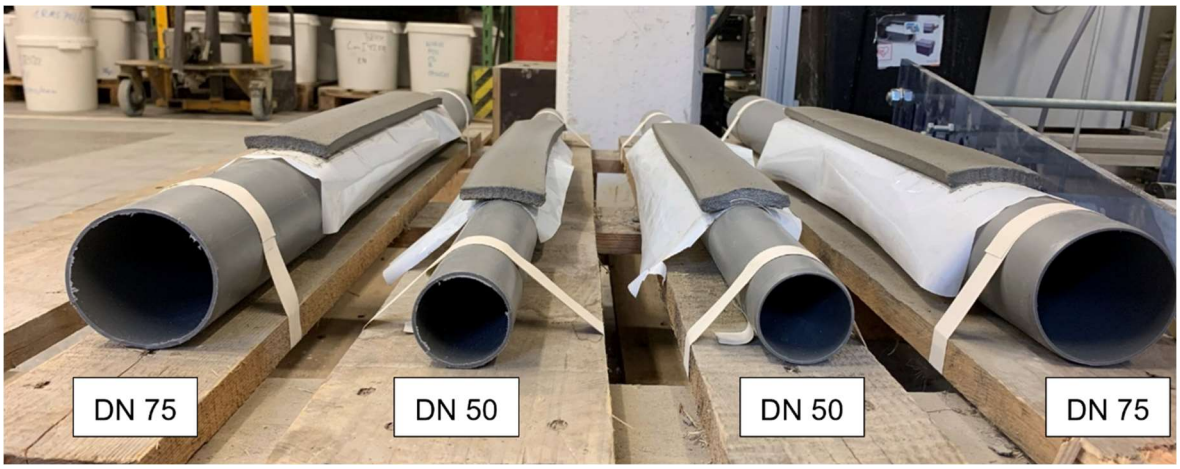

Figure 4-14: Transversally formed FRC on top of DN 50 and DN 75 pipes – free deformation (0.5 vol.-% of "soft" PVA fibers and no textile reinforcement)

For the bigger orange pipes (DN 110 and DN 160) it seemed more useful to put the concrete inside instead of on top of the pipes. Thus, the extruded concrete was placed on a slender wooden board and shoved into the pipe. In later tests, the bigger orange pipes were cut open in half cross-sections (Figure 4-15 and Figure 4-16). Thus, the concrete could be placed inside the pipes in a much more convenient way. However, cutting open would not have been useful for the smaller grey pipes, since they were too small to fit the 60 mm x

10 mm wide extruded concrete stripes inside and thus the extruded concrete was placed on top of them for all tests.

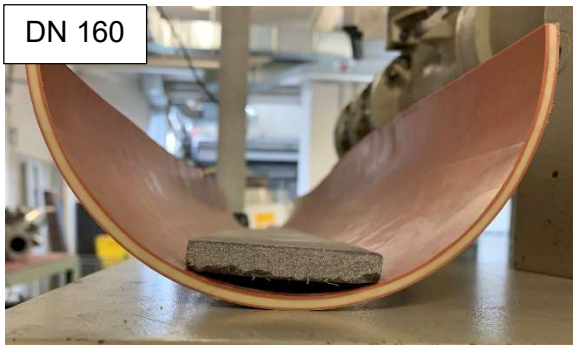

Figure 4-15: Transversally formed FRC in DN 160 pipe – free deformation (0.5 vol.-% of "hard" PVA fibers and no textile reinforcement)

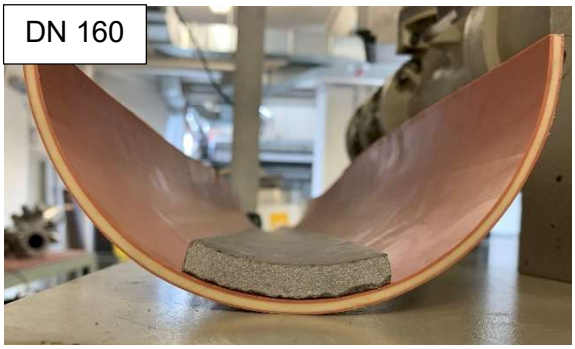

Figure 4-16: Transversally formed FRC in DN 160 pipe – forced deformation (0.25 vol.-% of "soft" PVA fibers and no textile reinforcement)

However, the first two test series, showed that the concrete mixture was too stiff to be formed transversally along the pipes cross-section solely by gravity. Thus, it must be distinguished between free and forced deformation (Figure 4-15 and Figure 4-16). Since the goal of this master's thesis is to find minimal bending radii for the extruded concrete, it was decided to force the concrete into the desired shape to see for which bending radii cracks would occur.

Figure 4-17: Transversally formed FRC on top of DN 50 pipe – free deformation (0.5 vol.-% of "soft" PVA fibers and no textile reinforcement)

Figure 4-18: Transversally formed FRC on top of DN 75 pipe – free deformation (0.5 vol.-% of "soft" PVA fibers and no textile reinforcement)

As the figures above show, it seemed that the extruded concrete had a minimal bending radius that it was willing to deform to without an extern al force (besides gravity). Thus, the distinction between desired bending radius and actual bending radius increased for smaller bending radii. Figure 4-17 shows a significant difference for the DN 50 pipe while for the DN 75 pipe the bending radius seemed to be achieved at least in the intermediate part of the cross-section (Figure 4-18).

To apply the forced deformation three different methods were tested. However, the approaches were similar: at first, another piece of plastic foil was placed on top of the fresh concrete to protect the surface. Then mechanical force was applied to push the fresh concrete into the desired shape without flattening it significantly. The first tool used was a

roller. Two types of rollers were available: one made from plastic with an uneven surface and another one made from steel with an even surface. However, with both, it was difficult to find a suitable pressure to form the concrete along the pipe without making it edgy. Furthermore, the plastic roller left marks in the fresh concrete while the steel roller made the concrete more edgy due to its higher weight (Figure 4-19).

Figure 4-19: Edgy surface caused by roller pressure

Thus, two new approaches were developed: 1) using another pipe of similar diameter and push the specimen in shape and 2) using gloves and apply pressure sensitive by hand. Option 1) turned out to be the best way of shaping the fresh concrete for the cut-open bigger orange pipes. Another pipe was placed on top of it and pushed with even pressure onto the concrete until it was in the desired shape. For the smaller grey pipes, option 2) turned out to be the best suiting. By hand it was possible to shape the concrete very sensitively without damaging it. Due to the low friction of the gloves on the plastic foil and by using the whole palm of the hand, it was furthermore possible to leave significantly less marks in the concrete than with the rollers. The figure below show the difference between free deformation and forced deformation.

Figure 4-20: Transversally formed FRC– free deformation (0.5 vol.-% of "soft" PVA fibers and no textile reinforcement)

Figure 4-21: Transversally formed FRC– forced deformation (0.5 vol.-% of basalt fibers and no textile reinforcement)

4.3.2 Folding in longitudinal direction

For the folding in longitudinal direction, a tool had to be developed that allowed flexible adjustment of the bending radius. Furthermore, different bending radii should be achieved simultaneously during one extrusion test series. The folding tool which existed at the laboratory (presented in Figure 2-19, page 19) did not fulfill these requirements since 1) the bending radius was not defined and 2) only one bending radius could be achieved per test series. Thus, a new folding tool has been developed.

During the development process the idea arose of using a tool that allowed free hanging of the concrete. The mathematical shape describing a free hanging rope solely influenced by gravity and self-weight, is the so-called catenary and was extensively described in chapter 3.2 from a mathematical point of view and in chapter 3.1.1 the relevance of this shape in architecture and civil engineering has been explained. The mechanism of hanging concrete allowed a change of the bending radius of the specimens by simply changing the distance between the fixing points. The further the two fixing points of the catenary were apart, the larger the bending radius and consequently, if the fixing points were put closer together, the bending radius decreased.

Figure 4-22 shows the mathematical principle behind the folding tool as it was designed. Three different catenaries of equal length (110 cm) can be seen. However, the distance between the fixing points varies. Here, one fixing point was left unmoved while the second fixing point was moved to achieve spacings of 45 cm, 60 cm, and 80 cm, respectively. Two parameters (rope length and distance between fixing points) defined the catenary mathematically. Resulting bending radii could be calculated with a solving algorithm in Microsoft Excel as explained subsequently to equation (3-12).

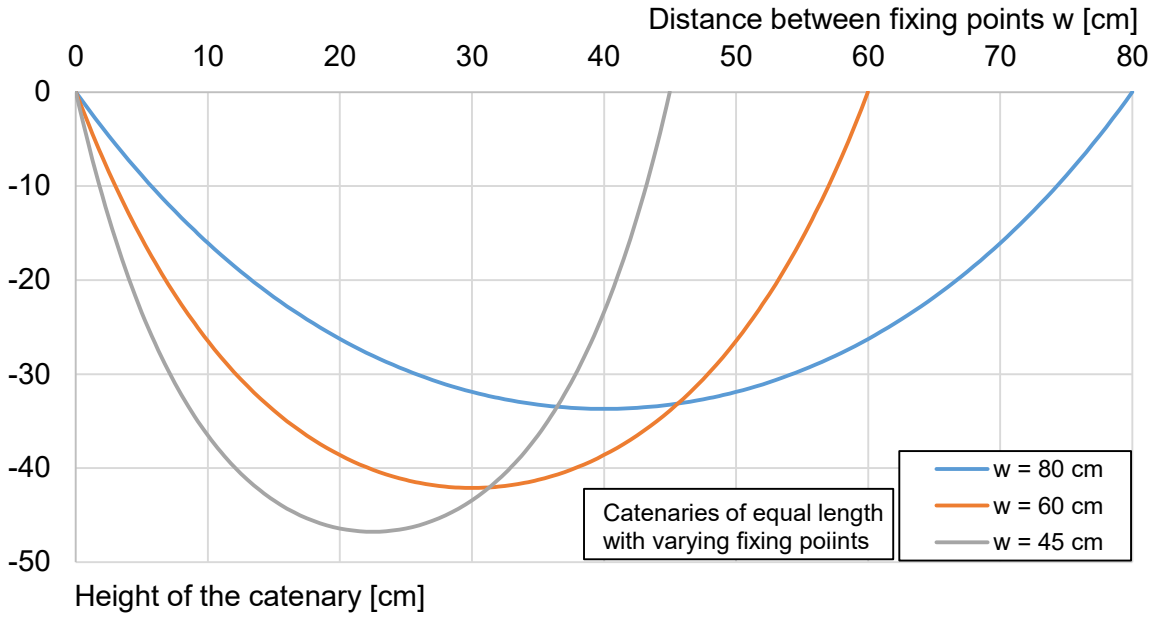

Figure 4-22: Catenaries with equal fixing points but different rope lengths

The table below gives the rope length l and the varying fixing point distances w of the catenaries shown in the figure above. Furthermore, the calculated bending radius at the vertex a and the arch height f can be seen. The associated equations can be found in Appendix A.4.

Table 4-6: Parameters describing the catenaries presented in Figure 4-22

Rope length l	Fixing point distance w	Bending radius a	Height f
[cm]			
110	80	28.1	33.7
110	60	14.9	42.1
110	45	8.9	46.8

A real folding tool was then developed from the basic idea and finally the tool was manufactured by the institute's workshop. The designed tool consists of five individually adjustable tracks. Each track has two clamping jaws (Figure 4-23) which serve as fixing points for the hanged concrete specimen. The length of the tracks is approx. 1.1 m with a width of approx. 12 cm.

After extrusion, the fresh concrete was carried on a plastic foil to the new folding tool. There it was put on a wooden board placed between the two fixing points, so that the fresh concrete would stay in place. The figure below shows the necessary steps for longitudinally forming the specimens.

Figure 4-23: Steps of the longitudinal folding procedure

In summary, the procedure of longitudinally folding elements was carried out as follows:

1) Placing the extrudate on a wooden board between two clamping jaws.
2) Clamping the plastic foil between two clamping jaws:
    a. Fixing one clamping jaw
    b. Loosely fixing the other clamping jaw while prestressing the plastic foil by hand and holding jaw and foil tight
3) Removing the wooden board so that the concrete is in free-hanging state and moving the clamping jaw that is not yet fixed.
4) Fixing the second clamping jaw in the desired position – concrete is longitudinally formed.

A clamping jaw in its disassembled and assembled state can be seen in Figure 4-24 and Figure 4-25. Furthermore, the wooden board on which the fresh concrete was placed while the plastic foil was clamped between the clamping jaws can be seen. The clamping jaws were mounted on movable rails. By fixing the screws of the clamping jaws two effects occurred: 1) the plastic foil was clamped and 2) the position of the clamping jaw was fixed. The board was then removed so that the concrete was in a free-hanging state. However, before removing the board the thin foil had to be prestressed to a certain extend by hand so that the concrete would not drop immediately after the board was removed. Yet, it was not possible for the free-hanging concrete to hang exactly horizontally since the necessary prestressing force would tend to become infinite. A mathematical explanation can be found in Appendix A.2. Thus, the initial state was not perfectly horizontal, and a minor drop occurred when the board was removed. However, this was not a crucial issue, since for the evaluation of the theoretically achieved bending radius afterwards, the rope length was measured in a straight state and thus, the rope length of the imaginable existing perfectly straight catenary was known.

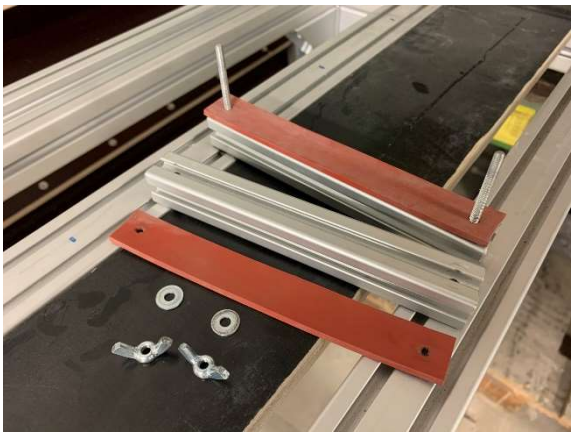

Figure 4-24: Structure of a clamping jaw - disassembled

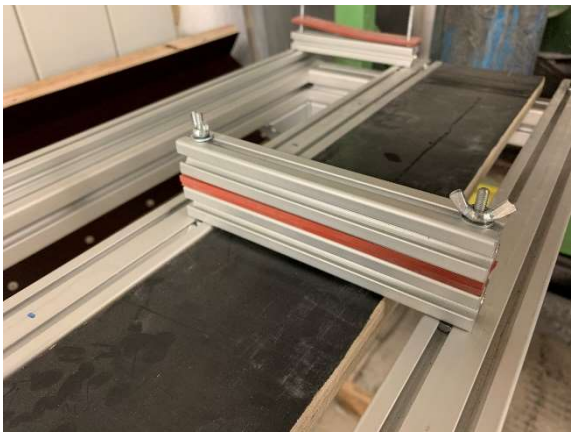

Figure 4-25: Structure of a clamping jaw - assembled

The whole procedure was repeated five times for every track. Thus, five different bending radii could be achieved in the concrete per test series. Exemplary the specimens of test series 2 can be seen in the figure below.

Figure 4-26: Test series 2 with longitudinally folded specimens

4.3.3 Double curved elements and three-point bending test

During the folding procedure, the question arose what the load-bearing capacity of the folded elements is. Therefore, a three-point bending test was proposed to determine the flexural strength. In [Woe17] four-point bending tests were carried out on folded specimen (Figure 2-23, page 20). Inspired by these tests, a similar test set-up was proposed. However, for a test like that, a new shape needed to be developed, since the hanging elements were not quite equal and furthermore, some of them were slightly twisted within their cross-section (Appendix A.9, Figure A-6 and Figure A-7), which would lead to possible stress peaks and thus to an early failure. The newly developed shape should not deviate significantly from the catenary in order to analyze the load-bearing behavior of comparable hanged elements. Here both ends of the shape should be folded up for a better anchorage of the textile reinforcement (Figure 4-27). The shape furthermore should represent the section of a possible future building component which could be a structural system for ceilings (more in chapter 5.7.2).

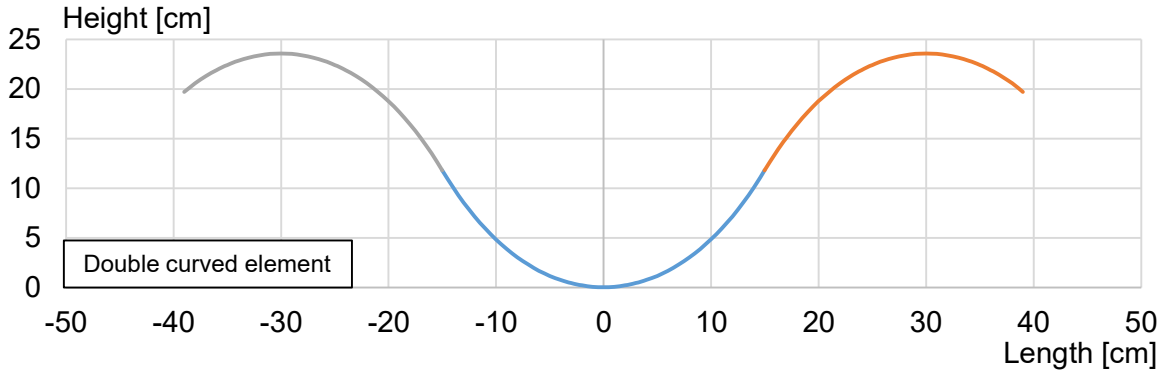

Figure 4-27: Mathematical designed shape for the double curved catenary elements

Typical flat slaps have thicknesses of approximately 20 to 30 cm. Thus, the height of the double curved elements was chosen to be of similar dimensions. Furthermore, the arc length of the specimens should be approx. 100 cm since much longer extrudates could not

be produced due to the length of the conveyor belt. Previous extrusion test series already showed that the concrete was capable of being bent in longitudinal direction with a comparable bending radius. To achieve a double curved element, three catenaries were combined i. e. there was one catenary as “valley” and two catenaries as “mountains”. The production of the formwork was carried out upside down (negative formwork). All three shapes basically followed the same mathematical equation. However, the two outer catenaries were mirrored and displaced. Furthermore, the three catenaries were not of equal length since the part of the arch beyond the high point was just for better anchorage of the textile reinforcement. Thus, it was not carrying any load in the test setup besides its self-weight. The resulting shape was then milled into polyurethane foam (PU-foam) at the Faculty of Architecture of the RWTH using a CNC[1] milling machine. The designed shape is presented in Figure 4-27 and the real PU formwork can be seen in Figure 4-28. The coordinates used for the CNC milling machine can be found in Appendix A.6.

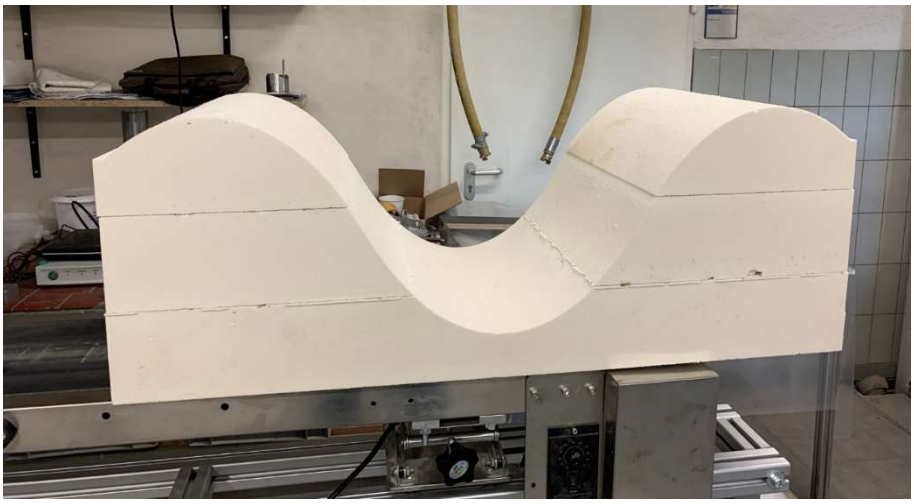

Figure 4-28: Double curved formwork milled into polyurethane foam via CNC mill

Starting with the 5th test series, concrete stripes of approx. 100 cm length were extruded and put on the double curved formwork (Figure 4-29 and Figure 4-30). By slowly lowering the extrudate into the formwork, gravity pulled the concrete into the desired shape. However, at some point the plastic foil tended to wrinkle and had to be straightened by hand. For each extrusion test series, three concrete specimens could be placed onto the double curved formwork simultaneously.

[1] CNC stands for “Computerized Numerical Control” and describes an electronic method for controlling tools that can produce complex parts with high precision.

Figure 4-29: Double curved elements – fresh FRC (test series 5)

Figure 4-30: Double curved elements – cured TRC (test series 8)

24 hours later the concrete was cured and put into water for at least 7 days. Afterwards it was put into a room with 65 % relative humidity at 20°C until testing. The three-point bending test set-up should approximate the situation of a future building component, namely a structural system for a ceiling. Therefore, the bearing conditions were chosen not to be completely free but rigid to a certain degree. To achieve this, sandpaper was placed on the bearing plate (Figure 4-32). The basic test set-up can be seen in the figure below.

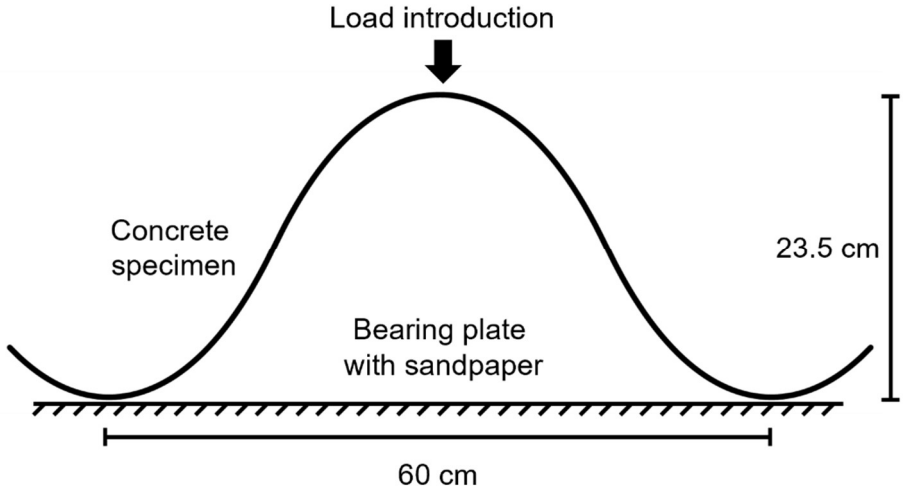

Figure 4-31: Basic experimental set-up for the three-point bending tests

Since one specimen from the 6th test series (with 0.25 vol.-% of basalt fibers) failed during transportation, the remaining 11 double curved elements were tested using this set-up. The load was introduced way-driven with a velocity of 2 mm/min. Exemplary one FRC specimen in said test set-up can be seen in the figure below. Results of the tests will be given in chapter 5.7.

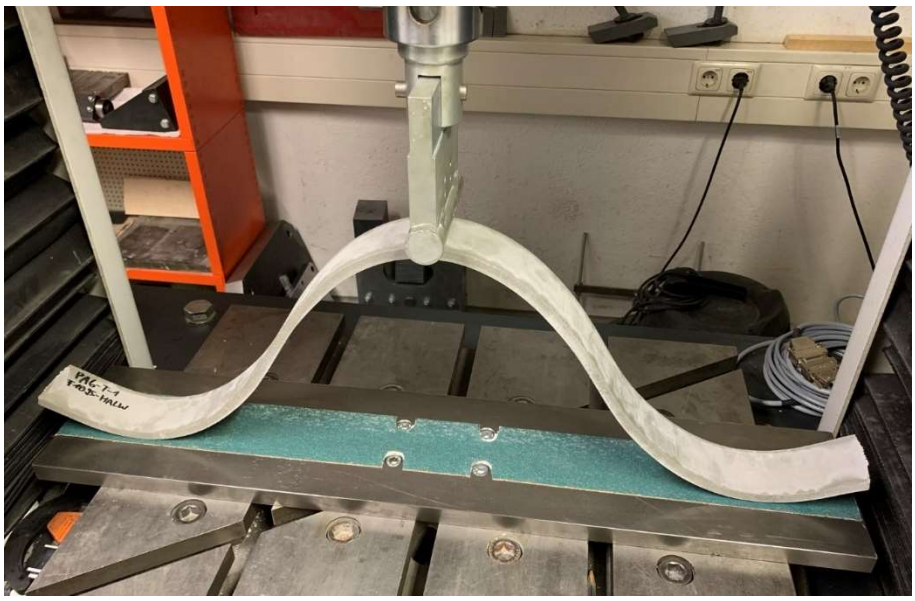

Figure 4-32: Three-point bending test set-up with FRC specimen

5 Evaluation and Discussion of Results

In the following chapter the results of forming the extruded concrete specimens and the three-point bending tests will be evaluated and discussed. The criterion for an unsuccessfully formed specimen was chosen to be the visibility of cracks[1]. The widths of occurring cracks were measured with a crack measuring ruler. Since the elements are very filigree with dimensions of 60 mm x 10 mm, already minor cracks were defined as a failure in bending. Further criteria were developed to evaluate the pliability of the specimens. Since the evaluation was mainly carried out visually with photographs, all photographs are provided digitally as well.

5.1 Measurements of bending radii and crack widths

Since the goal of this master's thesis is to analyze minimal possible bending radii of extruded concrete specimens, at first, the actually achieved bending radii had to be determined. Theoretically, the bending radii of the longitudinally formed specimens was already defined by the length of the plastic foil and the distance between the fixing points, which under normal circumstances result in a catenary. However, the theoretical bending radii had to be compared with the actually achieved bending radii. Thus, 3 parameters were measured on the cured hanging concrete specimens (Figure 5-1): the distance between the fixing points $w_{meas.}$, the real length of the plastic foil $l_{meas.}$, and the height of the arch $f_{meas.}$.

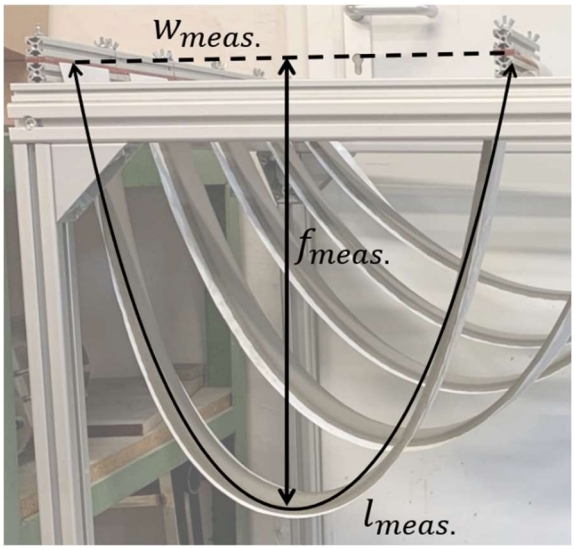

Figure 5-1: Measured parameters of longitudinally formed concrete specimens

With the real distance between the fixing points and the real length of the plastic foil the theoretical arch height $f_{calc.}$ and the theoretical bending radius $a_{calc.}$ of a catenary were calculated. The theoretical arch height was then compared to the measured arch height $f_{meas.}$ to get a first impression, whether the theoretical catenary was achieved or not. It turned out that for smaller fixing point distances and resulting larger arch heights, the deviations became larger. Consequently, this meant that the hanged concrete would follow the catenary only until a certain degree of bending, so that for smaller bending radii the

[1] The visibility of cracks was defined as: cracks are visible by eye and can furthermore be measured with a crack measuring ruler. This excludes cracks below 0.1 mm width.

specimens differed more from the catenary. In Appendix A.8 the difference between theoretical and measured arch height can be seen for all specimens.

To evaluate how this difference influenced the bending radii, afterwards, the physically achieved bending radii $a_{meas.}$ were measured. Therefore, the longitudinally formed concrete specimens were placed on paper and outer and inner circumference were drawn. These drawings where then photographed and the outer and inner bending radii were determined using the software COMEF by OEG GmbH in Frankfurt (Oder), Germany. Therefore, a 10 cm wide section in the apex zone of the hanged concrete specimens was chosen for the measurements (Figure 5-2). Within this section, 5 measurements were made for outer and inner bending radius each consisting of 5 measurement points to determine the bending radius i. e. in total 25 measurements were performed per bending radius. Thus, it is assumed that decent statistical validation of the measurements could be achieved.

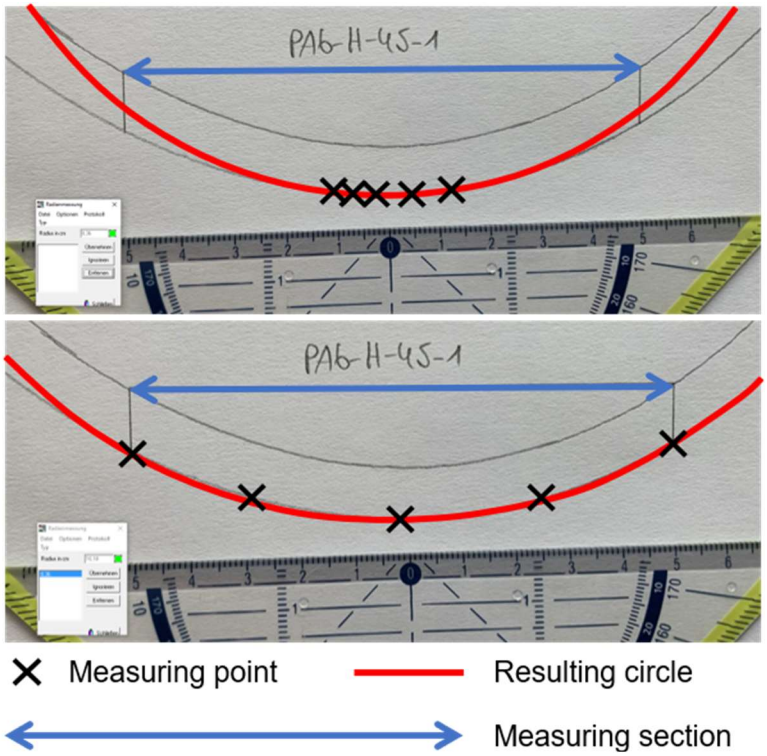

Figure 5-2: Variation of measured bending radii

However, since the specimens are not circle-shaped, finding a unique circle which determines the bending radius is not possible. Thus, for some specimens the 5 measurements differed relatively far. The reason for that can be seen in Figure 5-2: it can be difficult to determine a theoretical circle that suits the most. For the concrete specimen shown in the figure above the measurement in the top figure gives a bending radius of 8.4 cm while the lower figure gives a bending radius of 10.2 cm. However, both circles seem to approximate the bending radius in the apex zone properly. By measuring 5 times and using the arithmetic average of those measurements, it was concluded to have sufficient statistical validation to give a moderately precise average bending radius – in this case 9.8 cm.

However, some specimens had significant kinks or buckled so that it was not possible to determine the bending radius properly. To evaluate these specimens two properties were defined as failure in forming: 1) the visibility of a kink or buckling and 2) the standard

deviation of the bending radius measurements was larger than 10 % of the measured bending radii. The latter proves that a kink is present, since there is a large variation of measurable bending radii in the apex zone and thus no uniform bending. Extrudates fulfilling both criteria were considered as unsuccessfully formed specimens. Affected specimens can be seen in chapter 5.5.2. A table with all measured bending radii and standard deviations can be found in Appendix A.10.

Finally, the measured bending radii were compared to the theoretical bending radii. The following table gives the difference between theoretical and actually achieved bending radii for FRC in percent. Here, similar specimens were grouped to get better statistical validation. For the rounded fixing point distances of approximately 30 cm, 45 cm, 60 cm, and 70 cm at least 4 values existed and thus only these distances were chosen for comparison. The table shows that for larger fixing point distances and thus larger bending radii, the deviation between theoretical and actually achieved bending radii is smaller. For a fixing point distance of approx. 30 cm the average deviation between calculated bending radius (approx. 4.6 cm) and actually achieved bending radius is 67.4 % while for a fixing point distance of 70 cm the calculated bending radius of approx. 19.7 cm is on average missed only by 5.4 %. This fits with the above finding that the hanged concrete specimens deviated more from the catenary for smaller bending radii. Underlying data can be found in Appendix A.5.

Table 5-1: Deviation between theoretical and actually achieved bending radii for FRC

Approx. fixing point distance	Number of specimens	Average calculated bending radius	Average measured bending radius	Average deviation
[cm]	-	[cm]		[%]
30	4	4.6	7.8	67.4
45	5	8.8	10.8	22.2
60	5	14.5	15.6	7.5
70	4	19.7	20.8	5.4

For transversally formed concrete specimens, the theoretical bending radii were defined by the diameter of the used pipes. The bending radii were calculated by dividing the diameter of the pipe by 2. However, for the DN 50 and DN 75 pipes the thicknesses of the specimens were added and for the DN 110 and DN 160 pipes the thicknesses of the pipes were subtracted. This was done because the cracks would occur on the outer concrete surface which is subjected to tension. The thickness of the extrudates was assumed to be approx. 1 cm. The thickness of the larger pipes was measured to be approx. 4 mm. Table 5-2 summarizes the resulting theoretical bending radii. Furthermore, the bending radii were measured to evaluate the actually achieved bending radii. This was done in a similar way as for the bending radii of the longitudinal specimens. However, for the transversally formed specimens both ends of the extrudates were drawn on paper so that two arches had to be measured. On each arch 3 measurements were made with 5 measurement points each.

Thus, in total 30 measurements were performed per bending radius. The resulting measured bending radii can be found in Appendix A.11.

Table 5-2: Bending radii of pipes used for transversal forming

Pipe	Pipe radius	Added specimen thickness	Subtracted pipe thickness	Theoretical bending radius approx.
	[cm]			
DN 50	2.5	1.0	-	3.5
DN 75	3.8	1.0	-	4.8
DN 110	5.5	-	0.4	5.1
DN 160	8.0	-	0.4	7.6

For specimens that showed cracks, furthermore, the crack widths were determined. Therefore, a crack measuring ruler was used, which allows measurements up to 0.1 mm. The widths of smaller cracks were not determined. The figures below show exemplary the measurement of the crack widths for one specimen.

Figure 5-3: Measurement of crack width

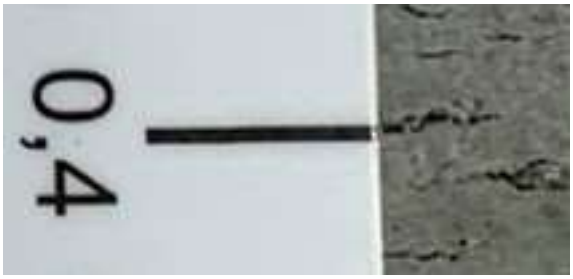

Figure 5-4: Measured crack of approx. 0.4 mm

5.2 Reference tests without fibers

One test series was carried out without any short fiber or textile reinforcement to analyze the influence of the reinforcement. Thereby, transversally as well as longitudinally formed concrete specimens were produced.

5.2.1 Transversally formed specimens

The transversally formed concrete specimens were produced with 4 different pipe diameters as mentioned in chapter 4.3.1. Visible cracks caused by forming occurred for the DN 75 and DN 50 pipes i. e. the specimens were unsuccessfully formed (Figure 5-5). The cracks occurred in longitudinal direction. For specimens formed with DN 50 pipes more visible

cracks appeared, and the cracks were wider than for the ones formed with DN 75 pipes (Figure 5-7).

Figure 5-5: Transversally formed concrete specimen with visible cracks of approx. 0.4 mm (no fibers and no textile reinforcement) – bending radius approx. 3.8 cm

However, for the DN 110 and DN 160 pipes no visible cracks occurred and thus, the forming was successful.

Figure 5-6: Transversally formed concrete specimen without visible cracks (no fibers and no textile reinforcement) – bending radius approx. 7.6 cm

Figure 5-6 shows that the concrete surface of the specimen formed using the bigger pipe diameter DN 160 is very smooth and nearly mirror-like. The same occurred for the other specimen made with the DN 160 pipe and the specimens formed with DN 110 pipes. This effect is caused by the fact that the surface of the concrete that is subjected to tension and thus is the one that is likely to get cracks from the forming procedure, lies on plastic foil. For the smaller pipes, the compressed surface of the concrete lies on the plastic foil which is unlikely to get cracks caused by forming it.

The figure below shows theoretical and measured bending radii and associated crack widths. As mentioned above crack widths below 0.1 mm were not measured.

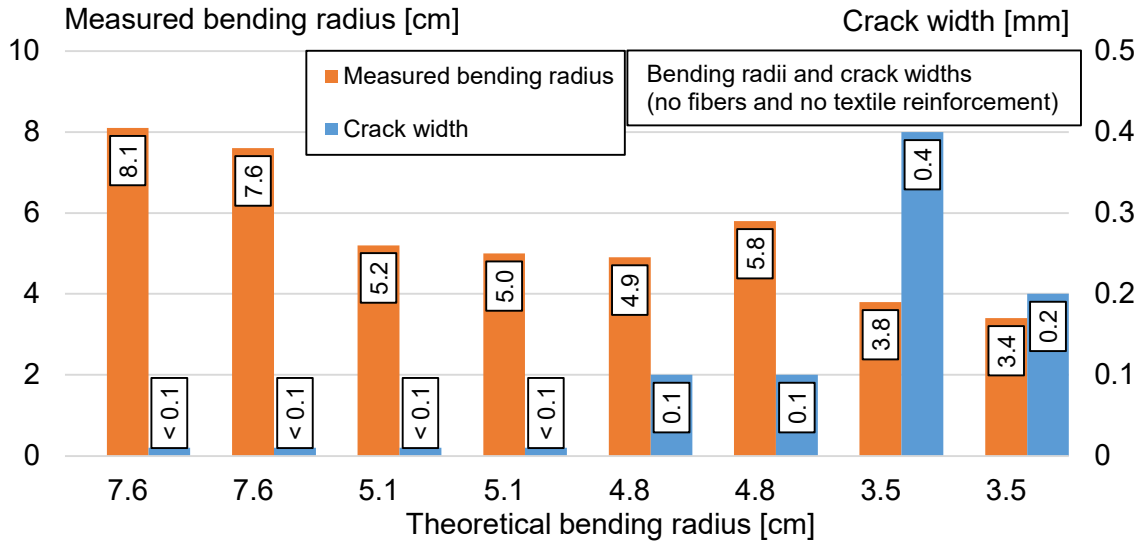

Figure 5-7: Theoretical and measured bending radii with corresponding crack widths (no fibers and no textile reinforcement)

Extrudates made from the base concrete mixture without fibers and textile reinforcement could be formed in transverse direction without visible cracks caused by forming for bending radii of up to approx. 5.0 cm. For bending radii of approx. 4.9 cm and below cracks occurred and thus, forming of the specimens was unsuccessful. One specimen that was formed on top of a pipe exhibited visible cracks already for a bending radius of approx. 5.8 cm.

For future investigations, it is recommended to use a microscope and analyze the cracked surface in more detail. Within this master's thesis only cracks visible by eye were evaluated with a crack measuring ruler. Furthermore, for the specimens that were pressed into pipes the outer bending radius of the concrete specimens which is susceptible to cracking lies on a plastic foil. The friction between fresh concrete and plastic foil leads to a stress transfer from the specimen into the plastic foil which carries the tensile stresses that would lead to cracks on the surface. Thus, forming specimens by pressing them into a pipe seems advantageous over forming them on top of a pipe.

5.2.2 Longitudinally formed specimens

The longitudinally hanged concrete specimens were produced as mentioned in chapter 4.3.2. The measured distances between the fixing points, the measured length of the plastic foil, theoretical, and actually achieved bending radii are given in Appendix A.10. The successfully achieved bending radii are furthermore shown in the figure below. Since no visible cracks occurred for all specimens of this test series, all formed extrudates were successful. An exemplary longitudinally formed concrete specimen is given in Figure 5-9.

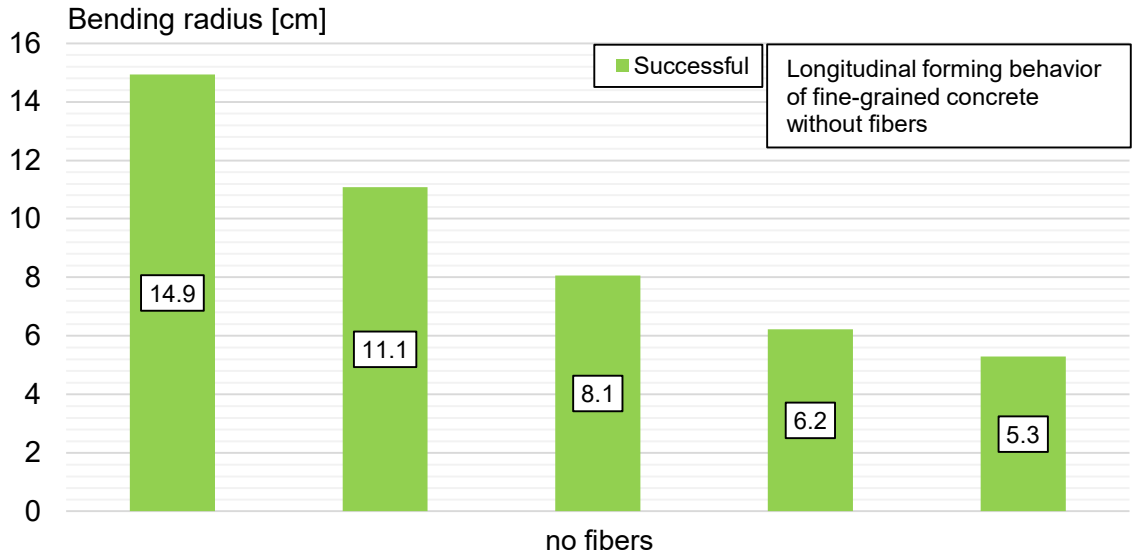

Figure 5-8: Successfully achieved bending radii of longitudinally formed specimens (no fibers and no textile reinforcement)

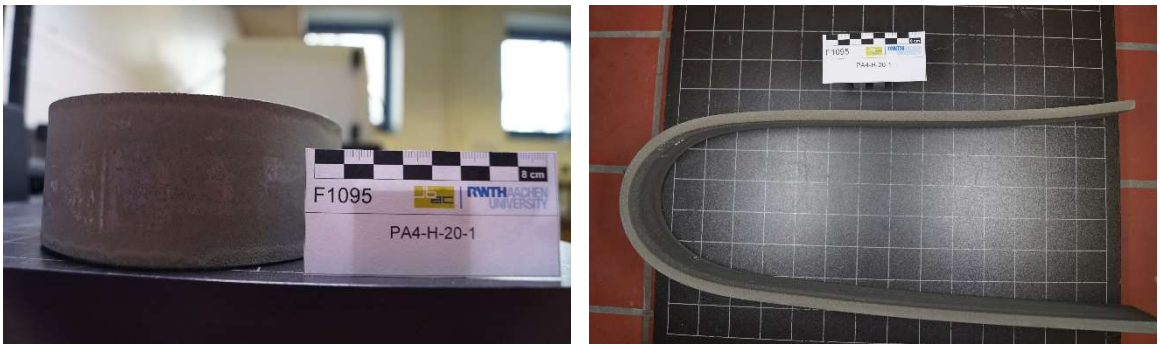

Figure 5-9: Longitudinally formed concrete specimen without visible cracks (no fibers and no textile reinforcement) – bending radius approx. 6.2 cm

To achieve bending radii in these orders, the fixing point distances had to be chosen very low. In this test series, the minimum fixing point distance was approx. 10 cm. Thus, some concrete specimens hanged vertical or even over vertical. In [Woe17] it is stated that the fold-in-fresh principle can be used for limited folding angles since the concrete would slip. However, the concrete mixture used within this master's thesis proved to be capable of achieving any angle due to its stiff consistency, extending the application spectrum of the fold-in-fresh principle.

Figure 5-10: Vertical hanging concrete specimen without slipping (no fibers and no textile reinforcement)

The extrudates made from the base concrete mixture without fibers and textile reinforcement could be formed in longitudinal direction without visible cracks for bending radii of up to approx. 5.3 cm. Since no cracks occurred for the minimal achieved bending radius, it cannot be stated whether cracks would occur for smaller bending radii or not.

5.3 Tests with 0.25 vol.-% of fibers and without textile reinforcement

Two test series were carried out with a fiber content of 0.25 vol.-%. Test series 5 was carried out with PVA fibers of the “soft” type and test series 6 was carried out with basalt fibers.

5.3.1 Transversally formed specimens

The transversally formed extrudates with 0.25 vol.-% of fibers showed similar results to the reference test series without fibers: visible cracks occurred for concrete specimens formed with DN 50 and DN 75 pipes for “soft” PVA and basalt fibers, respectively. For specimens formed with DN 160 and DN 110 pipes no visible cracks occurred.

Figure 5-11: Transversally formed concrete specimen with visible cracks of approx. 0.2 mm (0.25 vol.-% of “soft” PVA fibers and no textile reinforcement) – bending radius approx. 4.5 cm

The figure above shows a transversally formed concrete specimen with visible cracks. Cracks can be seen in the bottom right part of the left image. Furthermore, the left image shows the influence of the used roller. In this case a plastic roller was used, which left some obvious marks, especially on the edges. For this reason, the specimens were not pushed

into shape with a roller in later tests, but by hand. A transversally formed specimen of this test series without cracks can be seen in Appendix A.9, Figure A-8.

The figure below summarizes the measured bending radii and the corresponding measured crack widths for test series 5 with 0.25 vol.-% of “soft” PVA fibers. Here four specimens showed measurable cracks. One of those specimens with a bending radius of approx. 3.4 cm showed significant cracks of approx. 0.3 mm width which were located closer to the edges. The corresponding specimen can be seen in Appendix A.9, Figure A-9.

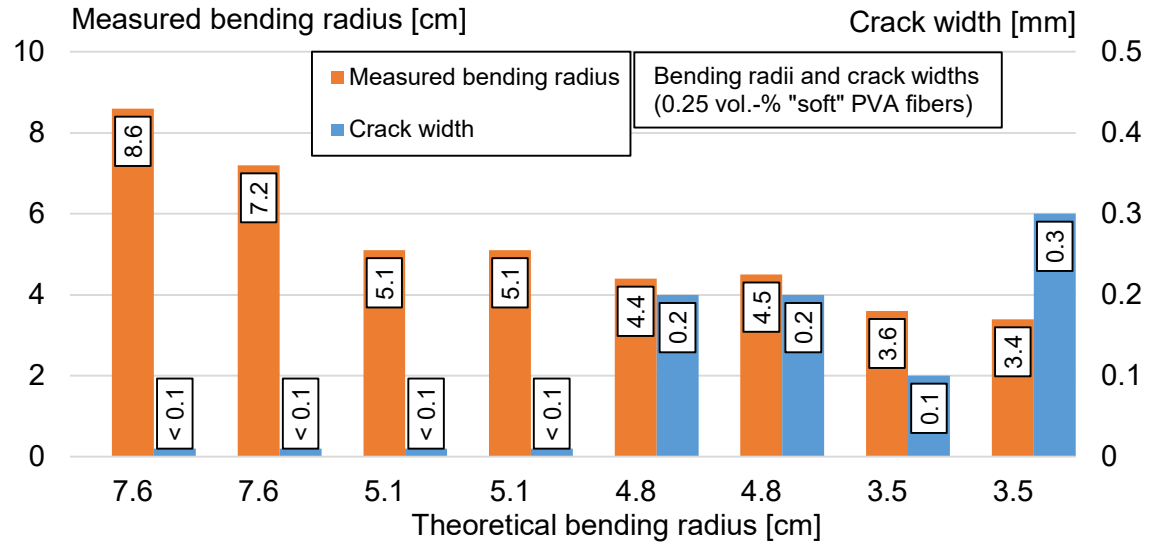

Figure 5-12: Theoretical and measured bending radii with corresponding crack widths (0.25 vol.-% of “soft” PVA fibers and no textile reinforcement)

Figure 5-13 shows the same measured parameters as the diagram above, however, for test series 6 with 0.25 vol.-% of basalt fibers. It shows similar results as the test series with 0.25 vol.-% of “soft” PVA fibers with on average slightly larger crack widths. An uncracked and a cracked specimen of this test series can be seen in Appendix A.9, Figure A-10 and Figure A-11.

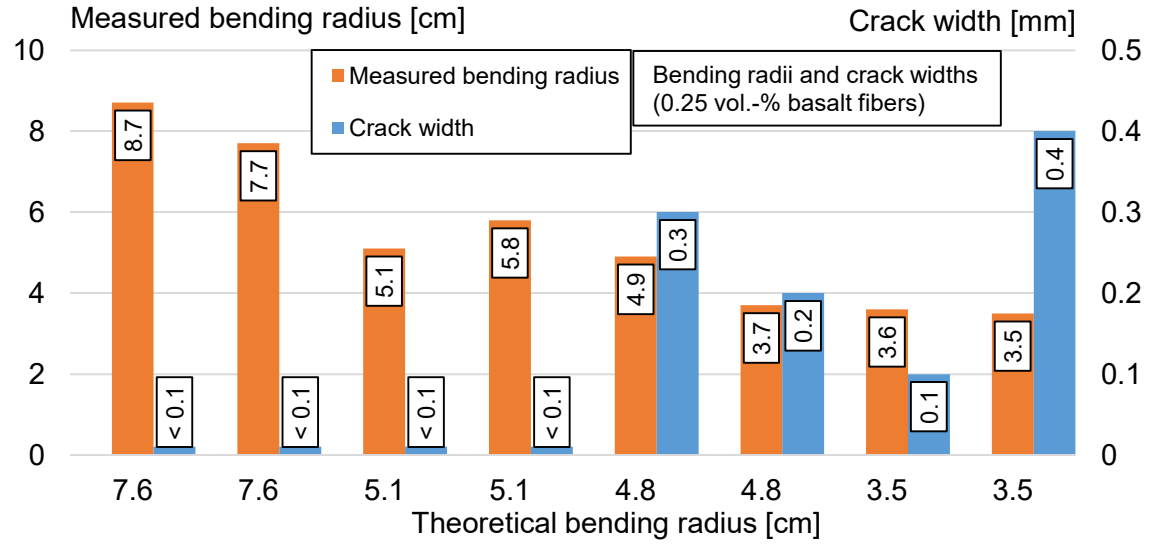

Figure 5-13: Theoretical and measured bending radii with corresponding crack widths (0.25 vol.-% of basalt fibers and no textile reinforcement)

Extrudates made from the concrete mixtures with 0.25 vol.-% of “soft” PVA fibers or basalt fibers showed similar results. The specimens could be formed in transverse direction without visible cracks for bending radii of up to approx. 5.1 cm. For bending radii of 4.9 cm and below cracks occurred and thus, the forming of the specimens was unsuccessful.

5.3.2 Longitudinally formed specimens

For all extrudates formed in longitudinal direction of these two test series no visible cracks occurred that were caused by forming and thus, all were successful. An exemplary longitudinally formed concrete specimen is given in the figure below. Furthermore, Figure 5-15 summarizes the successfully achieved bending radii. Relevant measured and calculated parameters can be found in Appendix A.10.

Figure 5-14: Longitudinally formed concrete specimen without visible cracks (0.25 vol.-% of basalt fibers and no textile reinforcement) – bending radius approx. 5.7 cm

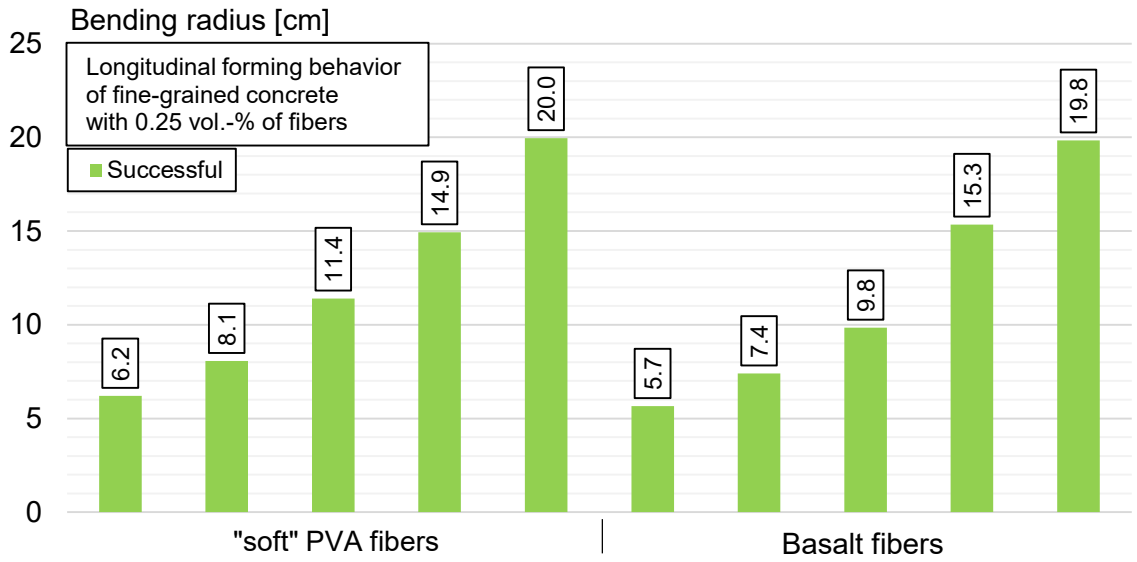

Figure 5-15: Successfully achieved bending radii of longitudinally formed specimens (0.25 vol.-% of “soft” PVA fibers or basalt fibers and no textile reinforcement)

The extrudates made from the concrete mixtures with 0.25 vol.-% of “soft” PVA fibers and basalt fibers showed similar results. The specimens could be formed in longitudinal direction without visible cracks for bending radii of up to approx. 5.7 cm. Since no visible cracks occurred for the minimal achieved bending radius, it cannot be stated whether cracks would occur for smaller bending radii or not.

5.4 Tests with 0.5 vol.-% of fibers and without textile reinforcement

Three test series were carried out with a fiber content of 0.5 vol.-% and no textile reinforcement. Test series 1 was carried out with PVA fibers of the “hard” type, test series 2 was carried out with “soft” PVA fibers, and test series 3 was carried out with basalt fibers.

5.4.1 Transversally formed specimens

The transversally formed extrudates with 0.5 vol.-% of fibers and no textile reinforcement must be distinguished in two groups: the first group consists of test series 1 and 2 with PVA fibers, where the bending was achieved solely by gravity. No mechanical force was applied from the outside to form the concrete. However, as mentioned in chapter 4.3.1, it was concluded to force the deformation starting with test series 3. Thus, the specimens of test series 3 form the second group in which mechanical force was applied to achieve the desired bending radii.

The two test series with PVA fibers showed no cracks for the transversally formed specimens. However, the specimens did not form properly around the used pipes. Thus, the achieved bending radii differed significantly from the intended ones and furthermore the results scattered a lot. Figure 5-16 shows the average standard deviation in percent of the average bending radii. For the test series with PVA fibers, the standard deviation is on average significantly higher. This proves that the specimens were not uniformly bent around the pipes and the bending radii varied significantly over the length of the specimens. The measured bending radii can be seen in Appendix A.9, Figure A-12 and Figure A-13.

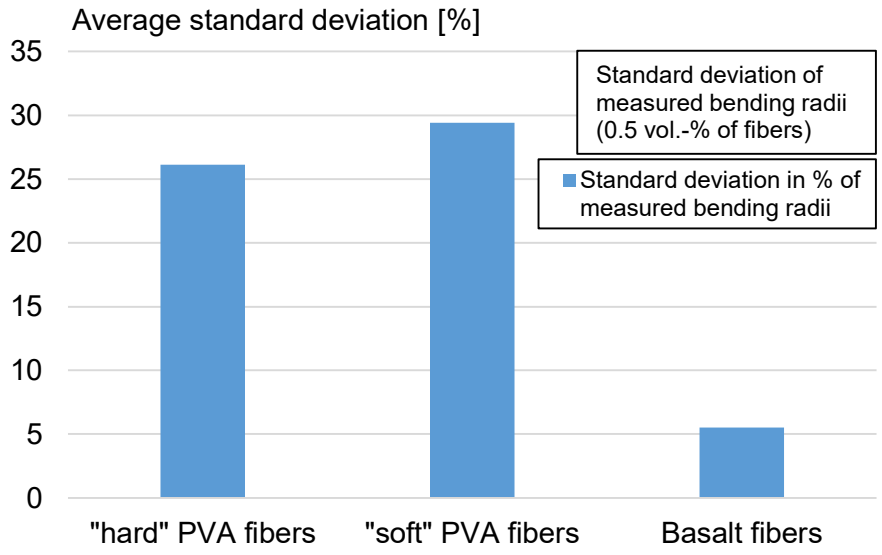

Figure 5-16: Average standard deviation in percent of the average bending radii for specimens with 0.5 vol.-% of fibers and no textile reinforcement

Figure 5-17 shows a specimen of the first test series with “hard” PVA fibers. Besides the fact that it was not properly bent, it can be seen that the fibers leave clear marks in the concrete (compared to “soft” PVA fibers, see e. g. Appendix A.9, Figure A-8). The “hard” PVA fibers are approx. 8 times thicker than the “soft” PVA fibers (Table 4-3, page 49) and thus significantly stiffer leading to those marks. At that point it was already known that new fibers of PVA type “soft” with improved properties were ordered, however, they were not available for the first test series.

Figure 5-17: Transversally formed concrete specimen without visible cracks (0.5 vol.-% of "hard" PVA fibers and no textile reinforcement) – bending radius approx. 28.0 cm

For the third test series with 0.5 vol.-% of basalt fibers, mechanical force was applied using a roller to bend the concrete specimen properly around the pipe. For the larger diameter pipes DN 110 and DN 160 a smaller pipe was used to apply the force on the concrete specimens. The results are similar as for the concrete specimens without fibers and 0.25 vol.-% of fibers: the specimens formed with the smaller pipes DN 50 and DN 75 showed cracks caused by the forming procedure (Appendix A.9, Figure A-14), while the specimens with larger bending radii did not show visible cracks caused by forming (Figure 5-18).

Figure 5-18: Transversally formed concrete specimen without visible cracks (0.5 vol.-% of basalt fibers and no textile reinforcement) – bending radius approx. 5.6 cm

Figure 5-19 shows the theoretical and measured bending radii and corresponding crack widths of the test series with 0.5 vol.-% of basalt fibers. Visible cracks occurred for bending radii of 4.8 cm and below. Furthermore, the crack widths increased for smaller bending radii. One bending radius could not be measured and thus, the theoretical value is given.

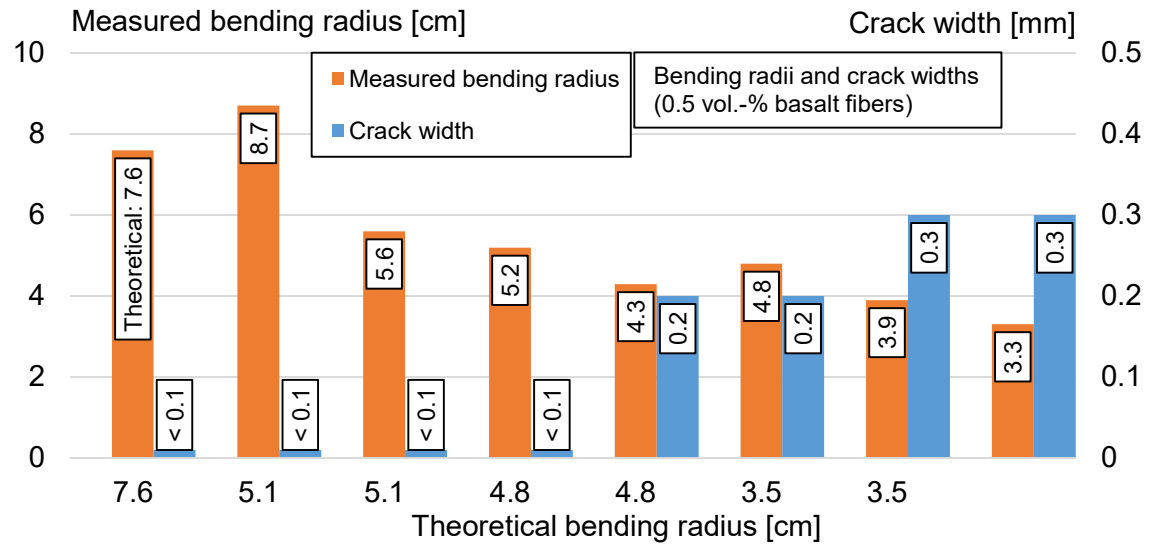

Figure 5-19: Theoretical and measured bending radii with corresponding crack widths (0.5 vol.-% of basalt fibers and no textile reinforcement)

As the figure above shows, extrudates made from the concrete mixtures with 0.5 vol.-% of basalt fibers could be formed in transverse direction without visible cracks for bending radii of up to approx. 5.2 cm. The two test series with 0.5 vol.-% of PVA fibers were both not properly formed and thus were not evaluated. However, they exhibited no visible cracks.

5.4.2 Longitudinally formed specimens

For all extrudates formed in longitudinal direction of these three test series no visible cracks occurred that were caused by forming and thus, the forming of all specimens was successful. Relevant measured and calculated parameters can be found in Appendix A.10. The figure below summarizes the successfully achieved bending radii. Furthermore, an exemplary longitudinally formed concrete specimen is given in Figure 5-21.

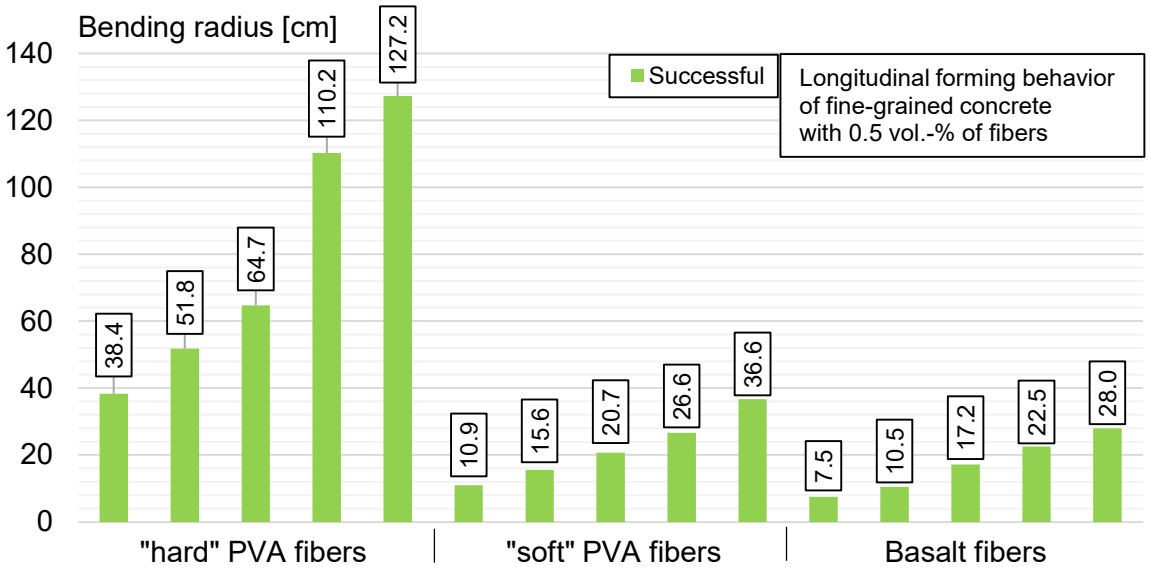

Figure 5-20: Successfully achieved bending radii of longitudinally formed specimens (0.5 vol.-% of "hard" PVA fibers. "soft" PVA fibers, or basalt fibers and no textile reinforcement)

Figure 5-21: Longitudinally formed concrete specimen without cracks (0.5 vol.-% of basalt fibers and no textile reinforcement) – bending radius approx. 7.5 cm

The extrudates made from the concrete mixtures with 0.5 vol.-% of “hard” PVA fibers, “soft” PVA fibers, and basalt fibers showed no visible cracks during longitudinal forming. The specimens could be formed for bending radii of up to approx. 38.4 cm (for “hard” PVA fibers), 10.9 cm (for “soft” PVA fibers), and 7.5 cm (for basalt fibers). However, those values do not allow for a comparison between the fiber types since all those values were the minimum intended bending radii and it cannot be state whether cracks would occur for smaller bending radii or not. For the first test series, more conservative assumptions for the bending radii were chosen than for the following test series which is why the minimal bending radii decrease in later test series.

5.5 Tests with textile reinforcement

Two test series were carried out with a fiber content of 0.5 vol.-% of “soft” PVA fibers and textile reinforcement. Test series 7 was carried out with textile reinforcement made from ar-glass and test series 8 was carried out with carbon textile reinforcement. Properties of the used textiles can be found in Table 4-4, page 50.

5.5.1 Transversally formed specimens

For the two test series with textile reinforcement, the same pipes were used as for the specimens without textile reinforcement. However, it turned out that the textile fabrics significantly increased the stiffness of the specimens, which previously formed well to the pipes without textile reinforcement, but now exhibited significant resistance. This effect was stronger for the carbon textile, but it also occurred for the ar-glass textile. Thus, to achieve forming around the pipe, much more force had to be applied and already during manufacturing a spring-like reaction of the specimens was observed i. e. after letting the force go, the specimens went back into a straighter position. Thus, no proper bending could be achieved. Comparable to the first and second test series, where no proper bending was achieved, the standard deviation of the measured bending radii was significantly higher for the textile reinforced specimens. Figure 5-22 shows the standard deviation of the measured bending radii in percent of the average measured bending radii. It shows that the standard deviation for the TRC specimens was on average significantly higher. This proves that the specimens were not uniformly bent around the pipes and the bending radii varied significantly over the length of the specimens.

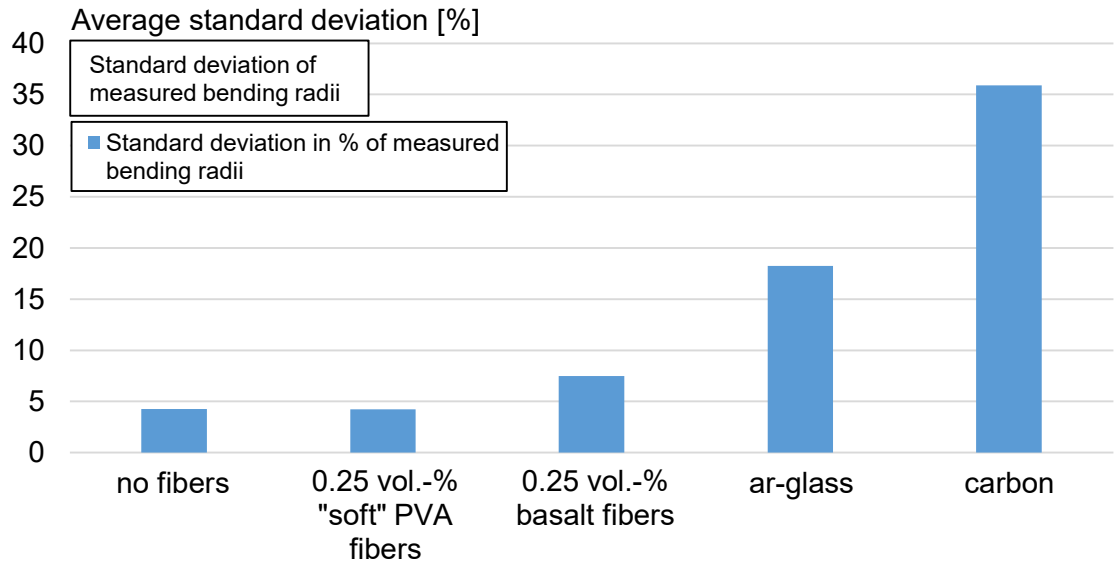

Figure 5-22: Average standard deviation in percent of the average bending radii for specimens of test series 4 to series 8

Furthermore, the ends of the concrete specimens were cut off after curing to make the TRC structure visible. The figure below shows a carbon textile reinforced specimen. An ar-glass reinforced specimen can be seen in Appendix A.9, Figure A-15.

Figure 5-23: Transversally formed concrete specimen without visible cracks (0.5 vol.-% of "soft" PVA fibers and carbon textile reinforcement) – bending radius approx. 5.0 cm

The movement of the textile reinforcement inside the concrete, which caused the spring-like behavior of the specimens, can be seen in Figure 5-24. Furthermore, it shows that the compound zone is damaged due to the movement of the fabrics and the shape of the cross-section changed to a flat top with curved edges. However, no visible cracks caused by bending occurred on the surfaces of the concrete specimens. Yet, the intended bending radii were not reached and unequal over the length of the specimens.

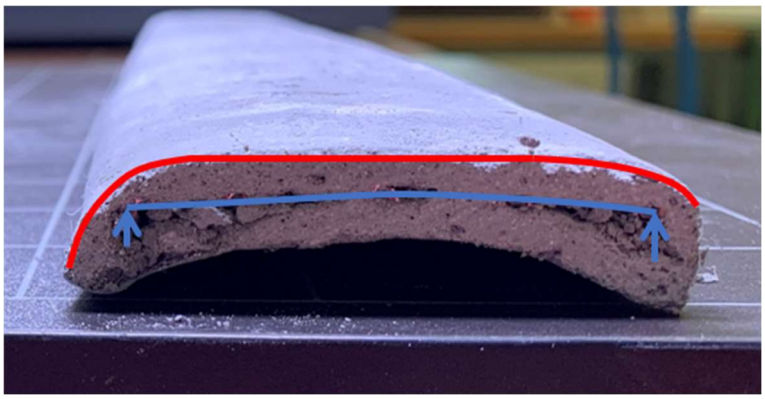

Figure 5-24: Movement of carbon textile reinforcement and change of cross-section shape caused by transverse forming

For the carbon textile reinforced specimen shown in Figure 5-24, the measurements of the bending radius scattered between 1.9 cm and 8.7 cm. This results from the flat top which is nearly not bent while the edges are strongly curved. For ar-glass reinforced specimens, the results scattered less on average (Figure 5-22), however, still significant. The measured average bending radii, as well as highest and lowest measured values are given in Appendix A.9, Figure A-16 and Figure A-17. The figures show the scatter of the results and the deviation from the intended bending radii. Thus, the transversally forming was unsuccessful.

5.5.2 Longitudinally formed specimens

For bending in longitudinal direction different types of failures occurred during the tests. Earlier tests with 0.5 vol.-% of “soft” PVA fibers proved that the concrete could perform bending with radii of up to 10.9 cm. However, the stiffness of the textile reinforcements limited proper bending.

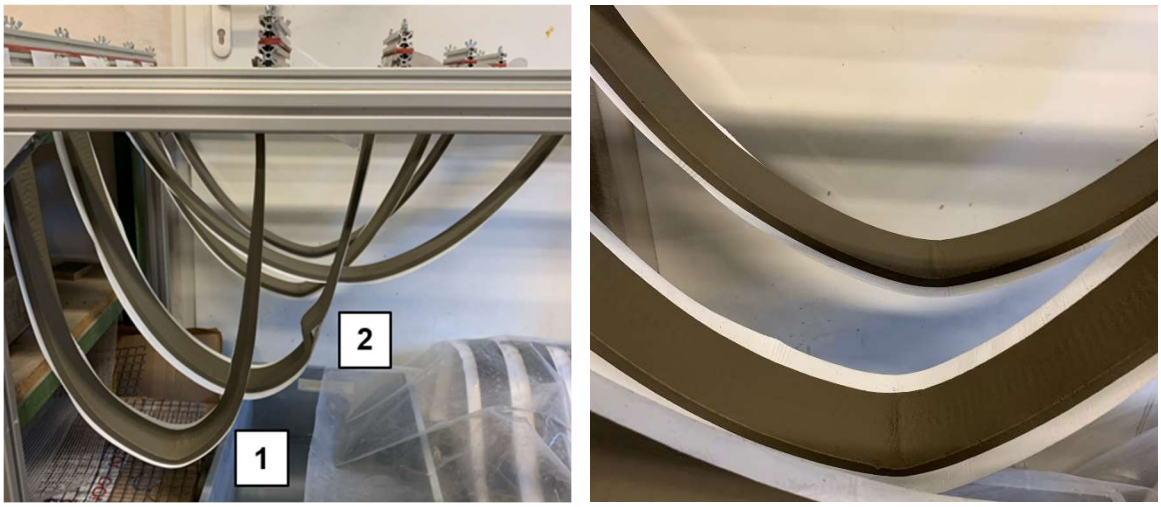

Figure 5-25: Test series with 0.5 vol.-% of “soft” PVA fibers and ar-glass textile reinforcement showing kinks and buckling during longitudinal forming – 1) kink in the apex zone 2) buckling

As the figures above show, the use of ar-glass reinforcement led to kinks and buckling in some concrete specimens. The kinks occurred just before a fixing point distance of approx. 70 cm which would correspond to a bending radius of approx. 19.8 cm considering a theoretical catenary. However, the concrete showed no visible cracks caused by bending on the surface. Yet, due to the kink it was not possible to properly determine the bending radii of those specimens. The standard deviation of the measured bending radii can be seen

in Appendix A.9, Figure A-20 for ar-glass as well as carbon textile reinforced specimens. The kink was probably caused by the fact that the ar-glass textile, which had a very small mesh size, prevented the concrete from its deformation due to compression on the surface of the inner bending radius and tension on the surface of the outer bending radius. Thus, the stress in the concrete increased and would be released after it reached a certain amount, causing a kink or buckling on either the point of maximum stress or near a point which already had a local failure and thus, was a stress peak. Specimens with kinks were counted as unsuccessful in longitudinal forming as explained in chapter 5.1. However, since they did not show cracks on the surface the failure might just be visual and the question arises, whether the load-bearing capacity of these elements is limited (more in chapter 5.7). The figure below shows a successfully formed specimen with a bending radius of approx. 30.6 cm. An unsuccessfully formed specimen can be seen in Appendix A.9, Figure A-18. Furthermore, a comparison of the surfaces of successfully and unsuccessfully formed specimens is given in Appendix A.9, Figure A-19.

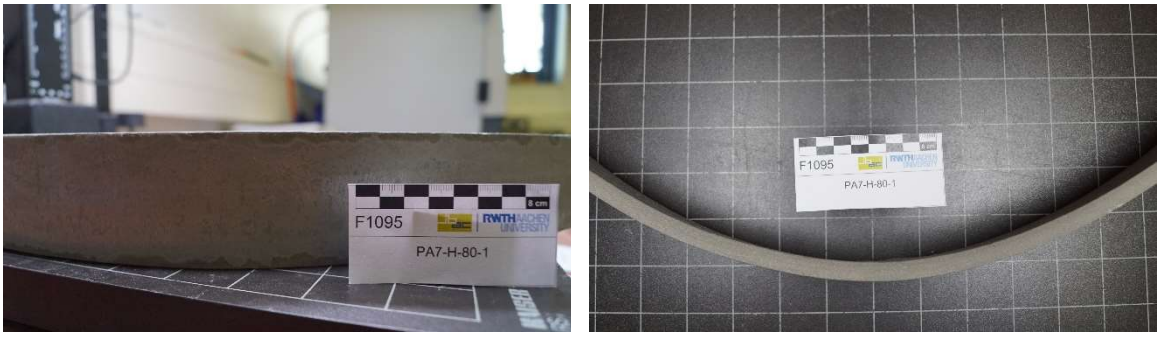

Figure 5-26: Longitudinally formed concrete specimen without visible cracks (0.5 vol.-% of "soft" PVA fibers and ar-glass textile reinforcement) – bending radius approx. 30.6 cm

One specimen exhibited significantly larger buckling than the others (Figure 5-25, page 83, number 2). This failure was probably caused by a small kink already existing in the specimen, so that a stress peak would occur, and the stresses relieved at this point formed a larger buckle. A figure that presents this specimen in more detail can be found in Appendix A.9, Figure A-21.

For the carbon textile reinforced specimens, kinks occurred as well (Figure 5-27). However, the kinks occurred for smaller bending radii than for the ar-glass reinforced specimens, starting with a fixing point distance of approx. 45 cm which would correspond to a bending radius of approx. 10.4 cm considering a catenary. Furthermore, the failure mode was different: it could be observed that the kink occurred in the textile and not as for the ar-glass in the concrete. The fine-grained concrete would maintain the shape of its cross-section until just before the kink occurred, and then it would deform lateral. Thus, the kinks in the carbon reinforced specimens were sharper and it can be assumed that the carbon textile is broken.

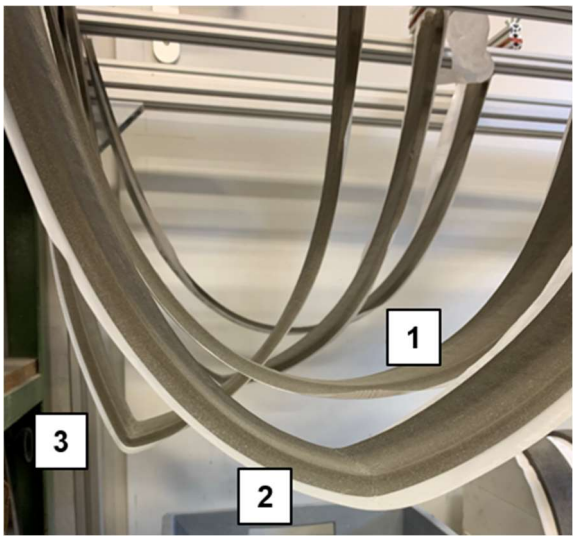

Figure 5-27: Test series with 0.5 vol.-% of "soft" PVA fibers and carbon textile reinforcement showing kinks during longitudinal forming – 1) no kink 2) kink occurred in carbon textile 3) further development of the kink

Consequently, it can be stated that the forming behavior of the carbon textile used within this master's thesis is particularly more brittle than the behavior of the used ar-glass. Table A-11 in Appendix A.10 shows that the carbon reinforced specimens deviated significantly from the catenary and thus, the resulting bending radii were significantly larger than expected. This is caused by the stiffness of the carbon textile which resists the free deformation due to gravity. However, with increased stiffness, the carbon textile exhibited more brittle behavior compared to the ar-glass. At a certain bending radius, the carbon textile would break, resulting in a kink in the concrete and a sudden lower hanging of the concrete. However, even for the sharpest kink (Figure 5-27, number 3) no visible cracks occurred on the surface of the concrete caused by forming. The figure below shows a successfully formed carbon textile reinforced specimen with a bending radius of approx. 25.5 cm. An unsuccessfully formed specimen with a sharp kink can be seen in Appendix A.9, Figure A-22.

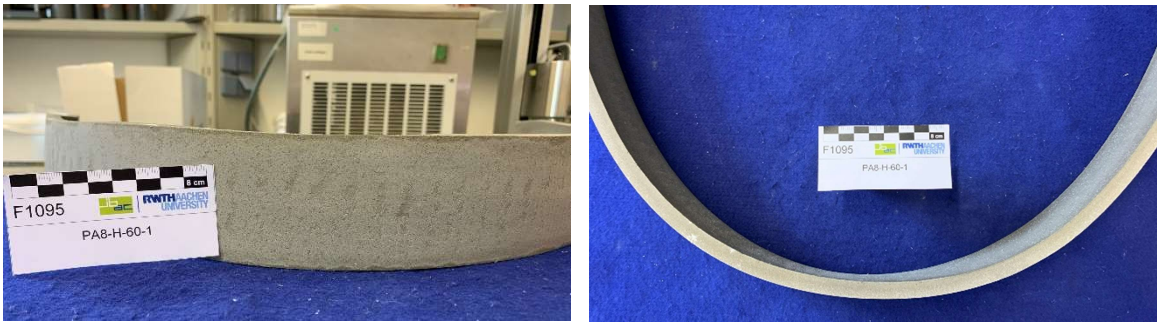

Figure 5-28: Longitudinally formed concrete specimen without visible cracks (0.5 vol.-% of "soft" PVA fibers and carbon textile reinforcement) – bending radius approx. 25.5 cm

Extrudates made from the concrete mixtures with 0.5 vol.-% of "soft" PVA fibers with ar-glass or carbon textile reinforcements showed different types of failure during longitudinal bending. The ar-glass seemed to have limited the movement of the fine-grained concrete causing buckling and kinks. The carbon textile seemed to be stiffer than the ar-glass leading to significantly lower bending radii than calculated. However, the carbon textile exhibited more brittle behavior leading to sudden kinks. For the ar-glass reinforced specimens, a

minimal bending radius of approx. 30.6 cm could be achieved (Figure 5-29), whereas for the carbon reinforced specimen a minimal bending radius of 19.7 cm could be achieved. Tables with measured values can be found in Appendix A.10 (Table A-10 and Table A-11).

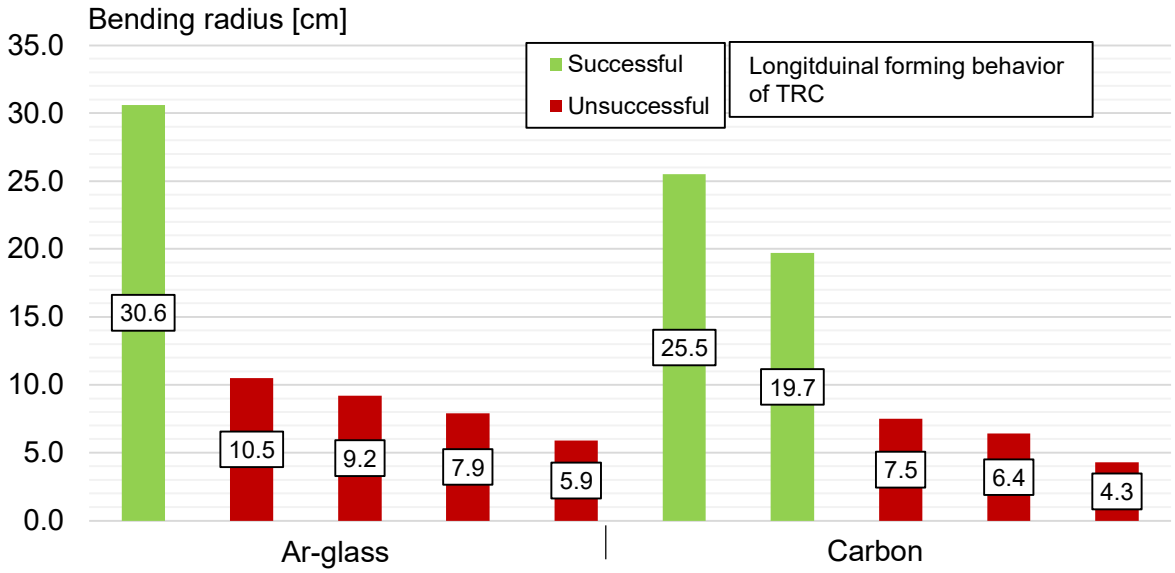

Figure 5-29: Successfully achieved and unsuccessful bending radii of longitudinally formed specimens (0.5 vol.-% of "soft" PVA fibers and textile reinforcement)

5.6 Double curved elements

In two test series furthermore, double curved elements were produced. Therefore, the developed negative formwork as explained in chapter 4.3.3 was used. The visual analysis of the specimens and resulting bending radii will be presented in this chapter. Since the specimens were placed in the formwork, the bending radius was already defined. However, the actually achieved bending radius was measured after curing to analyze possible differences.

5.6.1 Specimens with 0.25 vol.-% of fibers

For the test series with 0.25 vol.-% of "soft" PVA or basalt fibers, in total 6 double curved elements were produced. The bending radii of these elements were defined by the formwork. The catenary on which the production of the formwork was based on has a bending radius of 11.1 cm. However, slight differences to this value occurred since minor gaps formed between formwork and specimens. The maximum value measured within these two test series was 11.9 cm while the minimum value was 11.0 cm. On average the physically achieved bending radius was 11.3 cm and thus, it was very close to the desired radius. Considering the scatter of the measurements it can be stated that the concrete specimens adapted very well to the formwork.

Figure 5-30: Double curved concrete specimens without visible cracks (0.25 vol.-% of "soft" PVA fibers and no textile reinforcement) – bending radius of the intermediate curvature on average 11.1 cm

The double curved specimens of test series 5 with 0.25 vol.-% of "soft" PVA fibers showed overall no visible cracks caused by forming (Figure 5-30). Furthermore, the average achieved bending radius of the intermediate catenary was 11.1 cm and thus, it was nearly exactly the desired bending radius. However, the double curved elements of test series 6 with 0.25 vol.-% of basalt fibers showed cracks in transverse direction. Significant transverse cracks were found on the inside and on the outside of the curvature. However, the cracks on the inside are unlikely to be caused by bending since this area gets compressed during the forming process. Furthermore, many cracks were found to be close to the edges where imperfections are more likely to occur during extrusion and thus encourage crack development. Thus, it is concluded that those cracks were caused by shrinkage due to possibly unequal curing conditions. Furthermore, one specimen of this test series already failed when taking it out of the formwork. It can be seen in Appendix A.9, Figure A-23.

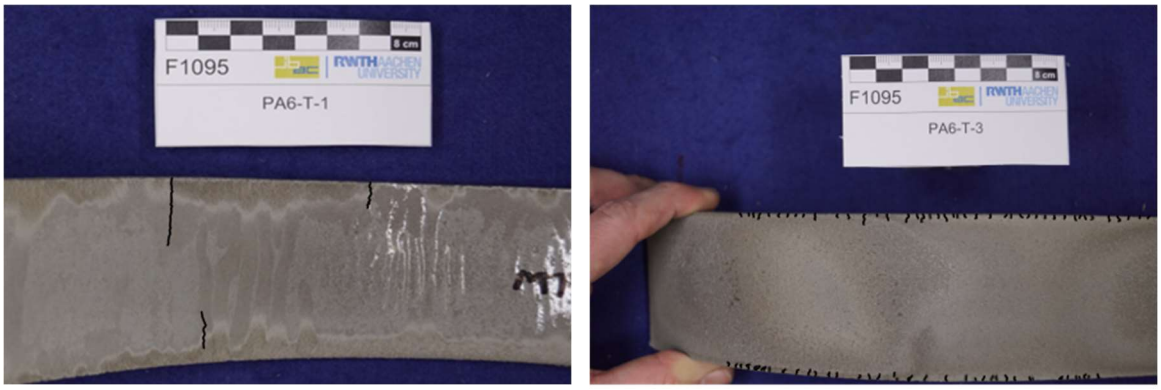

Figure 5-31: Double curved concrete specimens with visible cracks (0.25 vol.-% of basalt fibers and no textile reinforcement) – bending radius of the intermediate curvature on average 11.6 cm

5.6.2 Specimens with textile reinforcement

For the two test series with 0.5 vol.-% of "soft" PVA fibers and textile reinforcement, double curved elements for the purpose of testing their flexural strength in three-point bending test were produced.

As already mentioned before, slight differences between the bending radius of the formwork and the specimens occurred due to minor gaps. The maximum value of the bending radius measured for the ar-glass specimens was 12.3 cm while the minimum value was 11.2 cm. For the carbon reinforced specimens, the maximum value was 11.2 cm and the minimum value was 10.3 cm. Considering the scatter of the measurements it can be stated that the concrete specimens adapted very well to the formwork for both textiles.

The double curved elements with ar-glass reinforcement showed similar buckling behavior as the longitudinally formed ones. However, the buckling occurred only on the inner bending radius, which is under compression and furthermore, it did not lead to significant changes in the cross-section. For one of the three specimens with ar-glass a kink occurred in the apex zone leading to the most significant cross-section change of those three specimens. It is shown in Figure 5-32. However, the figure shows that no visible cracks caused by bending occurred.

Figure 5-32: Double curved concrete specimens with kink (0.5 vol.-% of "soft" PVA fibers and ar-glass textile reinforcement) – bending radius of the intermediate curvature approx. 11.2 cm

The double curved elements made with carbon reinforcement showed no defects in terms of kinks or buckling and furthermore, no visible cracks caused by bending could be seen (Figure 5-33).

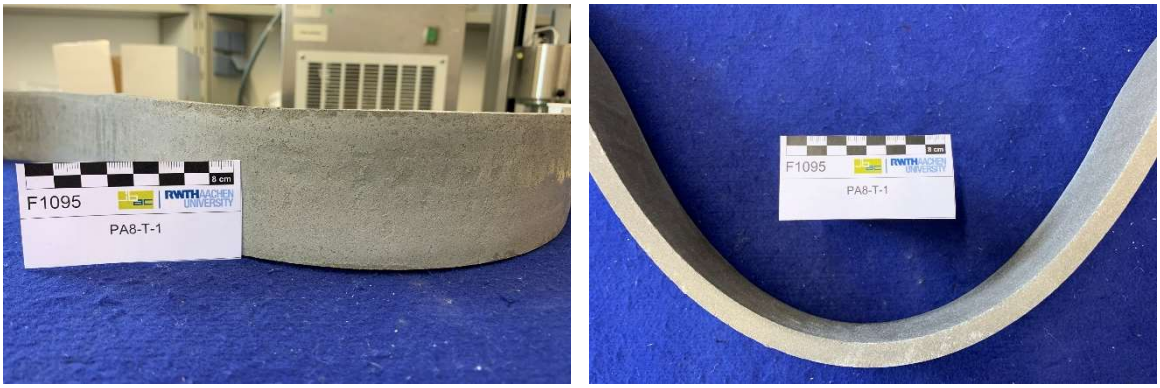

Figure 5-33: Double curved concrete specimens without visible cracks (0.5 vol.-% of "soft" PVA fibers and carbon textile reinforcement) – bending radius of the intermediate curvature approx. 11.2 cm

The bending radii achieved in the double-curved TRC elements are smaller than those in the free-hanging formed elements without significant kinks or buckling. This can be attributed to the fact that the specimens were not pulled down by gravity during forming and thus less compressive forces were generated that would lead to kinks. For the specimens with ar-glass, however, slight buckling occurred when they were placed in the formwork already. Properties of the used textiles can be found in Table 4-4, page 50. The results of the three-point bending tests are given in the following chapter.

5.7 Three-point bending tests

In total 11 three-point bending tests were carried out to analyze the flexural strength of the double curved elements. The test set-up and the execution of the tests was already explained in chapter 4.3.3. Within this chapter the resulting force-deflection diagrams are

given and analyzed. Furthermore, the stresses were calculated from the forces for better comparison of the results. However, the test set-up made this a complex problem, so that many assumptions had to be made. Therefore, the cross-section of the specimens was measured first. Then a static system had to be found representing the test set-up. However, the horizontal bearing resistance could not be determined and furthermore, the horizontal deflection has not been measured during the tests. Moreover, the TRC specimens are made from a composite material and the separate concrete and textile reinforcement areas were not determined. The calculated stresses and resulting stress-strain diagrams are given in Appendix A.13. However, it was concluded that the force-deflection diagrams suit better for comparison since the force is a real measured value without assumptions.

5.7.1 Specimens without textile reinforcement

5 specimens with 0.25 vol.-% of “soft” PVA fibers or basalt fibers and without textile reinforcement were tested first. Brittle behavior and a sudden failure were estimated, which the tests approved. The figure below shows the force-deflection diagram exemplary for a specimen with basalt fibers. The maximum applied force was approx. 234 N with a corresponding deflection of approx. 2.4 mm before brittle failure occurred.

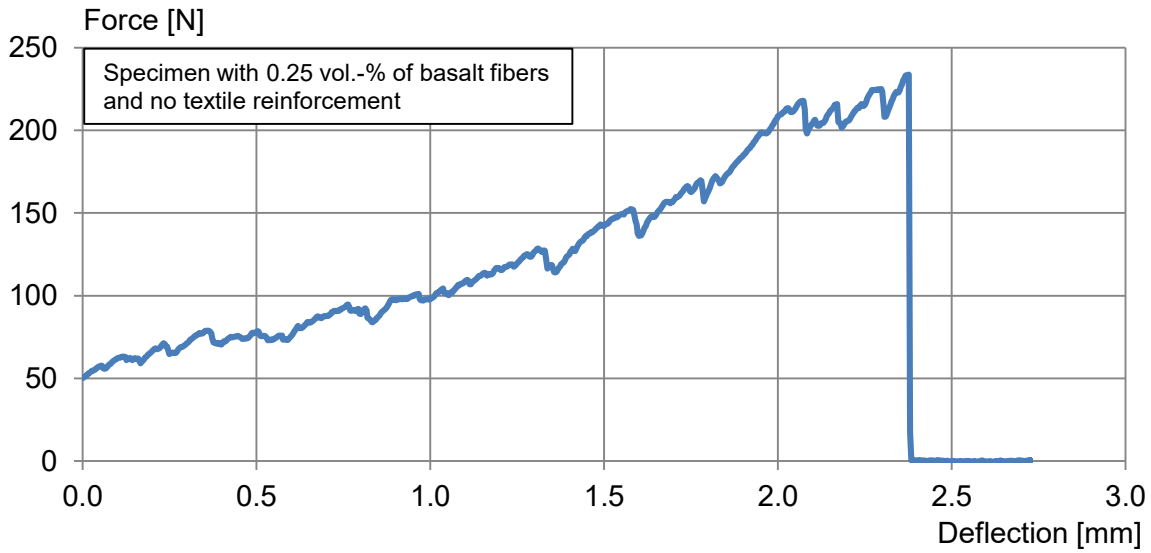

Figure 5-34: Load-deflection diagram of specimen with 0.25 vol.-% of basalt fibers and no textile reinforcement

The forces at failure for all 5 specimens without textile reinforcement are given in Figure 5-35. The testing age was 37 days for test series with “soft” PVA fibers and 41 days for the test series with basalt fibers. All specimens showed similar brittle behavior. Figure 5-36 shows a specimen shortly after failure. The critical crack occurred slightly off-center. As mentioned earlier, one specimen failed after curing and thus could not be tested on its flexural strength.

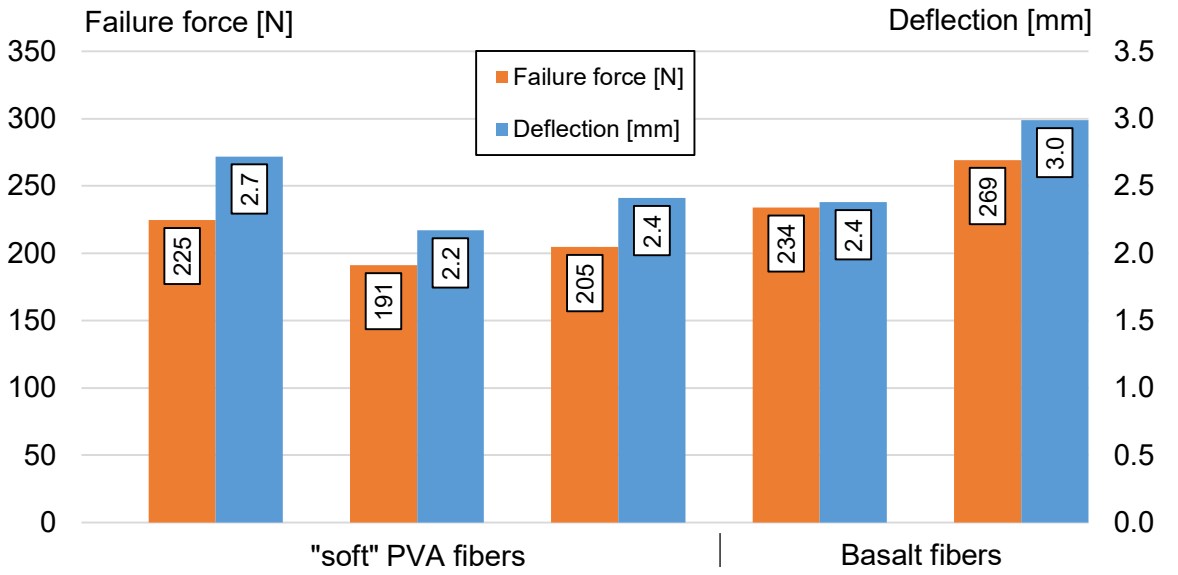

Figure 5-35: Force at failure and corresponding deflection for flexural tests of specimens with 0.25 vol.-% of fibers and no textile reinforcement

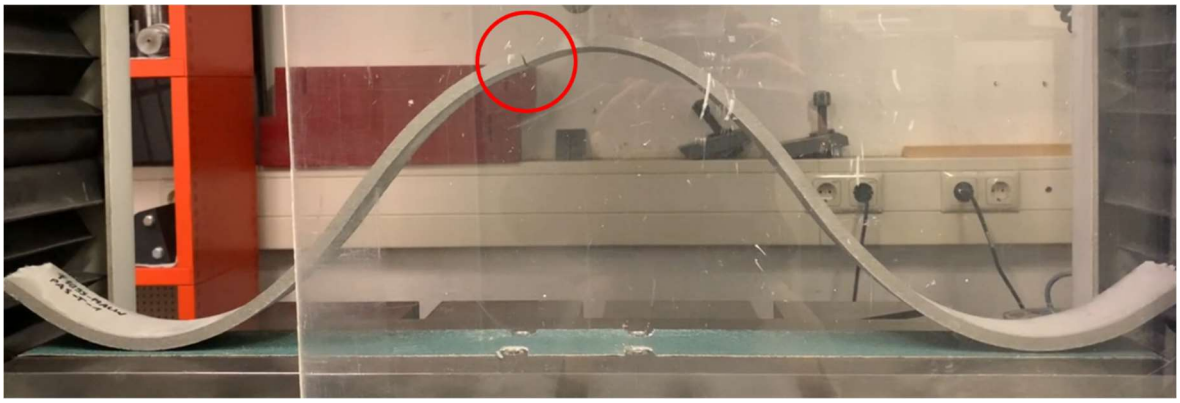

Figure 5-36: Specimen with 0.25 vol.-% of "soft" PVA fibers and no textile reinforcement shortly after failure

5.7.2 Specimens with textile reinforcement

Furthermore, 6 specimens with textile reinforcement and a fiber content of 0.5 vol.-% of "soft" PVA fibers were tested. The behavior of these specimens was expected to be more ductile. However, after the initial crack that led to failure in the FRC specimens, the textile kept the concrete together, but especially the ar-glass reinforced specimens deformed without significant resistance (Figure 5-37). The carbon reinforced specimens showed a slight increase in resistance after the initial crack, but the specimens deformed significantly as well (Figure 5-38). The diagrams below are a cut out of the whole measured force deflection diagram. Complete diagrams can be found in the digital appendix.

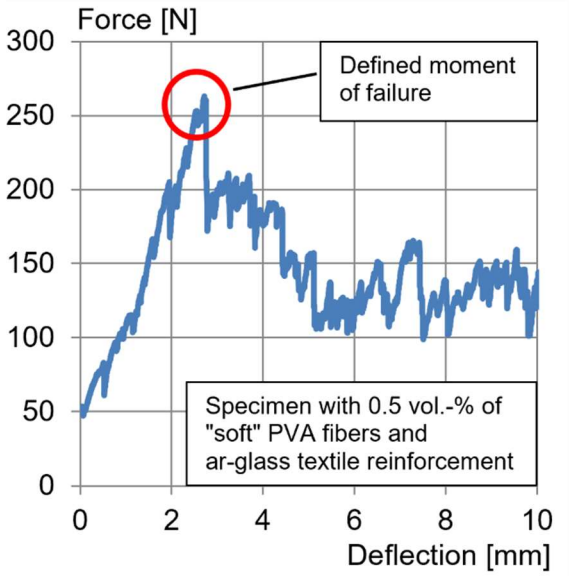

Figure 5-37: Load-deflection diagram of specimen with 0.5 vol.-% of "soft" PVA fibers and ar-glass textile reinforcement

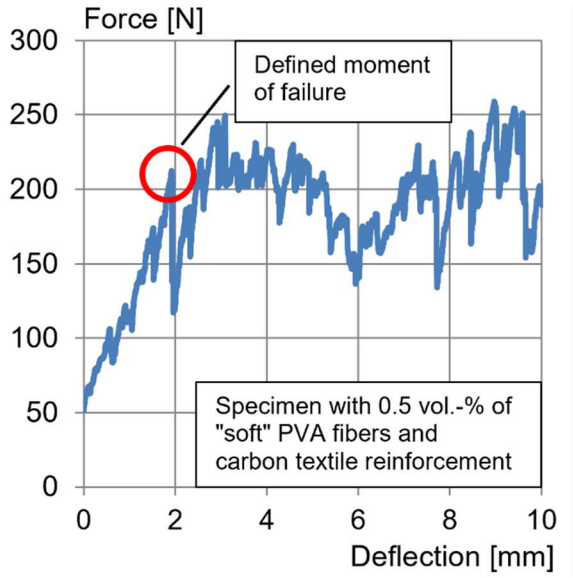

Figure 5-38: Load-deflection diagram of specimen with 0.5 vol.-% of "soft" PVA fibers and carbon textile reinforcement

The failure force was defined as the applied load when the initial crack occurred in the concrete (far left peak, marked with red circle in the diagrams above). As the force-deflection diagrams show, higher resistances could be achieved, however, for significant deflections. For the carbon textile reinforced specimen shown in Figure 5-38, a resistance of approx. 259 N and a corresponding deflection of approx. 9 mm could be achieved. However, deflections in this order for a span of approx. 60 cm are undesired for building components. The figure below summarizes measured failure forces and corresponding deflections. The testing age was 35 days for test series with ar-glass and 27 days for the test series with carbon.

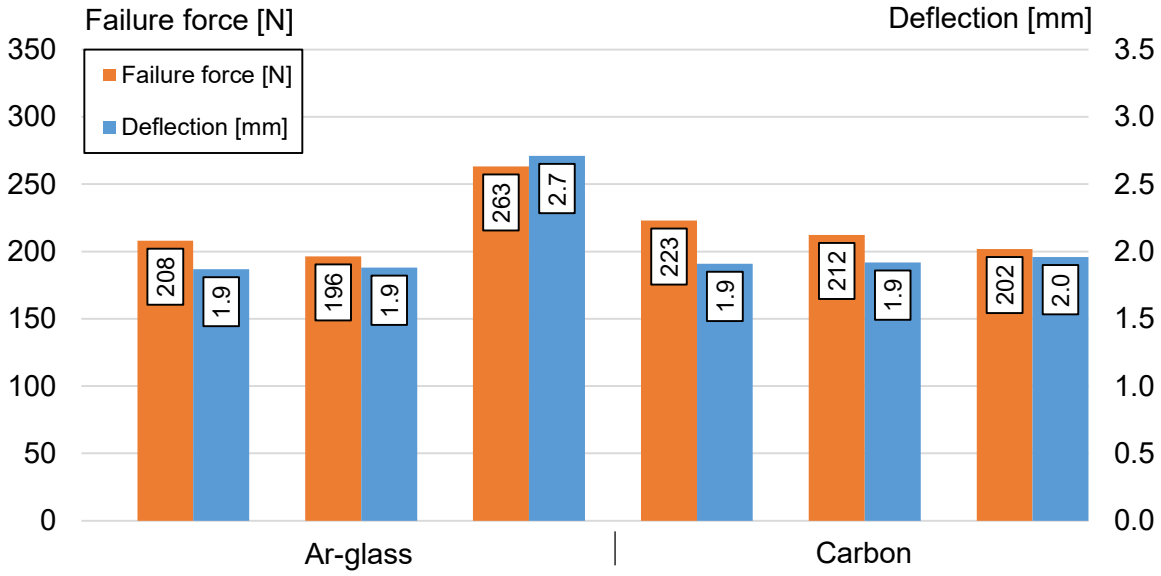

Figure 5-39: Force at failure and corresponding deflection for flexural tests of specimens with 0.25 vol.-% of fibers and no textile reinforcement

The figure below shows a specimen with ar-glass reinforcement at the beginning and the end of the three-point bending test. Besides the vertical movement, it shows that the friction between sandpaper and concrete specimen was not sufficient to keep the specimen in place. Thus, a horizontal movement can be seen as well.

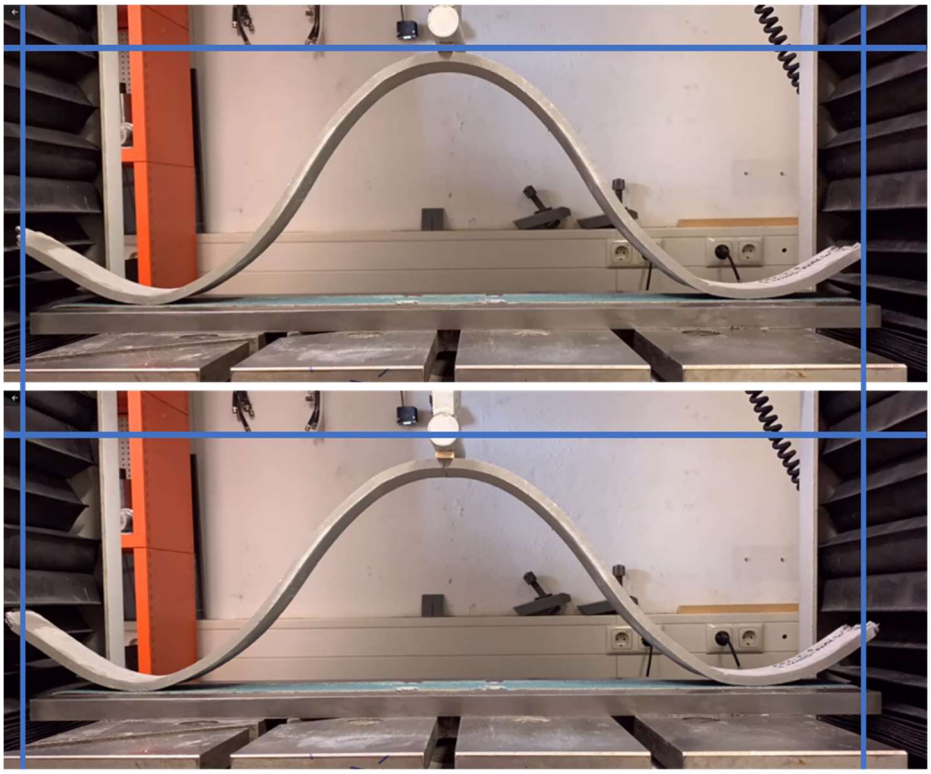

Figure 5-40: Specimen PA7-T-3 with 0.5 vol.-% of "soft" PVA fibers and ar-glass textile reinforcement – at the beginning of the flexural test (top figure) and at the end of the test (bottom figure)

Since the failure load was set to be the force at the initial crack, the textile reinforcements did not change the load-bearing capacity of the double curved elements significantly. However, the behavior of the specimens with textile reinforcement after the initial crack was unfavorable. One specimen with carbon textile reinforcement for example could carry a load of approx. 315 N. However, the corresponding deflection was approx. 17 mm. With a span of approx. 60 cm this gives a value of $L/35$ which is approx. 10 times the value as recommended for building components in DIN EN 1992-1-1 [DIN11].

The initial crack that led to a brittle failure in the FRC specimens occurred on average at approx. 225 N and a corresponding deflection of approx. 2.5 mm. For TRC specimens, more ductile behavior was expected. However, the initial crack occurred for similar loads – on average at approx. 218 N and a deflection of approx. 2 mm deflection – but no significant resistance was obtained afterwards. The specimens deformed significantly and only a slight increase in resistance could be obtained for the carbon textile reinforced specimens, whereas for the ar-glass reinforced specimens no load increase could be obtained. The fact that the TRC specimens showed the initial crack for lower deflections than the FRC specimens (Figure 5-41), is probably due to the disruption of the concrete structure by the textile reinforcement. In the following, exemplary one load-deflection diagram of each test series is given. The FRC specimens are shown until failure load while for the TRC specimens the failure load is marked with an arrow and subsequent behavior is shown

partially. The load-deflection diagrams of all specimens are given until the defined failure load in Appendix A.12. Complete diagrams can be found in the digital appendix.

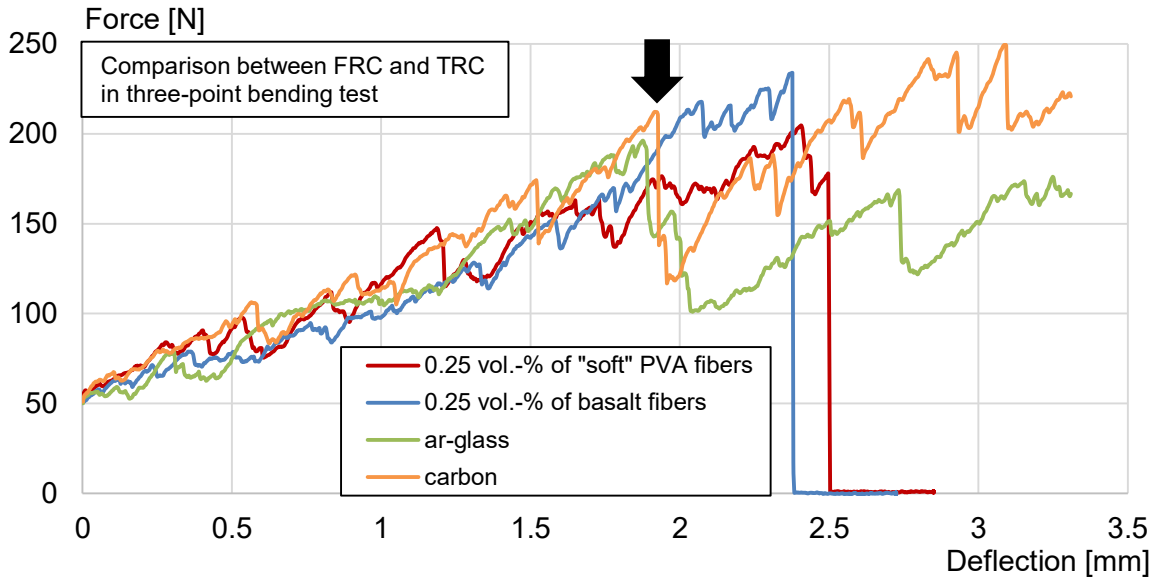

Figure 5-41: Load-deflection diagram of FRC and TRC specimens in comparison

It turned out that the sandpaper did not keep the specimens in place. The influence of the sandpaper can be described as follows: the force increases up to a certain value at which the frictional force is overcome, causing the specimens to slip horizontally leading to a sudden load drop. The specimen then comes to a stop, the load increases again, and the process repeats. In summary, the sandpaper could not represent the bearing situation in a future building component properly. The bearing conditions of the test set-up were based on a possible future building component. The double-curved elements could be used as a structural system for ceilings where the double curved TRC elements could be advantageous in terms of resource efficiency, durability, and load-bearing behavior over the current state of the art which is the use of reinforced concrete flat plates. Therefore, it was chosen to restrain the movement of the support in horizontal direction to a certain degree. The movement should neither be completely free, as it would be if the concrete specimens were placed directly on the steel bearing plate, nor should it be fully restraint. Thus, sandpaper was placed between bearing plate and specimen to increase friction and limit the movement partially. However, it turned out that the sandpaper had almost no restraining effect so that the specimens moved rather jerky. Certainly, a real structural component for a ceiling would rather be fully restrained in its horizontal movement than not restraint at all. Thus, it is proposed to change the test set-up in future investigations so that the horizontal movement of the components is more restraint, and a future building component is represented properly.

Inspired by the hanged concrete specimens, the catenary was chosen for the shape of the double curved elements which were tested on their flexural strength. Indeed, the catenary gives a moment-less arch if mirrored horizontally, but only if it is subjected solely by gravity. As investigations in [Lew16a] showed, the shape of a moment-less arch subjected to self-weight and an uniformly distributed load differs from the catenary. Furthermore, only two-dimensional forming was achieved, using the developed forming tools: either transversal or longitudinal. An efficient building component however, e. g. for a ceiling could be

three-dimensionally shaped i. e. in transverse and longitudinal direction at the same time. Finding ideal three-dimensional shapes, different form-finding methods could be used e. g. inflated membranes [Lew16b]. In any case, the objective for the production of efficient load-bearing TRC components should be to find shapes that are mainly subjected to normal stresses. Since the actual applied loads on real building components can be very complex, different shapes and load cases should be investigated. A parametric design tool such as the software Grasshopper[1] could help finding appropriate shapes according to actual loading. This would allow the design of support structures that are optimized according to the acting loads.

Furthermore, the tests carried out were of small-scale. A main advantage of extrusion is the continuous manufacturing process which allows extruded components to be produced in endless strings. However, they are limited in their size according to the cross-section of the mouthpiece. Thus, for larger application purposes in the future suitable connection methods must be found. In [Woe17] a screw connection of flat folded concrete elements was chosen for a prototype. However, a connection via full-surface mortar bonding is recommended.

[1] https://www.grasshopper3d.com

6 Summary and Outlook

Within this master's thesis fiber reinforced concrete (FRC) and textile reinforced concrete (TRC) were successfully extruded. The challenging demands on the rheology of the concrete mixture for extrusion have already been overcome in previous investigations [Jan19, Kra15] and thus, a mixture with sufficient green strength and processability was already found and just slightly adapted. A laboratory extruder of the Institute of Building Materials Research at RWTH Aachen University was then used to extrude concrete specimens. Thereby a rectangular cross section of 60 mm x 10 mm was used for the investigations. With a newly developed mouthpiece, it was possible to guide textile reinforcements into the concrete flow via a feeding channel. Two types of textiles were used: one made from alkali-resistant glass (ar-glass) and one made from carbon. Afterwards, the extruded TRC and FRC specimens were formed using the fold-in-fresh principle. Within this principle, concrete is formed in its fresh state while being soft enough and therefore pliable. Here, transverse and longitudinal forming were distinguished. However, there was no suitable procedure for the efficient folding or forming of extruded concrete available and thus, a new folding tool was developed.

For forming in transverse direction, the extruded specimens were placed on top of or inside pipes with varying diameters. In the process, the concrete specimens had to be pressed in shape since under gravitational deformation, the specimens did not form properly around the pipes. Resulting FRC specimens could be formed without visible cracks for bending radii of up to approx. 5.0 cm. Pressing the specimens into the pipes turned out to be superior to placing them on top of the pipes. Specimens placed on top of the pipes always showed visible cracks when properly bent, even for slightly larger bending radii than successfully achieved for specimens pressed into pipes. However, the TRC specimens exhibited a spring-like behavior i. e. even after pressing them into shape, they formed back into a straighter position and thus they could not be properly bent around the pipes. For future investigations, it is recommended to use a microscope and analyze the cracked surface in more detail. Within this master's thesis only cracks visible by eye were evaluated with a crack measuring ruler.

For longitudinal forming, concrete specimens were hanged between two clamping profiles on a plastic foil. By moving the clamping profiles on guide rails, the fixing point distance could be changed, leading to a variation in the bending radii. For fine-grained concrete specimens without textile reinforcement, the free deformation of the concrete did not lead to visible cracks caused by forming in any specimen. A minimal bending radius of approx. 5.3 cm has been achieved. It was intentionally achieved for a specimen without microfibers or textile reinforcement. However, it turned out that the concrete would approach a minimal bending radius under free deformation, as it deviated further from the theoretical bending radius for smaller bending radii (Figure 6-1, page 96). Specimens with textile reinforcement showed failures in form of kinks or buckling. The extrudates reinforced with ar-glass did not show visible defects for a bending radius of approx. 30.6 cm. For smaller bending radii, the concrete tended to buckle on the inner surface or showed a kink in the apex zone. Specimens reinforced with carbon textiles could be formed with a bending radius of approx. 19.7 cm without visible defects. However, specimens with smaller bending radii failed more sudden: a kink probably caused by a failure in the textile reinforcement occurred

abruptly. For future investigations, it is proposed to test further textiles and coatings on their bending behavior. Depending on the desired shape, it is also possible to use combined textiles with stiffer and more flexible sections as it was done in [Pid16].

Figure 6-1: Longitudinally formed concrete specimens (no fibers and no textile reinforcement)

The theoretical bending radii of the hanged specimens could be calculated assuming a free-hanging state. Thereby, the mathematical function describing the shape of a hanging rope or chain solely influenced by gravity – the so-called catenary – was used. Besides using this function for the calculation of the bending radius, this function has another advantage: mirroring this shape on a horizontal axis, results in a moment-less arch structure with normal stresses only [Lew16a], if subjected solely by gravity. Based on this finding, double curved elements following the mathematical shape of catenaries were produced, in order to evaluate the flexural strength of curved concrete structures. Therefore, a negative formwork was produced from polyurethane foam via a CNC milling machine. After extrusion, specimens made from FRC and TRC were produced using this formwork. The elements were then turned over for being tested on their flexural behavior in three-point bending tests which were inspired by the set-up in [Woe17]. However, it turned out that some elements were slightly twisted in themselves. Thus, for some specimens a compensation element had to be placed between specimen and testing machine. For future investigations, further improvements to produce straighter elements are proposed e. g. placing straight horizontal boundaries in the formwork. During the flexural tests the initial crack that led to a brittle failure in the FRC specimens occurred on average at approx. 225 N and a corresponding deflection of approx. 2.5 mm. For TRC specimens, more ductile behavior was expected. However, the initial crack occurred for similar loads and no significant resistance was obtained afterwards. The specimens deformed significantly and only a slight increase in resistance could be obtained for the carbon textile reinforced specimens, whereas for the ar-glass reinforced specimens no load increase could be obtained.

It is recommended that the test set-up itself and especially the bearing conditions are improved in future investigations. The bearing conditions were chosen based on a possible future building component: The double-curved elements could be used as structural system for ceilings where the double curved TRC elements could be advantageous in terms of resource efficiency, durability, and load-bearing behavior over the current state of the art, which is the use of reinforced concrete flat plates. Therefore, it was chosen to restrain the movement of the supports in horizontal direction to a certain degree. However, the used sandpaper had almost no restraining effect and should be replaced in future investigations.

Inspired by the hanged concrete specimens, the catenary was chosen for the shape of the double curved elements. Indeed, the catenary gives a moment-less arch if mirrored horizontally, but only if it is subjected solely by gravity. However, the shape of a moment-less arch subjected to self-weight and a uniformly distributed load differs from the catenary. Furthermore, within this master's thesis only two-dimensional forming was achieved, while an ideal structural shape should consider three dimensions. Finding ideal three-dimensional shapes which are mainly subjected to normal stresses is a complex process and depends on the load situation. Since the actual applied loads on real building components can be very complex, different shapes and load cases should be investigated. A parametric design tool could help finding appropriate shapes according to actual loading. This would allow the design of support structures that are optimized according to the acting loads. The specimens from this master's thesis have already shown that the flexibility of extruded concrete allows significant bending and thus, make it possible to produce complex shapes.

7 Literature

[Ald98] Aldea, C.; Marikunte, S.; Shah, S. P.: Extruded Fiber Reinforced Cement Pressure Pipe. In Advanced Cement Based Materials, 1998, 8; p. 47–55.

[Alf05] Alfani, R.: Rheological test methods for the characterization of extrudable cement-based materials - A review. In Materials and Structures, 2005, 38; p. 239–247.

[Api19] Apis Cor. https://www.apis-cor.com/gallary, Accessed: 31.05.2021.

[Ban05] Banthia, N.; Soleimani, S. M.: Flexural Response of Hybrid Fiber-Reinforced Cementitious Composites. In ACI Materials Journal, 2005, 102; p. 382–389.

[Bau06] Bauser, M.; Sauer, G.; Siegert, K.: Extrusion (2nd Edition), 2006.

[Ben93] Benbow, J.; Bridgwater, J.: Paste Flow And Extrusion. Oxford University Press, 1993.

[Ber07] Bernstein, L. et al.: Industry. In (Metz, B. et al. Eds.): Climate Change 2007. Mitigation. Cambridge University Press, 2007; 447-496.

[Bos16] Bosch Rexroth AG: Mechanik-Grundelemente. https://www.urt-utz.de/komponenten/profiltechnik-mge/, Accessed: 15.03.2021.

[Bra15] Brameshuber, W.: Extrusion of textile reinforced concrete. In (RILEM publications Ed.): Proceedings of: FERRO-11 - 11th International Symposium on Ferrocement and 3rd ICTRC - International Conference on Textile Reinforced Concrete, 2015; 427-434.

[Bra16] Brameshuber, W.: Manufacturing methods for textile-reinforced concrete: Textile Fibre Composites in Civil Engineering. Elsevier, 2016; p. 45–59.

[Bup07] Buphoff: Gateway Arch, 2007. Permission of Use: CC BY-SA 3.0. https://de.wikipedia.org/wiki/Gateway_Arch_National_Park#/media/Datei:STL_Skyline_2007_crop_(Gateway_Arch).jpg, Accessed: 16.04.2021.

[Bus18] Buswell, R. A. et al.: 3D printing using concrete extrusion: A roadmap for research. In Cement and Concrete Research, 2018, 112; p. 37–49.

[Car16] Carbon Concrete Composite - C³: https://www.bauen-neu-denken.de/pressematerial/. Copyright: Bundesministerium für Bildung und Forschung/Innovation & Stukturwandel/Thilo Schoch, Accessed: 01.05.2021.

[Car21a] Carbon Concrete Composite - C³: Bauen neu denken. https://www.bauen-neu-denken.de/wp-content/uploads/2021/01/2021-Factsheet-Pressemappe-Deutsch_neu.pdf, Accessed: 01.05.2021.

[Car21b] Carbon Concrete Composite - C³: Entwicklung der Publikationen zum Thema Carbonbetonbauweise. https://www.bauen-neu-denken.de/publikationen-2/, Accessed: 01.05.2021.

[Chi10] Chilton, J.: Potential unrealised? - The shells Heinz Isler might have built… In Conference: International Symposium of the International Association for Shell and Spatial Structures (IASS) in Shanghai, China, 2010.

[Cur07] Curbach, M. et al.: Segmentbrücke aus textilbewehrtem Beton: Konstruktion, Fertigung, numerische Berechnung. In Beton- und Stahlbetonbau, 2007, 102; p. 342–352.

[Cur09] Curbach, M.; Jesse, F.: Eigenschaften und Anwendung von Textilbeton. In Beton- und Stahlbetonbau, 2009, 104; p. 9–16.

[Cur11a] Curbach, M.; Ortlepp, R.: Leichtes Bauen mit ultrahochfestem und Textilbeton. In (Lehrstuhl Tragwerksplanung, Fakultät Architektur, Technische Universität Dresden Ed.): Wie wollen wir in Zukunft bauen? Festschrift zum 60. Geburtstag von Prof. Dr.-Ing. Wolfram Jäger, Dresden, 2011; p. 17–22.

[Cur11b] Curbach, M. Ed.: Textilbeton in Theorie und Praxis. Tagungsband zum 6. Kolloquium zu textilbewehrten Tragwerken (CTRS6) ; gemeinsames Abschlusskolloquium der Sonderforschungsbereiche 528 (Dresden) und 532 (Aachen), Berlin 19.9.2011 - 20.9.2011. Techn. Univ, Dresden, 2011.

[Cur12] Curbach, M.; Ortlepp, R.: Textile Bewehrungen zur bautechnischen Verstärkung und Instandsetzung. Abschlussbericht SFB 528, 2012.

[Cur19] Curbach, M.; Beckmann, B. Eds.: Antrag auf Einrichtung und Förderung des SFB/Transregios 280. Konstruktionsstrategien für materialminimierte Carbonstrukturen - Grundlagen für eine neue Art zu bauen, 2019.

[DIN11] DIN EN 1992-1-1: Eurocode 2: Bemessung und Konstruktion von Stahlbeton- und Spannbetontragwerken, 2011.

[DIN16] DIN EN 196-1: Prüfverfahren für Zement, 2016.

[DIN17] DIN EN 206: Beton - Festlegung, Eigenschaften, Herstellung und Konformität, 2017.

[DIN18] DIN EN 1451-1: Kunststoff-Rohrleitungssysteme zum Ableiten von Abwasser (niedriger und hoher Temperatur) innerhalb der Gebäudestruktur - Polypropylen (PP), 2018.

[Ehl12] Ehlig, D. et al.: Textilbeton - Ausgeführte Projekte im Überblick. In Beton- und Stahlbetonbau, 2012, 107; p. 777–785.

[Gär19] Gärtner, C.: C³ - Carbon Concrete Composite. https://www.bauen-neu-denken.de/c%c2%b3-projekt/, Accessed: 30.04.2021.

[Gri06] Gries, T. et al.: Textiles. In (RILEM Technical Committee 201-TRC Ed.): Textile Reinforced Concrete. State-of-the Art Report of RILEM Technical Committee 201-TRC, 2006; p. 11–27.

[Haj16] Hajiabadi, M.: Die Kettenlinie. WS 2016/17. https://download.uni-mainz.de/mathematik/Algebraische%20Geometrie/Lehre/Sem-Ausgewaehlte-hoehere-Kurven-WS2016-17/Hajiabadi%20Maikel_Die%20Kettenlinie_090217.pdf, Accessed: 21.04.2021.

[Hän19] Händle GmbH: Komplette Anlagen für die Produktion von faser-verstärkten, tement-gebundenen Paneelen, profilen und Platten. https://www.haendle.com/haendle/industrien/faserzement/?lang=%20en., Accessed: 21.03.2021.

[Heg06] Hegger, J. et al.: Applications of Textile Reinforced Concrete. In (RILEM Technical Committee 201-TRC Ed.): Textile Reinforced Concrete. State-of-the Art Report of RILEM Technical Committee 201-TRC, 2006; 237-270.

[Heg08] Hegger, J.; Horstmann, M.; Voss, S.: Anwendungsbeispiele für textilbewehrten Beton. In Betontechnik, 2008; 20-27.

[Hey98] Heyman, J.: Hooke's cubico–parabolical conoid. In Notes and Records of the Royal Society of London, 1998, 52; p. 39–50.

[Hin09] Hinzen, M.; Brameshuber, W.: Improvement of Serviceability and Strength of Textile Reinforced Concrete by using Short Fibres. In (Curbach, M.; Jesse, F. Eds.): Textile Reinforced Structures: Proceedings of the 4th Colloquium on Textile Reinforced Structures (CTRS4), 2009; p. 261–272.

[Hor06] Horikoshi, T. et al.: Properties of polyvinylalcohol fiber as reinforcing materials for cementitious composites. In International RILEM workshop on HPFRCC in structural applications, 2006.

[Hue06] Huerta, S.: Structural Design in the Work of Gaudí. In Architectural Science Review, 2006, 49; p. 324–339.

[ISO15] ISO / ASTM 52900: Additive manufacturing - General principles - Terminology, 2015.

[Jan19] Janissen, L.; Raupach, M.; Hartung-Mott, R.: Extrusion faserverstärkter Textilbetone. In Bautechnik, 2019, 96; p. 723–730.

[Jes10] Jesse, F.; Curbach, M.: Verstärken mit Textilbeton. In (Bergmeister, K.; Fingerloos, F.; Wörner, J.-D. Eds.): 2010 Beton-Kalender. Brücken - Betonbau im Wasser. Ernst & Sohn Verlag, Berlin, 2010; p. 458–565.

[Kra15] Kraus, M.; Hartung-Mott, R.; Brameshuber, W.: Extrudieren von Textilbeton. Entwicklung eines geeigneten Mundstückes. In BWI - BetonWerk International, 2015; p. 22–26.

[Kur16] Kurrer, K.-E.: Geschichte der Baustatik. Auf der Suche nach dem Gleichgewicht. Ernst & Sohn, Berlin, 2016.

[Lan92] Langhans, K.; Roeder, E.: Theoretische und experimentelle Untersuchungen zur Faserausrichtung beim Strangpressen von Kurzfaser-Verbundwerkstoffen. In Materialwissenschaft und Werkstofftechnik, 1992, 23; p. 174–179.

[Lew16a] Lewis, W. J.: Mathematical model of a moment-less arch. In Proceedings. Mathematical, physical, and engineering sciences, 2016, 472; p. 1–14.

[Lew16b] Lewis, W.: Form-Finding Approach To Modelling Minimal Structural Forms, With Analogy To Nature. In (Wroclaw branch of the Polish Academy of Sciences Ed.): Proceedings ISSA 2016: Innovative Structural Systems in Architecture, November 3 - 5, 2016, Wroclaw, Poland, 2016; p. 39–42.

[Lew17a] Lewis, W. J.: Form-finding. In (Lewis, W. J. Ed.): Tension Structures: Form and behaviour, Second edition. ICE Publishing, 2017; p. 23–36.

[Lew17b] Lewis, W. J.: Tension cables in suspension bridges. A case of form-finding. In (Lewis, W. J. Ed.): Tension Structures: Form and behaviour, Second edition. ICE Publishing, 2017; p. 101–133.

[Lew17c] Lewis, W. J.: Introduction. In (Lewis, W. J. Ed.): Tension Structures: Form and behaviour, Second edition. ICE Publishing, 2017; p. 1–22.

[Lie15] Lieboldt, M.: Feinbetonmatrix für Textilbeton. In Beton- und Stahlbetonbau, 2015, 110; p. 22–28.

[Mah03] Maher, A.; Burry, M.: The Parametric Bridge: Connecting Digital Design Techniques in Architecture And Engineering: Proceedings of the 2003 Annual Conference of the Association for Computer Aided Design in Architecture, 2003; p. 39–47.

[Moh21] Mohan, M. K. et al.: Extrusion-based concrete 3D printing from a material perspective: A state-of-the-art review. In Cement and Concrete Composites, 2021, 115; p. 103855.

[Mol05] Molter, M.: Zum Tragverhalten von textilbewehrtem Beton. Dissertation, 2005.

[Mot12] Mott, R.; Brameshuber, W.: Erste Erkenntnisse zum Extrudieren von Textilbeton. 4. Anwendertagung Textilbeton. In TUDALIT: Leichter bauen - Zukunft formen, 2012, 7; p. 23.

[Nem17] Nematollahi, B.; Xia, M.; Sanjayan, J.: Current Progress of 3D Concrete Printing Technologies. In (Cheng, M.-Y.; Chen, H.-M.; Chiu, K. C. Eds.): Proceedings of the 34th International Symposium on Automation and Robotics in Construction (ISARC). Tribun EU, s.r.o., Brno, 2017.

[Off04] Offermann, P. et al.: Technische Textilien zur Bewehrung von Betonbauteilen. In Beton- und Stahlbetonbau, 2004, 99; p. 437–443.

[Oss10] Osserman, R.: How the Gateway Arch Got its Shape. In (Williams, K.; Rees, J. M. Eds.): Recalling Eero Saarinen 1910–2010. Birkhäuser Basel, Basel, 2010; p. 167–189.

[Per18] Perrot, A. et al.: Extrusion of cement-based materials - an overview. In RILEM Technical Letters, 2018, 3; p. 91–97.

[Pid16] Pidun, K.; Hannawald, J.; Koch, A.: Entwicklung eines Verfahrens zur Herstellung eines Fassadenelementes aus umgeformtem Textilbeton. In BWI - BetonWerk International, 2016, 82; 38,40,42-45.

[Pol47] Poleni, G.: Memorie istoriche della gran cupola del tempio Vaticano, e de danni di ess, e de' ristoramenti loro, 1747.

[Pur06] Purnell, P. et al.: Durability. In (RILEM Technical Committee 201-TRC Ed.): Textile Reinforced Concrete. State-of-the Art Report of RILEM Technical Committee 201-TRC, 2006; p. 187–210.

[Rau19] Raupach, M.; Matschei, T.: Teilprojekt D02: Grundlagen für das Extrudieren von Carbonbetonstrukturen. In (Curbach, M.; Beckmann, B. Eds.): Antrag auf Einrichtung und Förderung des SFB/Transregios 280. Konstruktionsstrategien für materialminimierte Carbonstrukturen - Grundlagen für eine neue Art zu bauen, 2019; 253-262.

[Rem18] Rempel, S. et al.: Extremely Light and Slender Precast Pedestrian-Bridge Made Out of Textile-Reinforced Concrete (TRC). In (Hordijk, D. A.; Luković, M. Eds.): High Tech Concrete: Where Technology and Engineering Meet. Springer International Publishing, Cham, 2018; p. 2530–2537.

[Reu15] Reute, A.: Eine neue Art des Bauens. https://www.bauen-neu-denken.de/eine-neue-art-des-bauens/, Accessed: 30.04.2021.

[Sch09] Schladitz, F. et al.: Verstärkung einer denkmalgeschützten Tonnenschale mit Textilbeton. In Beton- und Stahlbetonbau, 2009, 104; p. 432–437.

[Sch15] Scheerer, S.: Was ist Textilbeton? In Beton- und Stahlbetonbau, 2015, 110; p. 4–7.

[SFB01] SFB 528: Arbeits- und Ergebnisbericht. für die Periode II/1999-I/2002. Textile Bewehrungen zur bautechnischen Verstärkung und Instandsetzung, Dresden, 2001.

[Sha01] Shao, Y.; Qiu, J.; Shah, S. P.: Microstructure of extruded cement-bonded fiberboard. In Cement and Concrete Research, 2001, 31; p. 1153–1161.

[Sim05] Sim, J.; Park, C.; Moon, D. Y.: Characteristics of basalt fiber as a strengthening material for concrete structures. In Composites Part B: Engineering, 2005, 36; p. 504–512.

[Son20] Sonderforschungsbereich/Transregio 280: https://tu-dresden.de/bu/bauingenieurwesen/imb/das-institut/news/sonderforschungsbereich-transregio-280. Copyright: Stefan Gröschel, Accessed: 01.05.2021.

[Sta18] Statista: Population living in urban areas worldwide from 1950 to 2050. https://www.statista.com/statistics/672054/change-in-urbanization-worldwide-by-region/, Accessed: 31.05.2021.

[Sta19] Statista: Development of the world population from 1950 to 2050. https://www.statista.com/statistics/262875/development-of-the-world-population/, Accessed: 31.05.2021.

[Sta99] Stang, H.; Li, V. C.: Extrusion of ECC-Material, 1999.

[Ste21] Steinmann, P.; Runesson, K.: Visco-Plasticity. In (Steinmann, P.; Runesson, K. Eds.): The Catalogue of Computational Material Models. Basic Geometrically Linear Models in 1D. Springer, Cham, 2021; p. 285–402.

[Tra01] Trautz, M.: Formunvollendet. Eine Trilogie von der Suche nach der Form statisch idealer Kuppeln. In deutsche bauzeitung, 2001, 135; p. 105–112.

[Uni19] United Nations Environment Programme (UNEP): Sand and sustainability: Finding new solutions for environmental governance of global sand resources. GRID-Geneva, Geneva, Switzerland, 2019.

[Val19] Valente, M.; Sibai, A.; Sambucci, M.: Extrusion-Based Additive Manufacturing of Concrete Products: Revolutionizing and Remodeling the Construction Industry. In Journal of Composites Science, 2019, 3; p. 88.

[Vos08] Voss, S.: Ingenieurmodell zum Tragverhalten von textilbewehrtem Beton. Dissertation, Aachen, 2008.

[Wei09] Weiland, S.: Interaktion von Betonstahl und textiler Bewehrung bei der Biegeverstärkung mit textilbewehrtem Beton. Dissertation, Dresden, 2009.

[Wie95] Wiens, U.; Breit, W.; Schiessl, P.: Influence of High Silica Fume and High Fly Ash Contents on Alkalinity of Pore Solution and Protection of Steel Against Corrosion. In ACI Symposium Publication, 1995, 153; p. 741–762.

[Woe13] Woerd, J. D. van der et al.: Oricrete. In Beton- und Stahlbetonbau, 2013, 108; p. 774–782.

[Woe14] Woerd, J. D. van der; Chudoba, R.; Hegger, J.: Entwurf und Herstellung von Faltwerken durch Faltung. In (Scheerer, S.; Curbach, M. Eds.): Leicht Bauen mit Beton. Forschung im Schwerpunktprogramm 1542 Förderphase 1, 2014; p. 60–69.

[Woe17] Woerd, J. D. van der et al.: Construction of a vault using folded segments made out of textile reinforced concrete by fold-in-fresh: Proceedings of the IASS Annual Symposium, 2017; p. 60–69.

[Woe18a] Woerd, J. D. van der; Hegger, J.; Chudoba, R.: Oricrete: Origami aus Beton. https://www.detail.de/artikel/oricrete-origami-aus-beton-31735/.

[Woe18b] Woerd, J. D. van der: Eine Methodik zur Realisierung dünnwandiger Faltwerke aus zementbasierten Verbundwerkstoffen durch Faltung. Dissertation, Aachen, 2018.

[Yos55] Yoshimura, Y.: On the mechanism of buckling of a circular cylindrical shell under axial compression. Technical Memorandum 1390, 1955.

[Zho05] Zhou, X.: Characterization of rheology of fresh fiber reinforced cementitious composites through ram extrusion. In Materials and Structures, 2005, 38; p. 17–24.

[Zho15] Zhou, X.; Li, Z.: Manufacturing cement-based materials and building products via extrusion: from laboratory to factory. In Proceedings of the Institution of Civil Engineers - Civil Engineering, 2015, 168; p. 11–16.

[Zie21] Ziegelwerk Bellenberg. https://www.ziegelwerk-bellenberg.de/unternehmen/ziegelherstellung.html, Accessed: 15.03.2021.

A Appendix

A.1 Development of publications on carbon concrete from 2000 to 2020

Table A-1: Development of publications on carbon concrete based on search results for carbon concrete on "Scopus" and "Web of Science" [Car21b]

Year	Scopus	Web of Science
2000	860	578
2001	1766	1210
2002	2726	1883
2003	3949	2602
2004	5354	3409
2005	6826	4154
2006	8450	5129
2007	10206	6196
2008	12175	7306
2009	14241	8515
2010	16575	9806
2011	19171	11273
2012	22186	12920
2013	25210	15173
2014	28564	17699
2015	32008	20465
2016	36078	23820
2017	40239	27447
2018	44425	31343
2019	49321	35229
2020	55372	43557

Scopus: https://www.scopus.com/home.uri

Web of Science: http://login.webofknowledge.com

A.2 Forces acting on a horizontal catenary

The force necessary to put a catenary in a horizontal state mathematically tends to go to infinity. Considering a defined catenary of rope length l and density μ under gravitational acceleration g, the vertical force at each hanging point can be calculated to.

$$F_V(x) = \mu * g * l * \frac{1}{2} \tag{A-1}$$

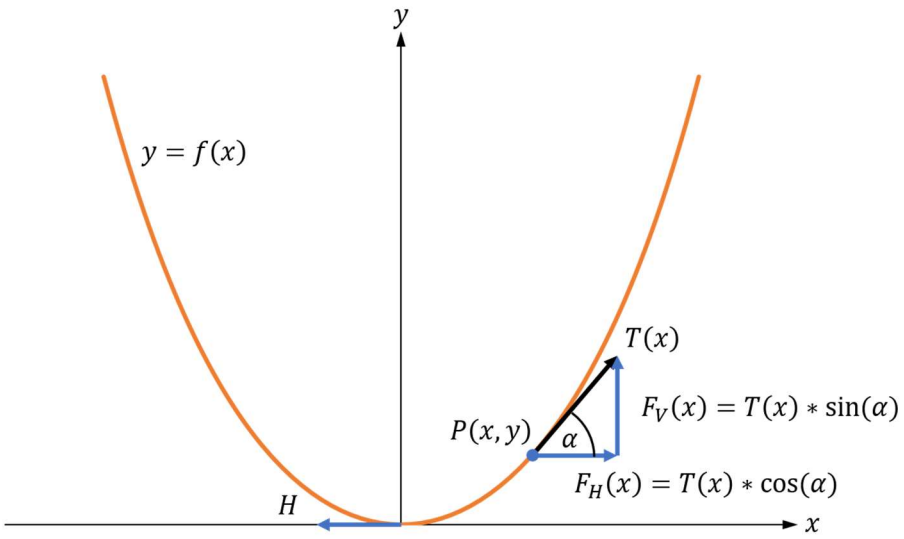

Figure A-1: Forces acting on a hanging chain

Where the vertical component of the force is:

$$F_V(x) = T(x) * \sin(\alpha) \tag{A-2}$$

$$\Rightarrow T(x) = \frac{F_V(x)}{\sin(\alpha)} = \frac{\mu * g * l}{2} * \frac{1}{\sin(\alpha)} \tag{A-3}$$

For $\alpha = 0°$ (horizontal line):

$$\sin(\alpha) = 0$$

$$\Rightarrow \frac{1}{\sin(\alpha)} \to \infty$$

$$\Rightarrow T(x) \to \infty$$

Thus, in practical terms it is impossible to receive a perfectly horizontal catenary.

A.3 Stresses and bending moments for different structural shapes in [Lew16a]

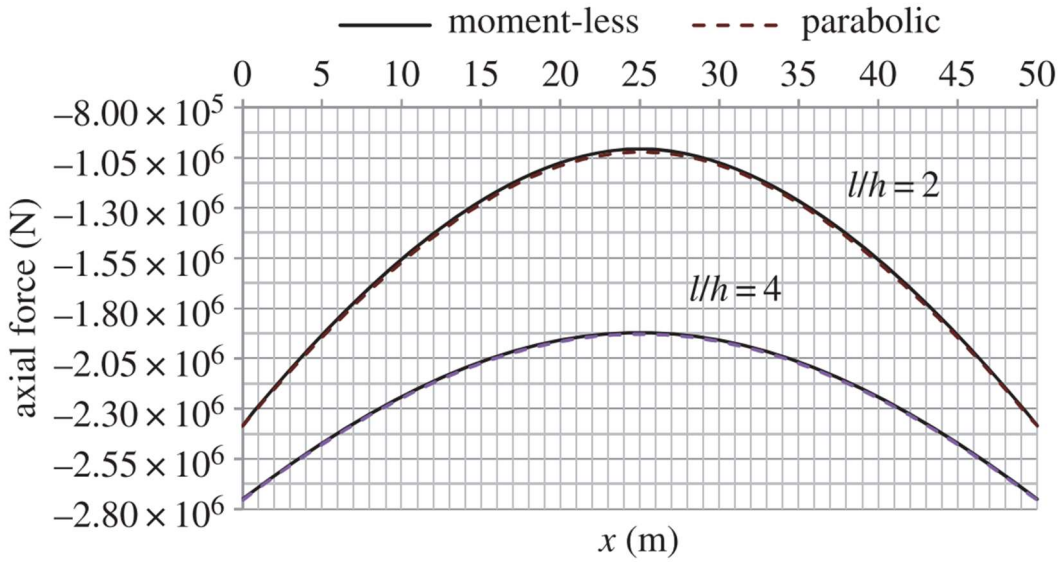

Figure A-2: Variation of axial force over the whole arch length, for the two types of arches of high and medium rise, respectively [Lew16a]

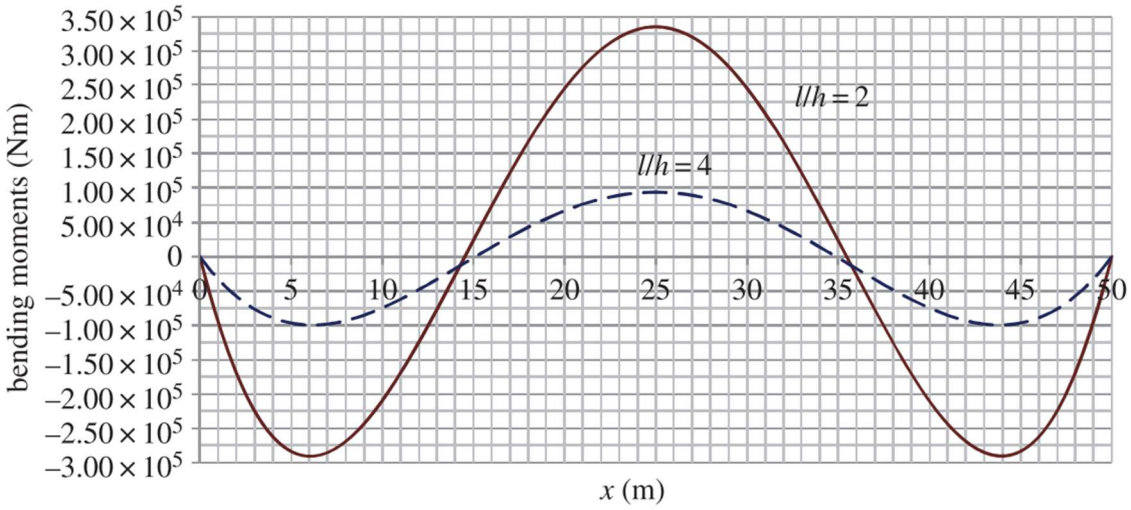

Figure A-3: Variation of bending moment in the parabolic arch of high and medium rise, r=2 [Lew16a]

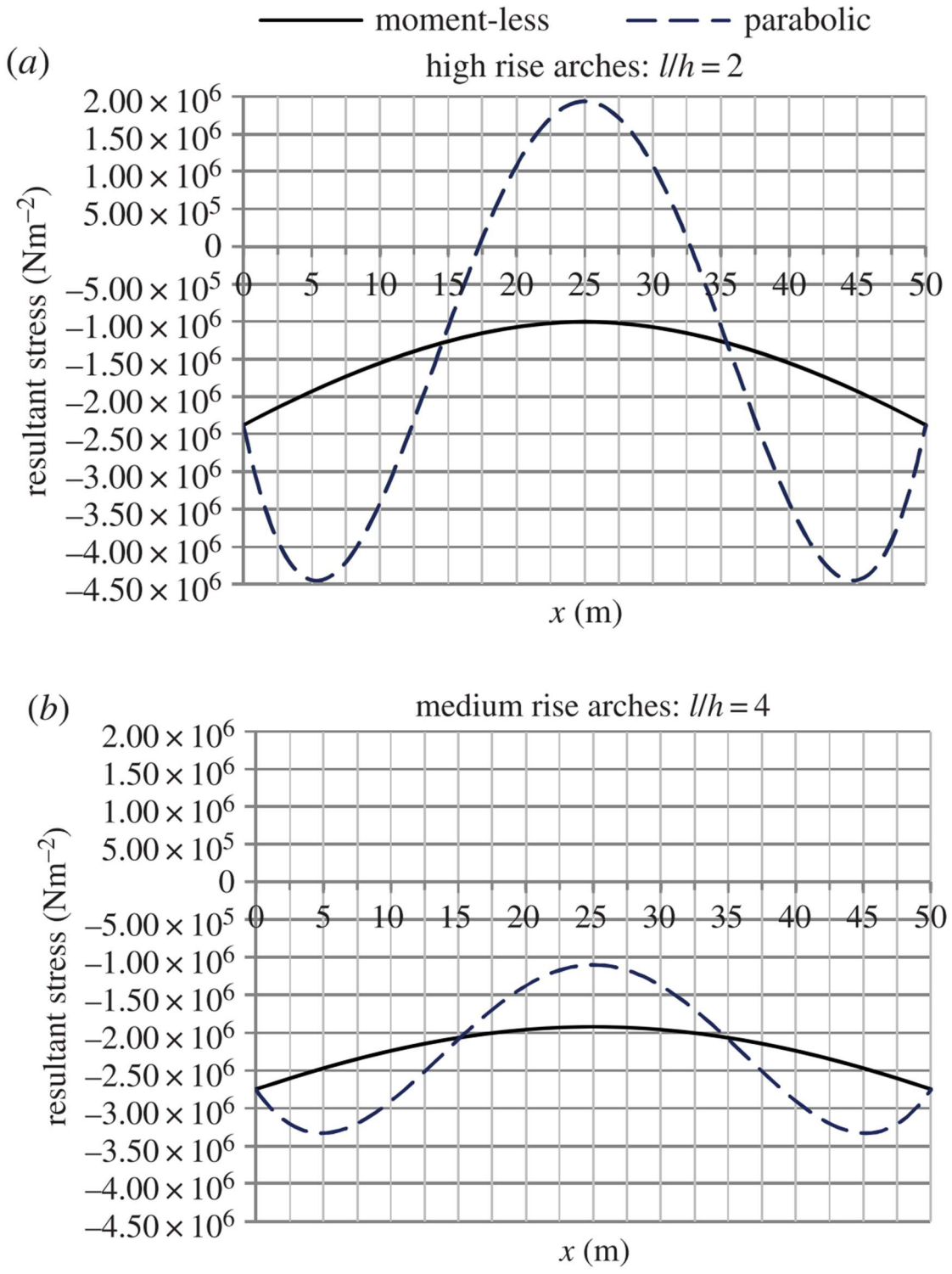

Figure A-4: Resultant stresses owing to the axial force in the moment-less arch, and combined axial force plus bending in the parabolic form [Lew16a]

A.4 Equations of the catenaries given in Figure 4-22

Table A-2: Mathematical description of the catenaries given in Figure 4-22

Length l	Fixing point distance w	Bending radius a	Height f	Equation in form $f(x) = a * \cosh\left(\frac{x - w/2}{a}\right) - a - f$
[cm]				-
110	80	28.1	33.7	$f(x) = 28.1 * \cosh\left(\frac{x - 80/2}{28.1}\right) - 28.1 - 33.7$
110	60	14.9	42.1	$f(x) = 14.9 * \cosh\left(\frac{x - 60/2}{14.9}\right) - 14.9 - 42.1$
110	45	8.9	46.8	$f(x) = 8.9 * \cosh\left(\frac{x - 45/2}{8.9}\right) - 8.9 - 46.8$

A.5 Deviation between theoretical and physically achieved bending radii

In order to compare the theoretical and physically achieved bending radii, the difference between both values in percent was calculated. As Figure 6-1, page 96**Fehler! Textmarke nicht definiert.** shows, it seems that there is a minimal bending radius that the concrete is willing to form into, solely influenced by gravity. Thus, the difference between theoretical bending radii and actually achieved bending radii, becomes larger for smaller bending radii. In order to evaluate this with a decent statistical validation, fixing point distances were rounded to form groups. For the rounded fixing point distances of approximately 30 cm, 45 cm, 60 cm, and 70 cm at least 4 values existed and thus, only these distances were chosen for comparison. The following table gives the underlying data for the average deviation presented in Table 5-1, page 70.

$$\Delta a = \frac{a_{meas.} - a_{calc.}}{a_{calc.}} * 100 \qquad \text{(A-4)}$$

With: $a_{meas.}$ Measured bending radius at the vertex [cm]
$a_{calc.}$ Calculated bending radius at the vertex [cm]
Δa Deviation between calculated and measured bending radius [%]

Table A-3: Difference between theoretical and physically achieved bending radius for rounded fixing point distances

Name of specimen	$w_{meas.}$	$w_{approx.}$	$a_{calc.}$	$a_{meas.}$	Δa	Average Δa
-	[cm]				[%]	
PA3-H-30-1	29.8	30	4.7	7.5	60.3	67.4
PA4-H-30-1	29.6	30	4.6	8.1	73.7	
PA5-H-30-1	29.7	30	4.7	8.1	73.0	
PA6-H-30-1	29.2	30	4.6	7.4	62.6	
PA2-H-45-1	45.2	45	8.9	10.9	23.3	22.2
PA3-H-45-1	44.8	45	8.7	10.5	19.9	
PA4-H-45-1	44.8	45	8.8	11.1	26.5	
PA5-H-45-1	45.0	45	8.8	11.4	29.4	
PA6-H-45-1	44.9	45	8.8	9.8	11.8	
PA2-H-60-1	59.9	60	14.5	15.6	7.5	7.5
PA3-H-60-1	59.8	60	14.5	17.2	18.4	
PA4-H-60-1	60.0	60	14.5	14.9	2.8	
PA5-H-60-1	59.6	60	14.4	14.9	3.7	
PA6-H-60-1	59.8	60	14.6	15.3	5.1	
PA2-H-70-1	69.7	70	19.7	20.7	5.4	5.4
PA3-H-70-1	69.7	70	19.6	22.5	15.0	
PA5-H-70-1	69.8	70	19.9	20.0	0.4	
PA6-H-70-1	69.7	70	19.7	19.8	0.6	

A.6 Coordinates of the double curved arch used for CNC milling

Table A-4: Coordinates of the double curved arch used for CNC milling

Left catenary		Intermediate catenary		Right catenary	
x [cm]	y [cm]	x [cm]	y [cm]	x [cm]	y [cm]
-39	19.69	-15	11.77	15	11.77
-38	20.54	-14	10.06	16	13.48
-37	21.27	-13	8.52	17	15.02
-36	21.89	-12	7.14	18	16.40
-35	22.40	-11	5.91	19	17.64
-34	22.82	-10	4.82	20	18.73
-33	23.14	-9	3.85	21	19.69
-32	23.37	-8	3.01	22	20.54
-31	23.50	-7	2.28	23	21.27
-30	23.55	-6	1.66	24	21.89
-29	23.50	-5	1.15	25	22.40
-28	23.37	-4	0.73	26	22.82
-27	23.14	-3	0.41	27	23.14
-26	22.82	-2	0.18	28	23.37
-25	22.40	-1	0.05	29	23.50
-24	21.89	0	0.00	30	23.55
-23	21.27	1	0.05	31	23.50
-22	20.54	2	0.18	32	23.37
-21	19.69	3	0.41	33	23.14
-20	18.73	4	0.73	34	22.82
-19	17.64	5	1.15	35	22.40
-18	16.40	6	1.66	36	21.89
-17	15.02	7	2.28	37	21.27
-16	13.48	8	3.01	38	20.54
-15	11.77	9	3.85	39	19.69
		10	4.82		
		11	5.91		
		12	7.14		
		13	8.52		
		14	10.06		
		15	11.77		

A.7 Concrete mixtures used within this master's thesis

Table A-5: Concrete mixtures of test series 1 to series 4

Component	Unit	Mix 1	Mix 2	Mix 3	Mix 4
Cement	kg/m³	700			700
Quarzitic aggregate 0.1 … 0.3 mm		671			678
Millisil W3 0 … 0.25 mm		277			283
Fly ash		210			210
Silica fume		70			70
Water		278			278
Methyl cellulose		7			7
PVA fibers "hard"	vol.-% of mixture	0.5	-	-	-
PVA fibers "soft"		-	0.5	-	-
Basalt fibers		-	-	0.5	-

Table A-6: Concrete mixtures of test series 5 to series 8

Component	Unit	Mix 5	Mix 6	Mix 7	Mix 8
Cement	kg/m³	700		700	
Quarzitic aggregate 0.1 … 0.3 mm		676		671	
Millisil W3 0 … 0.25 mm		279		277	
Fly ash		210		210	
Silica fume		70		70	
Water		278		278	
Methyl cellulose		7		7	
PVA fibers "hard"	vol.-% of mixture	-	-	-	-
PVA fibers "soft"		0.25	-	0.5	0.5
Basalt fibers		-	0.25	-	-

A.8 Difference between theoretical and calculated arch height of longitudinally formed specimens

The figure below shows the deviation between calculated and theoretical arch height $\Delta f_{absolute} = f_{measured} - f_{calculated}$ over the real fixing point distance $w_{measured}$. The theoretical arch height was calculated with the real fixing point distance and the length of the plastic foil under the assumption of a catenary.

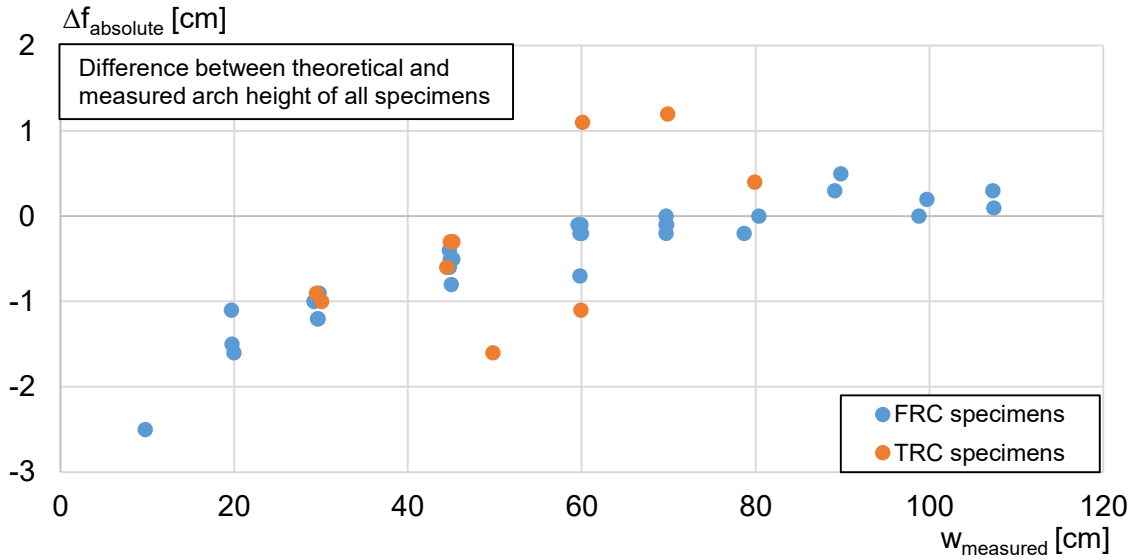

Figure A-5: Deviation of the real arch height from a theoretical catenary

A.9 Additional figures

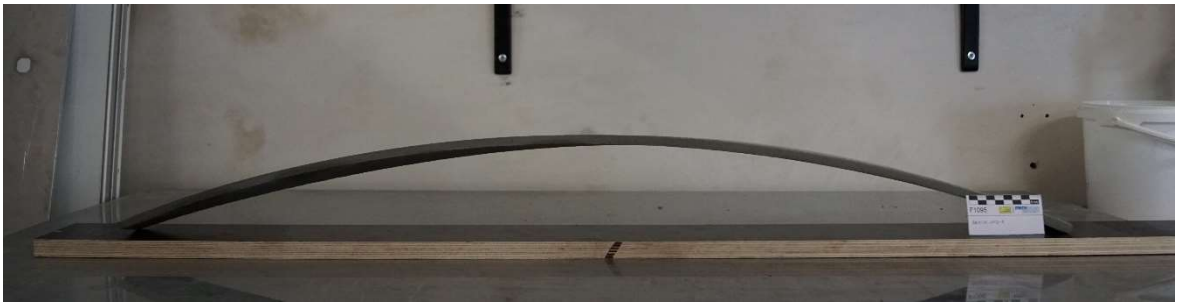

Figure A-6: Twisted longitudinally formed specimen (0.5 vol.-% of “hard” PVA fibers and no textile reinforcement)

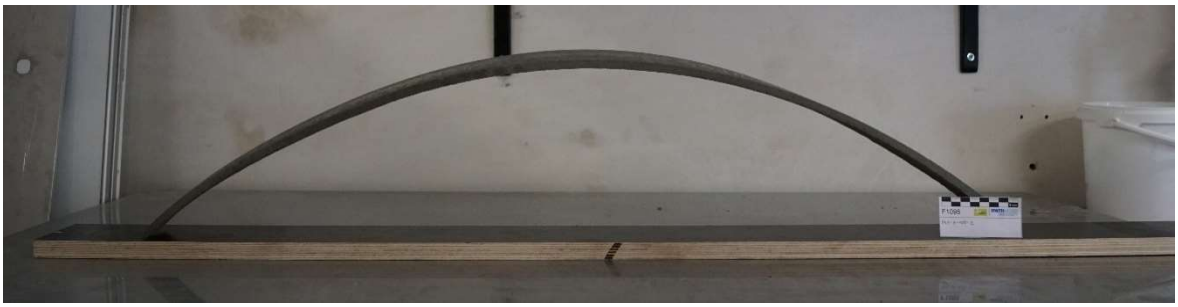

Figure A-7: Twisted longitudinally formed specimen (0.5 vol.-% of “hard” PVA fibers and no textile reinforcement)

Figure A-8: Transversally formed concrete specimen without visible cracks (0.25 vol.-% of “soft” PVA fibers and no textile reinforcement) – bending radius approx. 7.2 cm

Figure A-9: Transversally formed concrete specimen with visible cracks of approx. 0.3 mm (0.25 vol.-% of "soft" PVA fibers and no textile reinforcement) – bending radius approx. 3.4 cm

Figure A-10: Transversally formed concrete specimen without visible cracks (0.25 vol.-% of basalt fibers and no textile reinforcement) – bending radius approx. 5.1 cm

Figure A-11: Transversally formed concrete specimen with visible cracks of approx. 0.3 mm (0.25 vol.-% of basalt fibers and no textile reinforcement) – bending radius approx. 4.9 cm

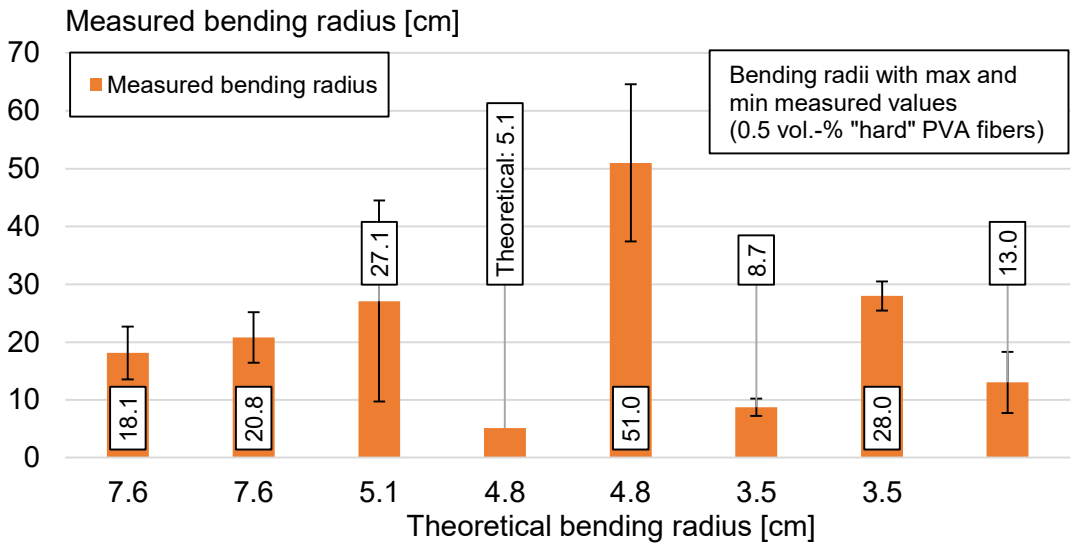

Figure A-12: Theoretical and measured bending radii with max and min measured values (0.5 vol.-% of "hard" PVA fibers and no textile reinforcement)

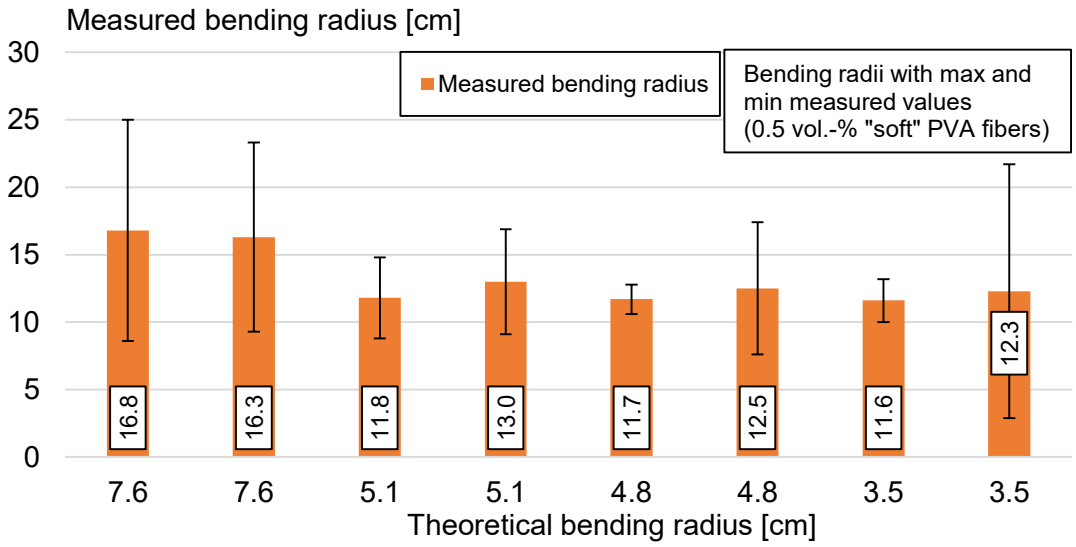

Figure A-13: Theoretical and measured bending radii with max and min measured values (0.5 vol.-% of "soft" PVA fibers and no textile reinforcement)

Figure A-14: Transversally formed concrete specimen with visible cracks of approx. 0.2 mm (0.5 vol.-% of basalt fibers and no textile reinforcement) – bending radius approx. 4.8 cm

Figure A-15: Transversally formed concrete specimen without visible cracks (0.5 vol.-% of "soft" PVA fibers and ar-glass textile reinforcement) – bending radius approx. 5.3 cm

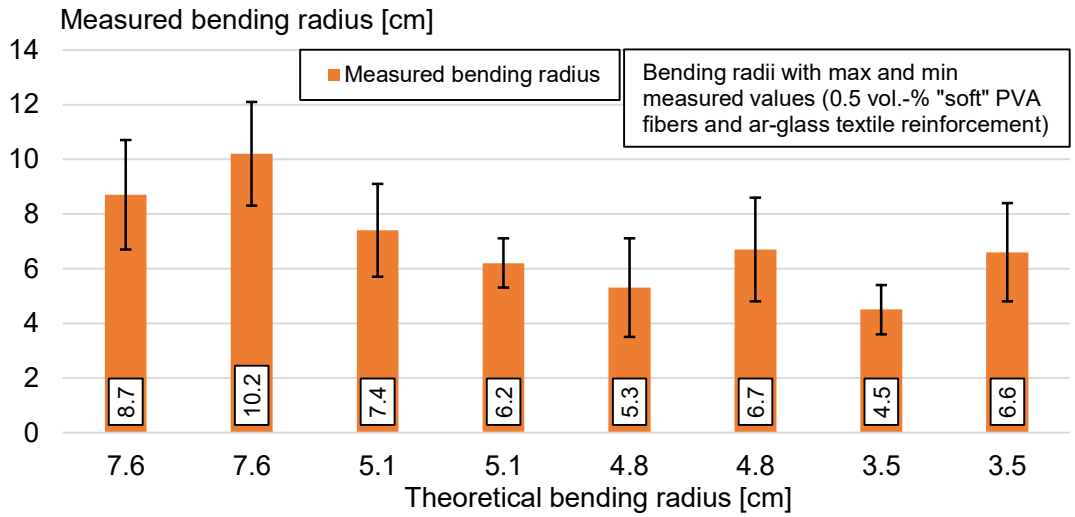

Figure A-16: Theoretical and measured bending radii with maximum and minimum measured values (0.5 vol.-% of "soft" PVA fibers and ar-glass textile reinforcement)

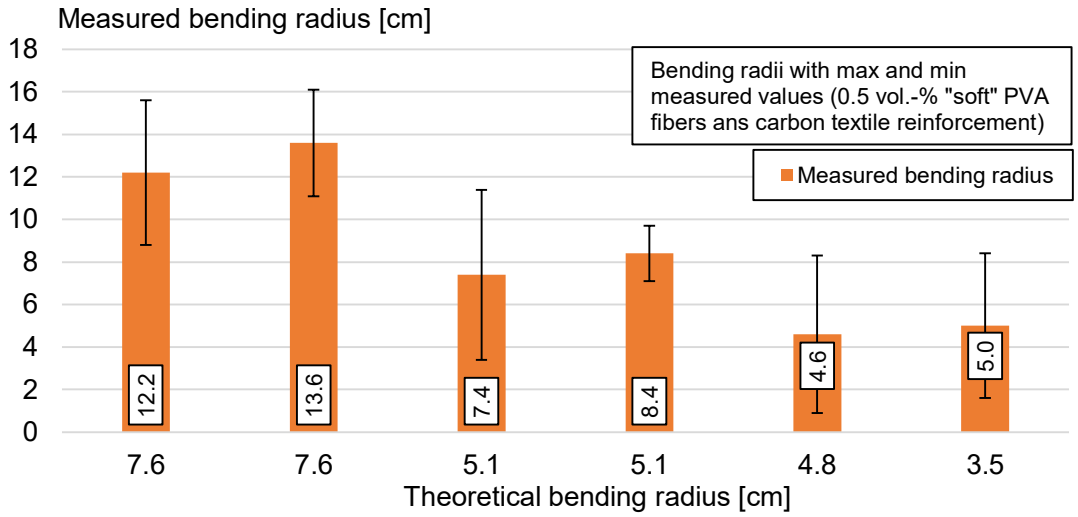

Figure A-17: Theoretical and measured bending radii with maximum and minimum measured values (0.5 vol.-% of "soft" PVA fibers and carbon textile reinforcement)

Figure A-18: Longitudinally formed concrete specimen with kink and buckling (0.5 vol.-% of "soft" PVA fibers and ar-glass textile reinforcement) – bending radius undetermined

Figure A-19: Comparison of cross-section failures caused by longitudinal forming (concrete mixture with 0.5 vol.-% of "soft" PVA fibers and carbon textile reinforcement

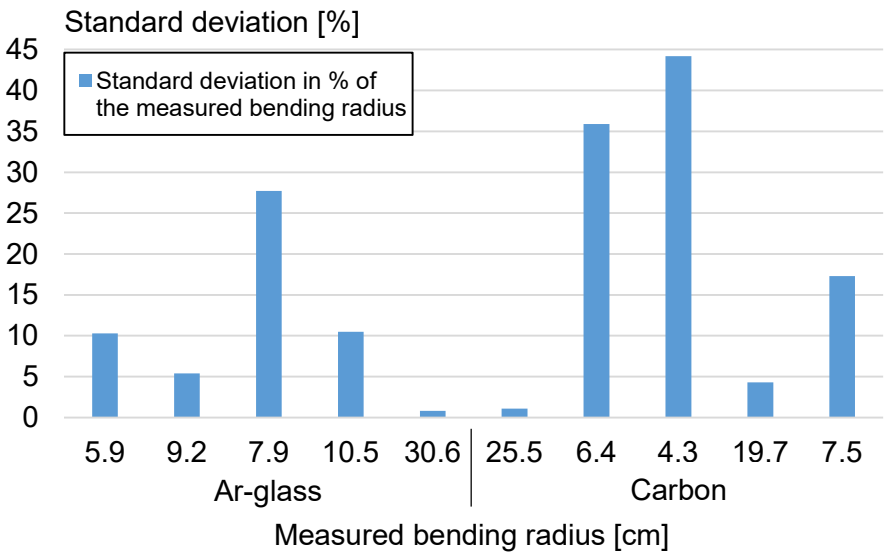

Figure A-20: Average standard deviation in percent of the measured bending radii for specimens with ar-glass or carbon textile reinforcement

Figure A-21: Longitudinally formed concrete specimen without cracks (0.5 vol.-% of "soft" PVA fibers and ar-glass textile reinforcement) – bending radius undetermined

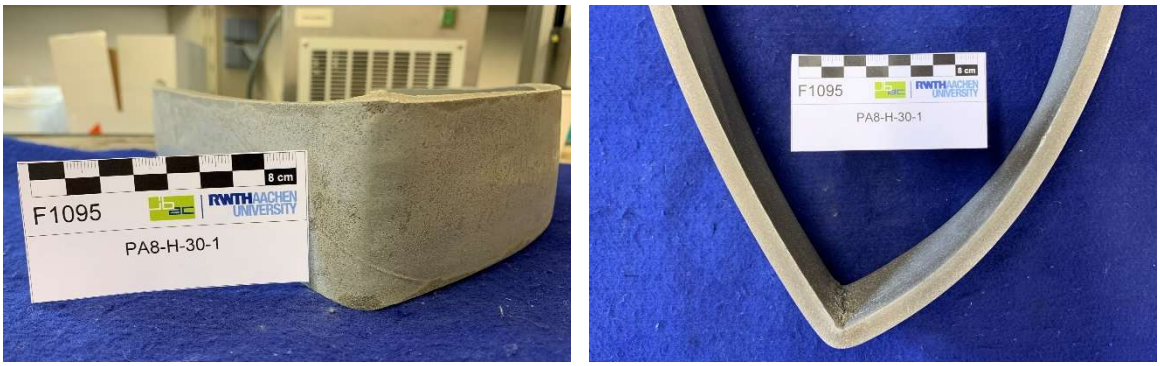

Figure A-22: Longitudinally formed concrete specimen with kink (0.5 vol.-% of "soft" PVA fibers and carbon textile reinforcement) – bending radius undetermined

Figure A-23: Specimen failed after curing (0.25 vol.-% of basalt fibers and no textile reinforcement)

A.10 Additional tables – Longitudinally formed specimen

In the following, additional tables are given with measured and calculated parameters of longitudinally formed specimens. Here, the measured fixing point distance $w_{meas.}$ and the measured length of the plastic foil $l_{meas.}$ are given. From those two parameters the theoretical bending radius at the vertex of a catenary of equal length and fixing point distance $a_{calc.}$ is calculated. Furthermore, the actually achieved (measured) bending radius of the specimen $a_{meas.}$ and the absolute difference between those two values $a_{abs.}$ is calculated. Finally, the standard deviation of the measured bending radii $\sigma_{abs.}$ is given and its percentage of the average bending radius $\sigma_{rel.}$. Specimens that showed a kink or buckling and a standard deviation greater than 10 % of the average bending radius were considered unsuccessfully formed.

Table A-7: Longitudinally formed concrete specimens of test series 4 (no fibers and no textile reinforcement) – all values are given in [cm]

Test number	$w_{meas.}$	$l_{meas.}$	$a_{calc.}$	$a_{meas.}$	$\Delta a_{abs.}$	$\sigma_{abs.}$	$\sigma_{rel.}$	Successful forming?
-	[cm]						[%]	[Yes/No]
PA4-H-60-1	60.0	112.7	14.5	14.9	0.4	0.3	1.9	Yes
PA4-H-45-1	44.8	112.4	8.8	11.1	2.3	0.2	1.6	Yes
PA4-H-30-1	29.6	112.4	4.6	8.1	3.5	0.1	0.9	Yes
PA4-H-20-1	20.0	112.0	2.7	6.2	3.5	0.1	1.3	Yes
PA4-H-10-1	9.8	112.1	1.1	5.3	4.2	0.1	1.9	Yes

Table A-8: Longitudinally formed concrete specimens of test series 5 and 6 (0.25 vol.-% of "soft" PVA fibers (test series 5) or basalt fibers (test series 6) and no textile reinforcement)

Test number	$w_{meas.}$	$l_{meas.}$	$a_{calc.}$	$a_{meas.}$	$\Delta a_{abs.}$	$\sigma_{abs.}$	$\sigma_{rel.}$	Successful forming?
-	[cm]						[%]	[Yes/No]
PA5-H-70-1	69.8	111.6	19.9	20.0	0.1	0.2	1.2	Yes
PA5-H-60-1	59.6	112.2	14.4	14.9	0.5	0.5	3.6	Yes
PA5-H-45-1	45.0	112.5	8.8	11.4	2.6	0.2	1.7	Yes
PA5-H-30-1	29.7	112.4	4.7	8.1	3.4	0.2	2.3	Yes
PA5-H-20-1	19.8	112.4	2.6	6.2	3.6	0.1	1.8	Yes
PA6-H-70-1	69.7	112.1	19.7	19.8	0.1	0.4	1.8	Yes
PA6-H-60-1	59.8	111.3	14.6	15.3	0.7	0.4	2.5	Yes
PA6-H-45-1	44.9	112.1	8.8	9.8	1.0	0.4	3.7	Yes
PA6-H-30-1	29.2	112.3	4.6	7.4	2.8	0.1	0.8	Yes
PA6-H-20-1	19.7	112.6	2.6	5.7	3.1	0.2	3.5	Yes

Table A-9: Longitudinally formed concrete specimens of test series 1, 2, and 3 (0.5 vol.-% of "hard" PVA fibers (test series 1), "soft" PVA fibers (test series 2), or basalt fibers (test series 3) and no textile reinforcement)

Test number	$w_{meas.}$	$l_{meas.}$	$a_{calc.}$	$a_{meas.}$	$\Delta a_{abs.}$	$\sigma_{abs.}$	$\sigma_{rel.}$	Successful forming?
-	[cm]						[%]	[Yes/No]
PA1-H-90-1	89.8	111.4	38.7	38.4	-0.3	2.7	7.0	Yes
PA1-H-100-1	98.8	110.4	59.9	64.7	4.8	3.8	5.9	Yes
PA1-H-100-2	99.7	111.8	59.5	51.8	-7.7	3.4	6.5	Yes
PA1-H-110-1	107.3	110.1	136.1	110.2	-25.9	4.0	3.6	Yes
PA1-H-110-2	107.4	110.8	123.8	127.2	3.4	11.1	8.7	Yes
PA2-H-45-1	45.2	112.7	8.9	10.9	2.0	0.2	1.9	Yes
PA2-H-60-1	59.9	112.6	14.5	15.6	1.1	0.4	2.4	Yes
PA2-H-70-1	69.7	112.4	19.7	20.7	1.0	0.5	2.6	Yes
PA2-H-80-1	78.7	112.5	26.0	26.6	0.6	0.5	1.8	Yes
PA2-H-90-1	89.1	112.7	36.7	36.6	-0.1	1.5	4.0	Yes
PA3-H-30-1	29.8	112.8	4.7	7.5	2.8	0.2	2.1	Yes
PA3-H-45-1	44.8	112.7	8.7	10.5	1.8	0.3	2.6	Yes
PA3-H-60-1	59.8	112.1	14.5	17.2	2.7	0.8	4.7	Yes
PA3-H-70-1	69.7	112.8	19.6	22.5	2.9	0.4	1.9	Yes
PA3-H-80-1	80.4	112.2	27.5	28.0	0.5	0.9	3.1	Yes

Table A-10: Longitudinally formed concrete specimens of test series 7 (0.5 vol.-% of "soft" PVA fibers and ar-glass textile reinforcement)

Test number	$w_{meas.}$	$l_{meas.}$	$a_{calc.}$	$a_{meas.}$	$\Delta a_{abs.}$	$\sigma_{abs.}$	$\sigma_{rel.}$	Successful forming?
-	[cm]						[%]	[Yes/No]
PA7-H-80-1	79.9	112.4	27.0	30.6	3.6	0.3	0.8	Yes
PA7-H-70-1	69.9	112.5	19.8	10.5	-9.3	1.1	10.5	No
PA7-H-60-1	60.1	112.4	14.6	7.9	-6.7	2.2	27.7	No
PA7-H-45-1	44.9	113.0	8.8	9.2	0.4	0.5	5.4	No[1]
PA7-H-30-1	30.1	113.1	4.7	5.9	1.2	0.6	10.3	No

Table A-11: Longitudinally formed concrete specimens of test series 8 (0.5 vol.-% of "soft" PVA fibers and carbon textile reinforcement)

Test number	$w_{meas.}$	$l_{meas.}$	$a_{calc.}$	$a_{meas.}$	$\Delta a_{abs.}$	$\sigma_{abs.}$	$\sigma_{rel.}$	Successful forming?
-	[cm]						[%]	[Yes/No]
PA8-H-60-1	59.9	112.3	14.5	25.5	11.0	0.3	1.1	Yes
PA8-H-50-1	49.8	112.5	10.4	19.7	9.3	0.8	4.3	Yes
PA8-H-45-1	44.5	112.8	8.6	6.4	-2.2	2.3	35.9	No
PA8-H-45-2	45.2	111.7	8.9	7.5	-1.4	1.3	17.3	No
PA8-H-30-1	29.5	112.8	4.6	4.3	-0.3	1.9	44.2	No

[1] Even though the standard deviation is less than 10 % of the average bending radius, this specimen was unsuccessfully formed due to a very clear kink (Figure A-21, page A16).

A.11 Additional tables – Transversally formed specimens

In the following additional tables for the transversally formed specimens are given. Here, the pipe diameter as well as the measured bending radius are given. Furthermore, the visibility of cracks is given and their measured widths. The last column states whether the forming was successful or not, or if no proper bending was achieved.

Table A-12: Transversally formed concrete specimens of test series 1 (0.5 vol.-% of "hard" PVA fibers and no textile reinforcement)

Test number	Pipe	Measured bending radius [cm]	Visible cracks?	Crack widths [mm]	Comment
PA1-R-160-1	DN 160	18.1	No	< 0.1	No proper bending achieved
PA1-R-160-2	DN 160	20.8	No	< 0.1	No proper bending achieved
PA1-R-110-1	DN 110	27.1	No	< 0.1	No proper bending achieved
PA1-R-110-2	DN 110	5.1[1]	No	< 0.1	No proper bending achieved
PA1-R-75-1	DN 75	51.0	No	< 0.1	No proper bending achieved
PA1-R-75-2	DN 75	8.7	No	< 0.1	No proper bending achieved
PA1-R-50-1	DN 50	28.0	No	< 0.1	No proper bending achieved
PA1-R-50-2	DN 50	13.0	No	< 0.1	No proper bending achieved

Table A-13: Transversally formed concrete specimens of test series PA2 (0.5 vol.-% of "soft" PVA fibers and no textile reinforcement)

Test number	Pipe	Measured bending radius [cm]	Visible cracks?	Crack widths [mm]	Comment
PA2-R-160-1	DN 160	16.8	No	< 0.1	No proper bending achieved
PA2-R-160-2	DN 160	16.3	No	< 0.1	No proper bending achieved
PA2-R-110-1	DN 110	11.8	No	< 0.1	No proper bending achieved
PA2-R-110-2	DN 110	13.0	No	< 0.1	No proper bending achieved
PA2-R-75-1	DN 75	11.7	No	< 0.1	No proper bending achieved
PA2-R-75-2	DN 75	12.5	No	< 0.1	No proper bending achieved
PA2-R-50-1	DN 50	11.6	No	< 0.1	No proper bending achieved
PA2-R-50-2	DN 50	12.3	No	< 0.1	No proper bending achieved

[1] This value was not measured. The theoretical value is given for completeness.

Table A-14: Transversally formed concrete specimens of test series PA3 (0.5 vol.-% of basalt fibers and no textile reinforcement)

Test number	Pipe	Measured bending radius [cm]	Visible cracks?	Crack widths [mm]	Comment
PA3-R-160-1	DN 160	7.6[1]	No	< 0.1	Successfully formed
PA3-R-160-2	DN 160	8.7	No	< 0.1	Successfully formed
PA3-R-110-1	DN 110	5.6	No	< 0.1	Successfully formed
PA3-R-110-2	DN 110	5.2	No	< 0.1	Successfully formed
PA3-R-75-1	DN 75	4.3	Yes	0.2	Unsuccessfully formed
PA3-R-75-2	DN 75	4.8	Yes	0.2	Unsuccessfully formed
PA3-R-50-1	DN 50	3.9	Yes	0.3	Unsuccessfully formed
PA3-R-50-2	DN 50	3.3	Yes	0.3	Unsuccessfully formed

Table A-15: Transversally formed concrete specimens of test series PA4 (no fibers and no textile reinforcement)

Test number	Pipe	Measured bending radius [cm]	Visible cracks?	Crack widths [mm]	Comment
PA4-R-160-1	DN 160	8.1	No	< 0.1	Successfully formed
PA4-R-160-2	DN 160	7.6	No	< 0.1	Successfully formed
PA4-R-110-1	DN 110	5.2	No	< 0.1	Successfully formed
PA4-R-110-2	DN 110	5.0	No	< 0.1	Successfully formed
PA4-R-75-1	DN 75	4.9	Yes	0.1	Unsuccessfully formed
PA4-R-75-2	DN 75	5.8	Yes	0.1	Unsuccessfully formed
PA4-R-50-1	DN 50	3.8	Yes	0.4	Unsuccessfully formed
PA4-R-50-2	DN 50	3.4	Yes	0.2	Unsuccessfully formed

[1] This value was not measured. The theoretical value is given for completeness.

Table A-16: Transversally formed concrete specimens of test series PA5 (0.25 vol.-% of "soft" PVA fibers and no textile reinforcement)

Test number	Pipe	Measured bending radius [cm]	Visible cracks?	Crack widths [mm]	Comment
PA5-R-160-1	DN 160	8.6	No	< 0.1	Successfully formed
PA5-R-160-2	DN 160	7.2	No	< 0.1	Successfully formed
PA5-R-110-1	DN 110	5.1	No	< 0.1	Successfully formed
PA5-R-110-2	DN 110	5.1	No	< 0.1	Successfully formed
PA5-R-75-1	DN 75	4.4	Yes	0.2	Unsuccessfully formed
PA5-R-75-2	DN 75	4.5	Yes	0.2	Unsuccessfully formed
PA5-R-50-1	DN 50	3.6	Yes	0.1	Unsuccessfully formed
PA5-R-50-2	DN 50	3.4	Yes	0.3	Unsuccessfully formed

Table A-17: Transversally formed concrete specimens of test series PA6 (0.25 vol.-% of basalt fibers and no textile reinforcement)

Test number	Pipe	Measured bending radius [cm]	Visible cracks?	Crack widths [mm]	Comment
PA6-R-160-1	DN 160	8.7	No	< 0.1	Successfully formed
PA6-R-160-2	DN 160	7.7	No	< 0.1	Successfully formed
PA6-R-110-1	DN 110	5.1	No	< 0.1	Successfully formed
PA6-R-110-2	DN 110	5.8	No	< 0.1	Successfully formed
PA6-R-75-1	DN 75	4.9	Yes	0.3	Unsuccessfully formed
PA6-R-75-2	DN 75	3.7	Yes	0.2	Unsuccessfully formed
PA6-R-50-1	DN 50	3.6	Yes	0.1	Unsuccessfully formed
PA6-R-50-2	DN 50	3.5	Yes	0.4	Unsuccessfully formed

Table A-18: Transversally formed concrete specimens of test series PA7 (0.5 vol.-% of "soft" PVA fibers and ar-glass textile reinforcement)

Test number	Pipe	Measured bending radius [cm]	Visible cracks?	Crack widths [mm]	Comment
PA7-R-160-1	DN 160	8.7	No	< 0.1	No proper bending achieved
PA7-R-160-2	DN 160	10.2	No	< 0.1	No proper bending achieved
PA7-R-110-1	DN 110	7.4	No	< 0.1	No proper bending achieved
PA7-R-110-2	DN 110	6.2	No	< 0.1	No proper bending achieved
PA7-R-75-1	DN 75	5.3	No	< 0.1	No proper bending achieved
PA7-R-75-2	DN 75	6.7	No	< 0.1	No proper bending achieved
PA7-R-50-1	DN 50	4.5	No	< 0.1	No proper bending achieved
PA7-R-50-2	DN 50	6.6	No	< 0.1	No proper bending achieved

Table A-19: Transversally formed concrete specimens of test series PA8 (0.5 vol.-% of "soft" PVA fibers and carbon textile reinforcement)

Test number	Pipe	Measured bending radius [cm]	Visible cracks?	Crack widths [mm]	Comment
PA8-R-160-1	DN 160	12.2	No	< 0.1	No proper bending achieved
PA8-R-160-2	DN 160	13.6	No	< 0.1	No proper bending achieved
PA8-R-110-1	DN 110	7.4	No	< 0.1	No proper bending achieved
PA8-R-110-2	DN 110	8.4	No	< 0.1	No proper bending achieved
PA8-R-75-1	DN 75	4.6	No	< 0.1	No proper bending achieved
PA8-R-50-1	DN 50	5.0	No	< 0.1	No proper bending achieved

A.12 Load-deflection diagrams of three-point bending tests

In the following the load-deflection diagrams of all 11 three-point bending tests are given. The textile reinforced specimen showed large deflections without breaking. However, no significant resistance was observed after the initial crack and thus, the tests were stopped after approx. 10 mins. The FRC specimens showed brittle behavior and a sudden failure. The given TRC load-deflection diagrams are cut-outs until the defined failure load. Complete diagrams can be found in the digital appendix.

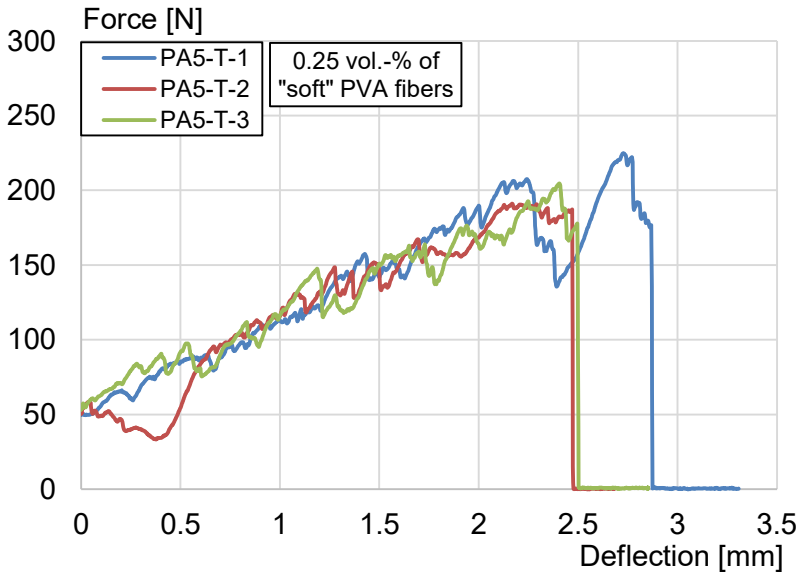

Figure A-24: Load-deflection diagram of specimens with 0.25 vol.-% of "soft" PVA fibers and no textile reinforcement

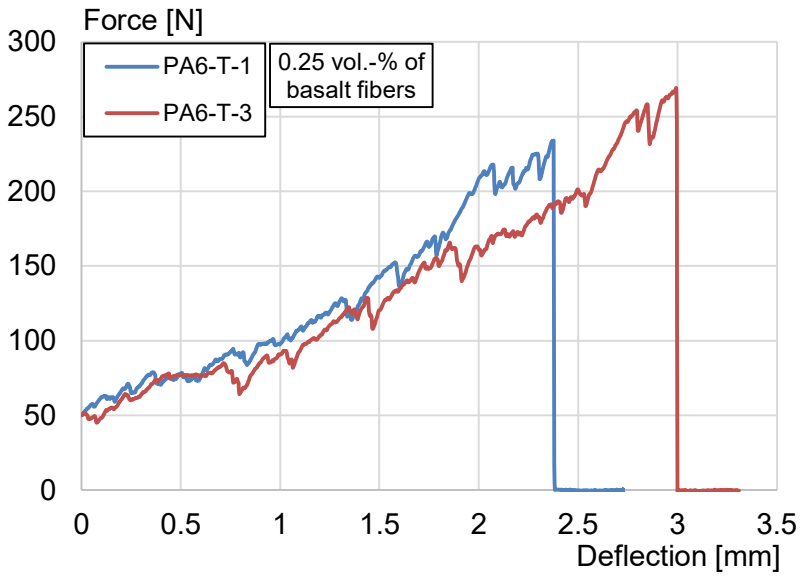

Figure A-25: Load-deflection diagram of specimens with 0.25 vol.-% of basalt fibers and no textile reinforcement

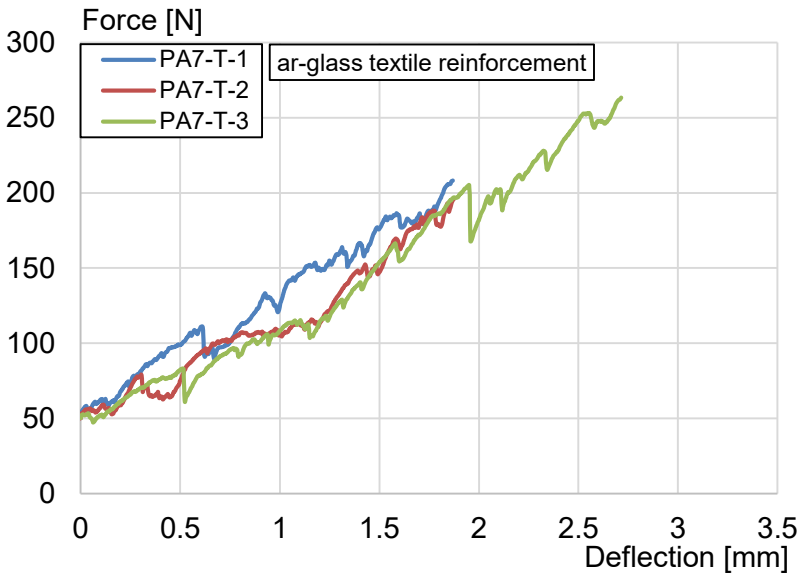

Figure A-26: Load-deflection diagram of specimens with 0.5 vol.-% of "soft" PVA fibers and ar-glass textile reinforcement

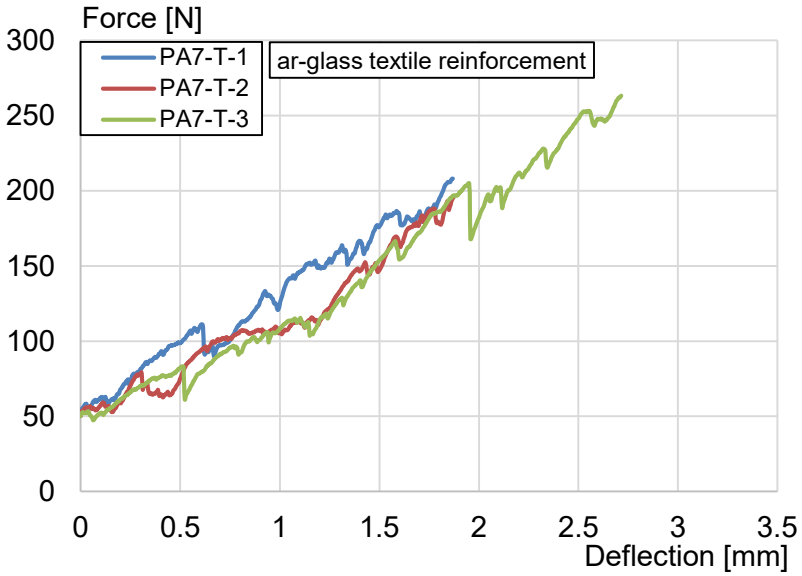

Figure A-27: Load-deflection diagram of specimens with 0.5 vol.-% of "soft" PVA fibers and carbon textile reinforcement

A.13 Stress-deflection diagrams of three-point bending tests

For better comparison and a classification of the test results, stress-deflection diagrams are usually used instead of force-deflection diagrams. Usually, however, standardized test procedures are used in which the stresses are calculated with the specimen geometries, applied forces, and measured deflections. The test method used within this master's thesis is based on that of a three-point bending test, which is usually performed with flat specimens and not curved ones. Furthermore, there is usually no horizontal support force in the flat element, but this is the case in the tests performed in this master thesis due to the partial horizontal deformation restraint. The resulting horizontal forces generate a normal force in the specimen, which must be considered in the stress calculation and further reduces the acting moment in the considered critical cross-section. Thus, assumptions must be made in order to derive stresses from the measured forces:

- The horizontal support force was assumed to be 0, since the specimens significantly deformed in horizontal direction which consequently means that the horizontal resistance was low.
- The distance between the support points was assumed to be 60.0 cm for all specimens. This corresponds to the distance between the high points of the formwork. Since the horizontal deflection of the specimens was not measured, the real distance in the moment of failure was unknown.
- The normal force in the considered cross-section was assumed to be 0, so that the stress was calculated solely from the acting moment.

A sketch showing the static system is presented below.

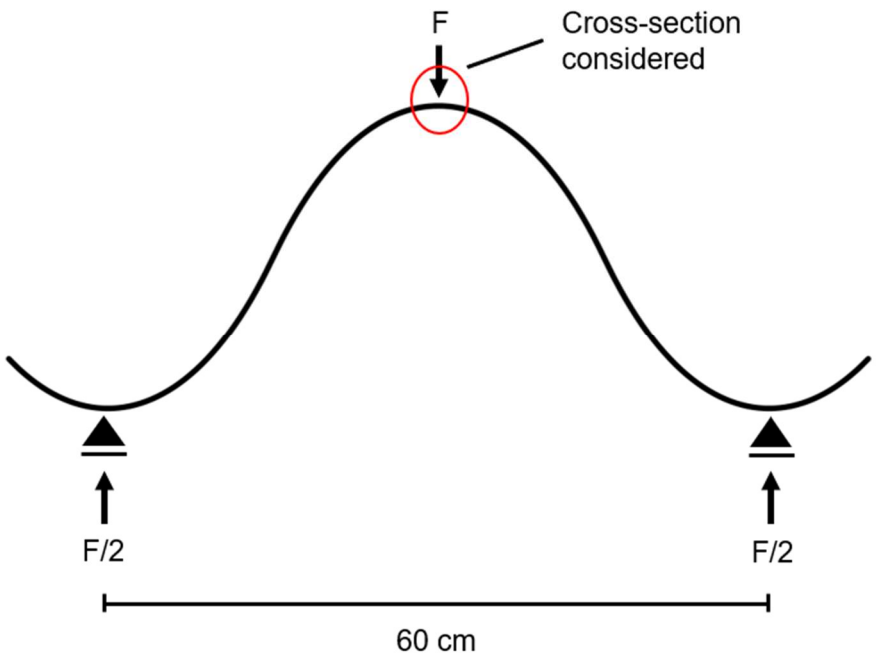

Figure A-28: Static system used for stress calculation of three-point bending tests

First, the cross-section of the elements was measured. Therefore 5 measurements were performed for the thickness and one for the width of the specimens. With the arithmetic average of the thickness and the width of the specimen, the section modulus was then calculated. Using the failure force, the moment in the apex zone was then calculated and

furthermore, the stress. Finally, the stress to force value was calculated to transform the force-deflection diagrams into stress-deflection diagrams, which are presented in Figure A-29 to Figure A-32. Used formulas can be seen below. The measurements and calculated values are given in Table A-20.

$$W = \frac{b * {d_m}^2}{6} \tag{A-5}$$

With: W Section modulus [mm³]
b Width of the specimen [mm]
d_m Average thickness of the specimen [mm]

$$M_{Fail} = \frac{F_{Fail} * l}{4} \tag{A-6}$$

With: M_{Fail} Failure moment [Nmm]
F_{Fail} Failure force [N]
l Distance between the supports [mm]

$$\sigma_{Fail} = \frac{M_{Fail}}{W} \tag{A-7}$$

With: σ_{Fail} Failure stress [N/mm²]
M_{Fail} Failure moment [Nmm]
W Section modulus [mm³]

Table A-20: Measured and calculated values of specimens used in three-point bending tests

Test number	Average thickness d_m	Width b	Section modulus W	Failure force F_{Fail}	Failure moment M_{Fail}	Failure stress σ_{Fail}	Stress / Force ratio
-	[mm]		[mm³]	[N]	[Nmm]	[N/mm²]	-
PA5-T-1	10.1	60.1	1021.0	224.6	33690	33.0	0.15
PA5-T-2	10.2	60.4	1047.5	191.1	28665	27.4	0.14
PA5-T-3	10.0	59.7	995.5	204.6	30690	30.8	0.15
PA6-T-1	10.0	59.3	988.3	233.9	35085	35.5	0.15
PA6-T-3	10.0	59.5	991.8	269.2	40380	40.7	0.15
PA7-T-1	11.4	62.2	1346.4	208.1	31215	23.2	0.11
PA7-T-2	10.6	60.4	1131.8	196.4	29460	26.0	0.13
PA7-T-3	10.5	60.1	1104.9	263.2	39480	35.7	0.14
PA8-T-1	10.1	61.0	1036.6	223	33450	32.3	0.14
PA8-T-2	11.7	60.9	1389.7	212.3	31845	22.9	0.11
PA8-T-3	11.6	61.0	1368.3	212.5	31875	23.3	0.11

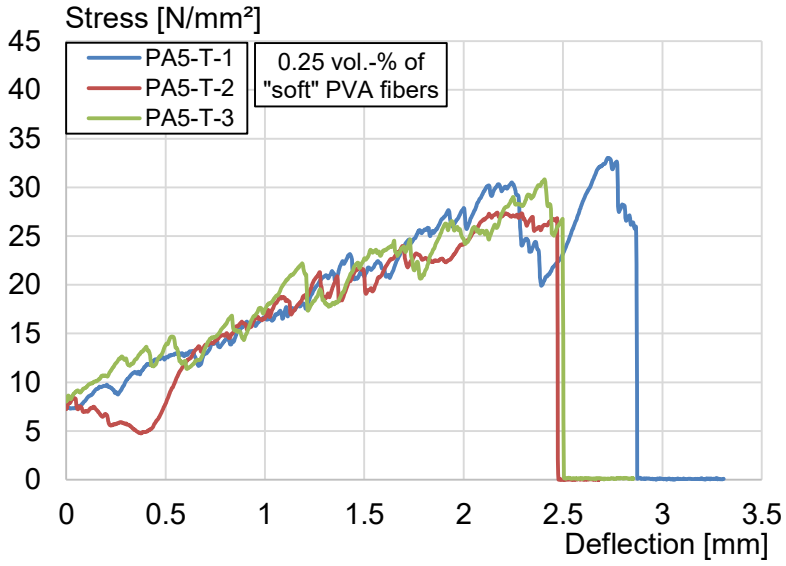

Figure A-29: Stress-deflection diagram of specimens with 0.25 vol.-% of "soft" PVA fibers and no textile reinforcement

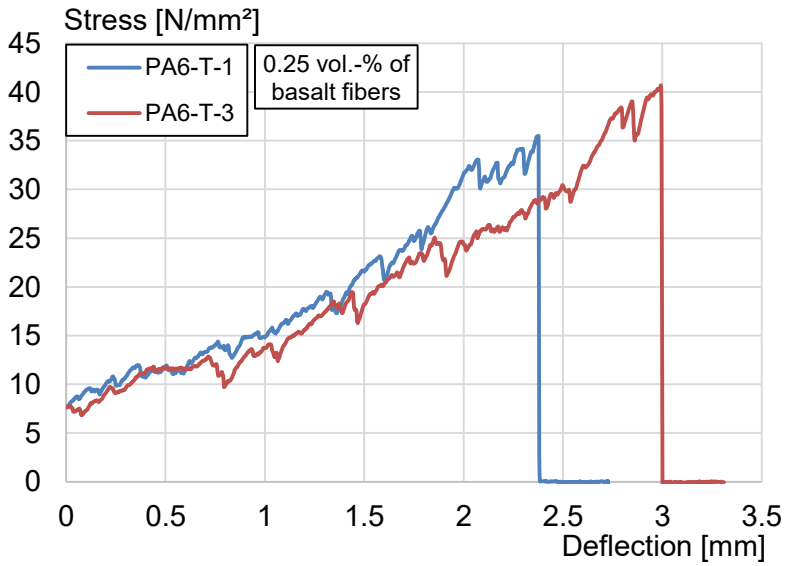

Figure A-30: Stress-deflection diagram of specimens with 0.25 vol.-% of basalt fibers and no textile reinforcement

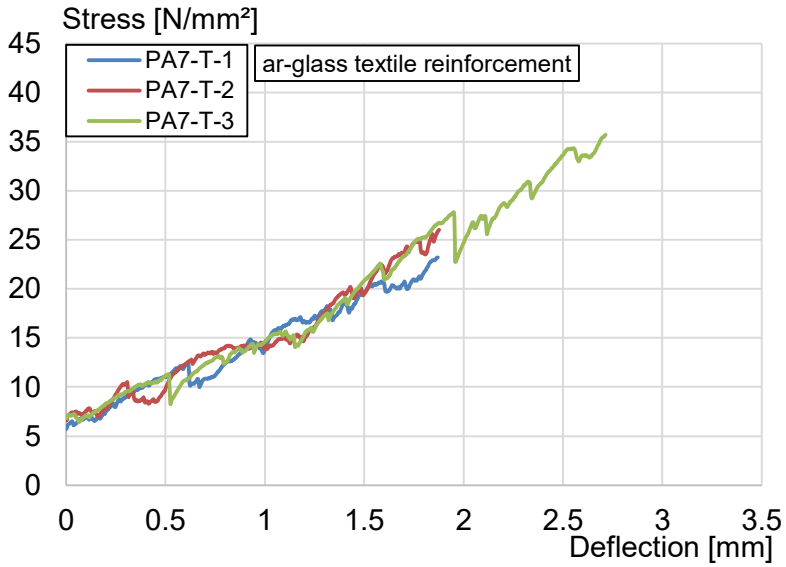

Figure A-31: Stress-deflection diagram of specimens with 0.5 vol.-% of "soft" PVA fibers and ar-glass textile reinforcement

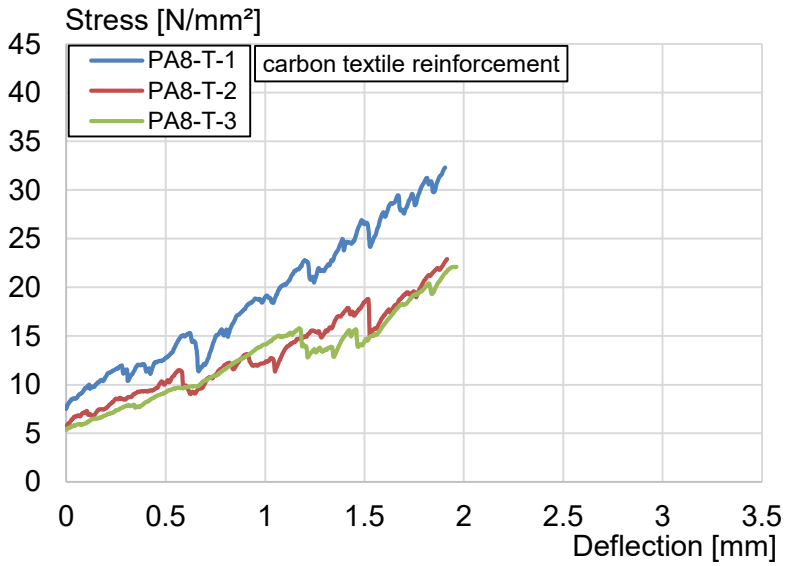

Figure A-32: Load-deflection diagram of specimens with 0.5 vol.-% of "soft" PVA fibers and carbon textile reinforcement